Studies on ^{68}Ga-Based Agents for PET Imaging of Cancer and Inflammation

by

Tiina Ujula

From Turku PET Centre, Institute of Clinical Medicine, Department of Clinical Physiology and Nuclear Medicine; Institute of Biomedicine, Department of Cell Biology and Anatomy, University of Turku, Turku; and Drug Discovery Graduate School (DDGS), Finland

Supervised by:

Professor Anne Roivainen, PhD
Turku PET Centre
Turku Center for Disease Modeling
University of Turku
Turku, Finland

and

Professor Pirkko Härkönen, MD, PhD
Department of Cell Biology and Anatomy
University of Turku
Turku, Finland

Reviewed by:

Professor Marion de Jong, PhD
Department of Nuclear Medicine
University Hospital Rotterdam
Rotterdam, The Netherlands

and

Adjunct Professor Kirsi Timonen, MD, PhD
Department of Clinical Physiology and Nuclear Medicine
University Hospital of Kuopio
Kuopio, Finland

Dissertation opponent:

Cristina Nanni, MD
Department of Nuclear Medicine
University of Bologna
Bologna, Italy

Per aspera ad astra

ABSTRACT

Tiina Ujula (née Pöyhönen)

Studies on ^{68}Ga-Based Agents for PET Imaging of Cancer and Inflammation

Turku PET Centre, Institute of Clinical Medicine, Department of Clinical Physiology and Nuclear Medicine; and Institute of Biomedicine, Department of Cell Biology and Anatomy, University of Turku, Turku, Finland
Annales Universitatis Turkuensis, Medica-Odontologica, 2010, Turku Finland

Positron emission tomography (PET) is based on the use of radiolabeled agents and facilitates *in vivo* imaging of biological processes, such as cancer. Because the detection of cancer is demanding and is often obscured by inflammation, there is a demand for better PET imaging agents.

The aim was to preliminarily evaluate new PET agents for imaging cancer and inflammation using experimental models. ^{68}Ga-chloride and peptides, ^{68}Ga-labeled through 1,4,7,10-tetraazacyclododecane-1,4,7,10-tetraacetic acid (DOTA), targeting matrix metalloproteinase-9 (MMP-9) were tested for tumor imaging. In addition, a ^{68}Ga-DOTA-conjugated peptide targeting vascular adhesion protein-1 (VAP-1), was tested for inflammation imaging.

The ^{68}Ga-based imaging agents described here showed potential features by passing the essential *in vitro* tests, proceeding further to preclinical *in vivo* evaluation and being able to visualize the target. The target uptake and target-to-background ratios of ^{68}Ga-based agents were, however, not optimal. ^{68}Ga-chloride showed slow clearance caused by its binding to blood transferrin. In the case of ^{68}Ga-DOTA-peptides low *in vivo* stability and/or low lipophilicity led to too rapid blood clearance and urinary excretion.

The properties of ^{68}Ga-labeled peptides are modifiable, as shown with matrix metalloproteinase-9 targeting ligands. In the conclusion of this PhD thesis, ^{68}Ga-based agents for PET imaging of cancer and inflammation could be applied in the development of drugs, earlier diagnostics and following-up of the efficacy of therapies.

Keywords: Gallium-68, positron emission tomography, cancer, inflammation, experimental models

TIIVISTELMÄ

Tiina Ujula (o.s. Pöyhönen)

Tutkimuksia syövän ja tulehduksen PET-kuvantamisen ^{68}Ga-merkkiaineista

Positroniemissiotomografiaa (PET) käytetään elimistön (*in vivo*) toiminnalliseen kuvantamiseen radioleimattujen aineiden avulla. PET soveltuu esimerkiksi syövän tutkimiseen ja diagnosointiin, joka on haasteellista. Usein syöpään liittyvä tulehdus häiritsee PET-kuvantamista ja siksi tarvitaan entistä parempia merkkiaineita.

Tutkimuksen tarkoituksena oli tehdä alustava arvio uusista syövän ja tulehduksen PET-merkkiaineista käyttäen kokeellisia malleja. Syöpäkasvainten kuvantamiseen testattiin ^{68}Ga-kloridia ja peptidejä, jotka ^{68}Ga-leimattiin 1,4,7,10-tetra-atsasyklododekaani-1,4,7,10-tetrametaanikarboksyylihapon (DOTA) avulla ja jotka kohdentuivat matriksin metalloproteinaasi-9 -proteiiniin (MMP-9). Lisäksi tulehduksen kuvantamiseen testattiin ^{68}Ga-leimattua DOTA-peptidiä, joka kohdentui verisuonen seinämän adheesioproteiini-1:een (VAP-1).

Tutkimustulosten perusteella testatuilla kuvantamisen ^{68}Ga-merkkiaineilla on lupaavia ominaisuuksia: Ne läpäisivät vaaditut *in vitro* -testit, etenivät prekliiniseen *in vivo* -arviointiin, ja mahdollistivat kohteen visualisoinnin. Merkkiaineiden kertyminen kohteeseen ja kohde-tausta-suhde eivät kuitenkaan olleet optimaalisia. ^{68}Ga-kloridi sitoutui veren transferriiniin, jolloin poistuma verenkierrosta oli hidasta. ^{68}Ga-DOTA-peptidien tapauksessa yhdisteiden heikohko *in vivo* stabiilisuus ja/tai alhainen vesiliukoisuus johti nopeaan poistumaan virtsan erityksen kautta.

Matriksin metalloproteinaasi-9:ään kohdentuvilla ligandeilla osoitettiin, että ^{68}Ga-leimatut peptidit ovat muokattavissa. Väitöskirjan yhteenvetona voidaan todeta, että syövän ja tulehduksen kuvantamisen ^{68}Ga-merkkiaineita voitaisiin hyödyntää lääkekehityksessä, entistä varhaisemmassa diagnostiikassa ja hoidon tehon seurannassa.

Avainsanat: Gallium-68, positroniemissiotomografia, syöpä, tulehdus, kokeelliset mallit

CONTENTS

ABBREVIATIONS

B_{max}	concentration of receptors or transporters
BP	binding potential
BxPC-3	pancreatic cancer cell line, originated from a human ductal adenocarcinoma
C8161T/M1	invasive subpopulation, isolated from a lung metastatic tumor of the initial C8161cell line, which originates from human cutaneous malignant melanoma
^{11}C	carbon-11 isotope
CHO	chinese hamster ovary cells
^{11}C-choline	[methyl-^{11}C]choline
^{11}C-MeAIB	[N-methyl-^{11}C]α-methylaminoisobutyric acid
^{11}C-MET	[^{11}C-methyl]methionine
CT	computed tomography
^{11}C-TYR	^{11}C-tyrosine
^{64}Cu	copper-64 isotope
DOTA	1,4,7,10-tetraazacyclododecane-1,4,7,10-tetraacetic acid, a chelate
Eβ+	positron energy
ECM	extracellular matrix
EDTA	ethylene-diamine-N,N,N',N'-tetraacetic acid; a chelate
FN	false negative
FP	false positive
^{18}F	fluorine-18 isotope
^{18}F-FDG	2-[^{18}F]fluoro-2-deoxy-D-glucose, ^{18}fluorine labeled (2S,3R,4S,5S,6R)-3-fluoranyl-6-(hydroxymethyl)oxane-2,4,5-triol (IUPAC)
^{18}F-FET	O-2-^{18}F-fluoroethyl-L-tyrosine
^{18}F-FLT	3'-deoxy-3'-[^{18}F]fluorothymidine
^{18}F-DOPA	^{18}F-fluorodihydroxyphenyl-L-alanine
γ	gamma quantum
^{66}Ga	gallium-66 isotope
^{67}Ga	gallium-67 isotope
^{68}Ga	gallium-68 isotope
^{67}Ga-citrate	gallium-67(3+); 2-hydroxypropane-1,2,3-tricarboxylate
$^{68}GaCl_3$	gallium-68(3+); trichloride, i.e. shortly ^{68}Ga-chloride
^{68}Ga-DOTA-BZH$_3$	^{68}Ga-DOTA-PEG$_2$-[D-Tyr^6, β-Ala^{11}, Thi^{13}, Nle^{14}] BN(6-14) amide
^{68}Ga-DOTA-α-MSH analogue	^{68}Ga-DOTA-α-melanocyte-stimulating hormone analogue, ^{68}Ga-DOTA-ReCCMSH(Arg^{11}) targeting melanocortin-1 receptors
^{68}Ga-DOTA-lanreotide	[^{68}Ga-DOTA-2-NaI, Tyr^3, ThrNH$_2^8$]octreotide
^{68}Ga-DOTA-NOC	[^{68}Ga-DOTA, 1-NaI^3]-octreotide
^{68}Ga-DOTA-TATE	[^{68}Ga-DOTA, Tyr^3, Thr^8]octreotide
^{68}Ga-DOTA-TOC	[^{68}Ga-DOTA, Tyr^3]octreotide
^{68}Ga-DOTAVAP-P1	^{68}Ga-DOTA-peptide targeting vascular adhesion protein-1
^{68}Ga-DOTA-lactam-TCTP-1	lactam-bridged ^{68}Ga-DOTA-peptide targeting matrix metalloproteinase-9
^{68}Ga-DOTA-lin-TCTP-1	linear ^{68}Ga-DOTA-peptide targeting matrix metalloproteinase-9
^{68}Ga-DOTA-TCTP-1	original ^{68}Ga-DOTA-peptide targeting matrix metalloproteinase-9
^{68}Ge	germanium-68 isotope
GRP	gastrin-releasing peptide
HCl	hydrochlorid acid, i.e. gastric acid
HE	hematoxylin and eosin, histological staining
HPLC	high-performance liquid chromatography
HRRT	high resolution research tomograph, a PET camera

^{123}I	iodine-123 isotope
^{123}I-VIP	^{123}I -labeled peptide targeting vasoactive intestinal peptide receptors
^{111}In	indium-111 isotope
i.p.	intraperitoneal(ly)
i.v.	intravenous(ly)
K_d	equilibrium dissociation constant
^{177}Lu	lutetium-177 isotope
MMP-9	matrix metalloproteinase-9
MRI	magnetic resonance imaging
NET	neuroendocrine tumor
PEG	polyethyleneglycol, a linker
PET	positron emission tomography
p.i.	post injection
ROI	region of interest
s.c.	subcutaneous(ly)
SPECT	single photon emission computed tomography
SRA	specific radioactivity
SSAO	semicarbazide-sensitive amine oxidase, also called VAP-1
SUV	standardized uptake value
TAC	time-activity curve
TiO_2	titaniumdioxide
$T_{1/2}$	physical half-life
^{99m}Tc	technetium-99m isotope
^{99m}Tc-VIP	^{99m}Tc-labeled peptide targeting vasoactive intestinal peptide receptors
TCTP	tumor cell targeting peptide
VAP-1	vascular adhesion protein-1, also called SSAO
VAP-P1	peptide targeting vascular adhesion protein-1
WBC	white blood cell
TN	true negative
TP	true positive
^{90}Y	yttrium-90 isotope
%ID/g	percentage of the injected dose per gram

TERMINOLOGY

Biomarker	"A characteristic that is objectively measured and evaluated as an indicator of normal biological processes, pathogenic processes, or pharmacological responses to a therapeutic intervention" (Beckmann *et al.*, 2007).
Contrast agent	An agent for ultrasound, CT or MRI, that is used for detecting certain details of anatomy more clearly (Dzik-Jurasz, 2004).
Imaging agent	Covers contrast agents, molecular imaging probes, radiopharmaceuticals and tracers (Dzik-Jurasz, 2004).
Imaging biomarker	A biomarker, that is especially used "for diagnosing and monitoring disease and tracking therapeutic response" (Agdeppa and Spilker, 2009).
Molecular imaging	"Characterization and measurement of biological processes in living animals, model systems, and humans at the cellular and molecular level using remote imaging detectors" (Sharma *et al.*, 2002).
Molecular imaging probe	Specifies a molecule (receptor, enzyme or transporter) of interest and provides physical contrast. Labeled small molecules (M < 1000 g/mol), peptides, enzymes, substrates and antibodies have all been used in this manner. Also the terms imaging probe or, especially, targeted imaging probe can be used (Dzik-Jurasz, 2004).
Radiopharmaceutical	"A radioactive compound used for diagnosis and the therapeutic treatment of human diseases" (Saha, 2004b).
Specific radioactivity	Specific radioactivity [SRA (Bq/mol or Bq/kg)] is "for a given radionuclide the activity divided by the mass of the sum of all radioactive and stable isotopes isotopic with the element involved" (de Goeij *et al.*, 2005).
Tracer	A radiopharmaceutical for nuclear medicine (PET or SPECT) that is administered as so small a dose, so-called tracer dose, which should not have pharmacological effects. This has led to the established term "tracer" (Sharma *et al.*, 2002; Dzik-Jurasz, 2004; Beckmann *et al.*, 2007; Nunn, 2007, Agdeppa and Spilker, 2009). The term tracer refers to a compound being processesed to a radiopharmaceutical or used as a radiopharmaceutical (Saha, 2004a).

LIST OF ORIGINAL PUBLICATIONS

This dissertation is based on the following original publications, which are referred to in the text by the corresponding Roman numerals, papers I – III.

I   Ujula T., Salomäki S., Autio A., Luoto P., Tolvanen T., Lehikoinen P., Viljanen T., Sipilä H., Härkönen P., Roivainen A. (2010). ^{68}Ga-chloride PET reveals human pancreatic adenocarcinoma xenografts in rats − comparison with FDG. *Mol Imaging Biol* **12**, 259-268.

II Ujula T., Salomäki S., Virsu P., Lankinen P. S., Mäkinen T. J., Autio A., Yegutkin G. G., Knuuti J., Jalkanen S., Roivainen A. (2009). Synthesis, ^{68}Ga labeling and preliminary evaluation of DOTA peptide binding vascular adhesion protein-1: a potential PET imaging agent for diagnosing osteomyelitis. *Nucl Med Biol* **36**, 631-641.

III Ujula T., Huttunen M., Luoto P., Peräkylä H., Simpura I., Wilson I., Bergman M., Roivainen A. (2010). Matrix metalloproteinase 9 targeting peptides: syntheses, ^{68}Ga-labeling and preliminary evaluation in a rat melanoma xenograft model. *Bioconjug Chem* **21**, 1612–1621.

The original publications have been reprinted with the permission of the copyright holders.

1. INTRODUCTION

In medical imaging, the capability to perform whole-body screening is an important issue. Timely identification of disease and localization of the pathogenic tissues are critical for the adequate treatment of patients. *In vivo* imaging of anatomical changes is known to poorly reflect the underlying biology. The special advantages of positron emission tomography (PET) and other modern imaging techniques, such as ultrasound and functional magnetic resonance imaging (MRI), are their ability to illustrate the functional status of the disease, which is essential for defining the prognosis and helping to choose the right treatment (Evans and Peters, 2002; Dzik-Jurasz, 2004). PET is justified if an added value compared to other more available techniques can be shown, like patient management can be altered and cost-effectiveness can be demonstrated. This is fullfilled when PET diagnosis leads to a more appropriate therapy in clinical oncology, cardiology, neurology or inflammatory and infectious diseases. PET can be utilized as well for following the efficacy of a treatment. When developing new cancer therapies the estimation of the response is extremely important. PET may help to identify earlier the downstream effects of cancer drugs even before tumor shrinkage occurs. The trend in medicine is personalized medicine, which means an increasing need to monitor the physiological state of an individual in a noninvasive manner (De Winter *et al.*, 2002; Agdeppa and Spilker, 2009).

In theory, any biochemical processes and molecules in the body can be detected and quantified with PET after the administration of imaging agents labeled with a positron emitting isotope (Fig. 1). PET allows for the obtaining of real-time quantitative distribution and the biokinetics of the labeled agents. According to the United States Food and Drug Assosiation (FDA), there are four broad indications for the use of imaging agents: "i) structural characterization, ii) disease or pathology detection or assessment, iii) functional, physiological or biochemical assessment, and iv) diagnostic or patient management" (Agdeppa and Spilker, 2009).

The functional information of PET can be combined with the anatomical image obtained by computed tomography (CT) or MRI with PET-CT or PET-MRI technologies, which provide more accurate estimates of the functions of organs and abnormalities in tissues, and simplifying the interpretation of the PET data. For example, after cytostatic therapies PET-CT may allow the imaging of the molecular response at the same time as measuring tumor size (Beckmann *et al.*, 2007; Agdeppa and Spilker, 2009). PET can be also utilized in the basic research and development of pharmaceuticals or radio-pharmaceuticals, e.g. to clarify targeting property, nonspecific binding and distribution kinetics of compounds. Advantageously, preclinical PET results can be translated into clinical studies, which cuts experiments and cost (Beckmann *et al.*, 2007). For preclinical purposes, high resolution (1-2 mm) small animal PET and small animal PET-CT cameras have been developed. Other imaging modalities can also be exploited in medicine, such as optical imaging. Although, the weakness of optical imaging is low tissue penetration of fluorescence or bioluminescence emitted from optical imaging agents. Optical imaging can be used e.g.

in breast cancer surgery, and it is widely used preclinically in different mouse models *in vivo* (Dzik-Jurasz, 2004; Beckmann *et al.*, 2007; Oude Munnink *et al.*, 2009).

The diagnosis of cancer is demanding and it is often obscured by inflammation and, on the other hand, untreated chronic inflammation can lead to the development of cancer. The complex interaction of cancer and inflammation is not fully understood (Marx, 2004). The mechanism of and interrelationships between these pathophysiological states might be clarified with a proper imaging technique. Before anything, the ability to differentiate the diseases from each other is needed when searching for the right treatment for a patient. The most used PET imaging agent for cancer and inflammation is fluorine-18(^{18}F)-labeled glucose analog, 2-[^{18}F]fluoro-2-deoxy-D-glucose (^{18}F-FDG). ^{18}F-FDG is a specific marker for glucose consumption, which is increased during cancerous growth and inflammation. Several imaging agents for cancer and inflammation have been developed, but none of them has managed to replace ^{18}F-FDG (van Waarde and Elsinga, 2008; Halter *et al.*, 2004). For these reasons there is a demand for better tumor and inflammation PET imaging agents. To meet this challenge, in this thesis work new imaging agents targeting tumor or inflammation were evaluated using experimental models.

New radiopharmaceuticals are the cornerstones for the survival and strength of nuclear medicine. The production of the majority of isotopes used for the labeling of PET agents requires a cyclotron and qualified personnel. The centers lacking cyclotron would benefit from an alternative technique to produce PET isotopes, such as the relatively low-cost production of Gallium-68(^{68}Ga)-isotopes with a generator (Breeman and Verbruggen, 2007) (Fig. 1). In the present study, different ^{68}Ga-based imaging agents were tested. ^{68}Ga-chloride (^{68}GaCl$_3$) and ^{68}Ga-labeled peptides targeting matrix metalloproteinase-9, over-expressed in cancer, was studied for tumor imaging. ^{68}Ga-labeled 1,4,7,10-tetraazacyclododecane-1,4,7,10-tetraacetic acid(DOTA)-conjugated peptide, targeting inflammation-inducible vascular adhesion protein-1, was studied for inflammation imaging.

Production of Imaging Agents

Isotope production in a cyclotron or in a generator (here)

Synthesis

PET image

Head

Heart

Liver

Kindney

Urinary bladder

Tail

PET imaging

Administration to a study subject (human or animal)
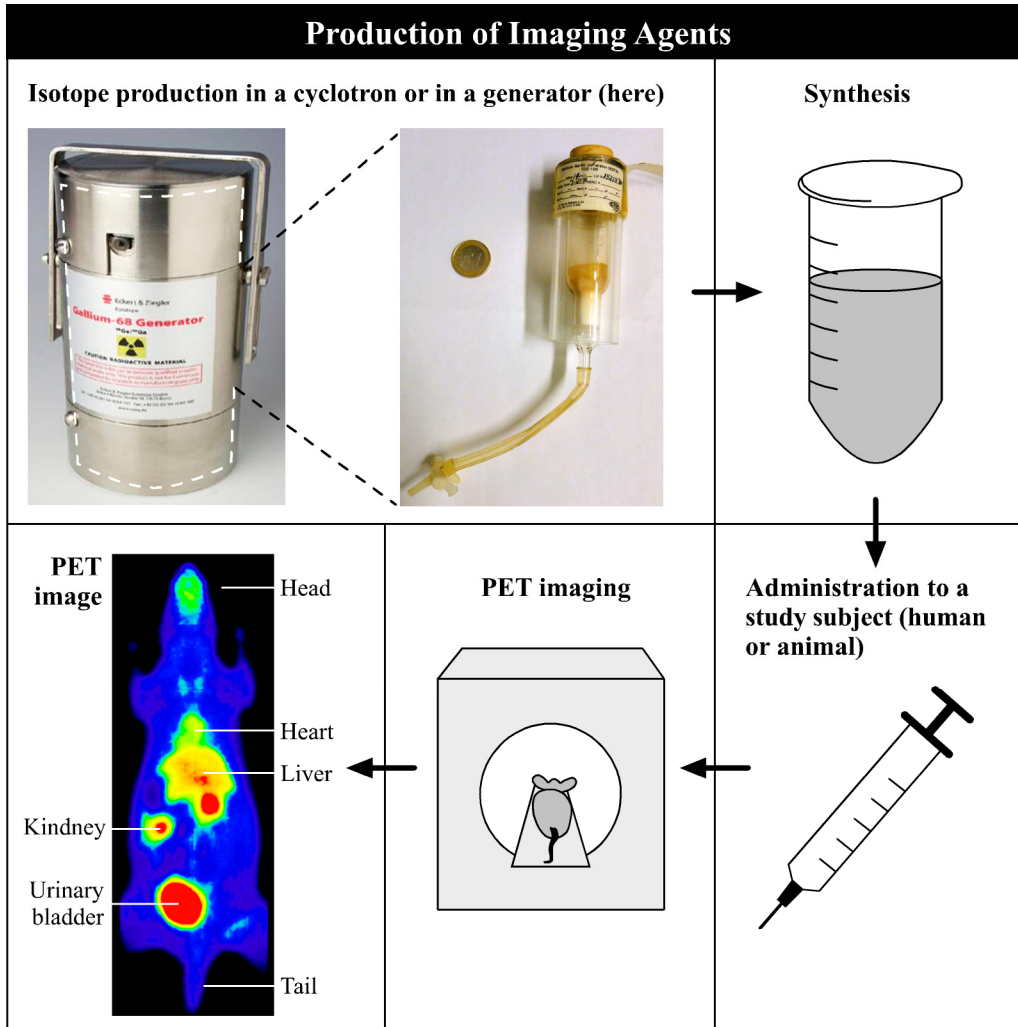
Figure 1. The principle of PET imaging. Radionuclides can be produced in a cyclotron or in a generator. A cyclotron is generally relatively large (even the size of a room), while a generator is quite small (next to the column, inside the generator's shell, is a coin illustrating the size). During synthesis a radionuclide is attached to the targeting molecule to develop an imaging agent. After administration the imaging agent gravitates to the target. The positrons released from the target, travel in the tissue until they meet their anti-particle, i.e. an electron, and a coincidence happens causing the release of gamma(γ)-quantums. The PET camera is able to detect the γ-quantums and with mathematical image construction a three-dimensional image is received. The figure of the generator's shell is reprinted from a commercial of Eckert&Ziegler, Berlin.

2. REVIEW OF THE LITERATURE

2.1. Gallium-Based Imaging Agents

2.1.1. History

Cyclotron produced Gallium-67(^{67}Ga) (half-life (T$_{1/2}$) of 78 h, decay 100 % by electron capture) in the form of ^{67}Ga-citrate (gallium-67(3+); 2-hydroxypropane-1,2,3-tricarboxylate) has been used as an imaging agent in scintigraphy/single photon emission computed tomography (SPECT) for decades for the purpose of detecting certain tumors and infection/inflammation, in spite of its disadvantages, resulting mainly from such unfavorable physical characteristics as high radiation exposure and long examination time. The first tumor uptake studies with ^{67}Ga-citrate were performed in the 1960's (Edwards and Hayes, 1969), but it was soon recognized that it was useful in the identification of inflammation as well (Higasi *et al.*, 1971; Lavender *et al.*, 1971; Ito *et al.*, 1971). Also, ^{68}Ga was tested for PET imaging (Anger H. O. and Gottschalk, 1963; Shealy *et al.*, 1964). For a long period of time ^{68}Ga was almost forgotten, but during the last decade it has gone through a renaissance.

2.1.2. The Generator Produced ^{68}Ga

Gallium has two natural isotopes, i.e. 60 % is ^{69}Ga and the rest is ^{71}Ga. Three radio-isotopes can be produced for nuclear medicine purposes. ^{66}Ga (T$_{1/2}$ of 9.5 h) and ^{68}Ga (T$_{1/2}$ of 68 min) are short-lived positron emitters, i.e. they decay β^+-emission, and for that reason they can be used for PET imaging. ^{68}Ga disintegrates 89 % by positron emission of 1.9 MeV max energy and 11 % by electron capture to stable zinc (^{68}Zn) (Velikyan, 2005). The half-life is suitable for labeling many ligands for PET imaging and it is short enough to cause minimal radioactive burden for a patient (Lundqvist and Tolmachev, 2002). ^{67}Ga decays via gamma (γ) emission and is utilized in SPECT imaging.

The production of ^{68}Ga does not require a cyclotron since it is available from a Germanium-68(^{68}Ge)/^{68}Ga-generator. Although, ^{68}Ga could be produced by cyclotron, as well [^{68}Zn(p,n)^{68}Ga reaction]. ^{68}Ge, instead, is produced by cyclotron from ^{69}Ga [^{69}Ga(p,2n)^{68}Ge] (Lundqvist and Tolmachev, 2002). *The first ^{68}Ge/^{68}Ga-generator* was developed by Gleason in 1960. ^{68}Ga was separated from its parent ^{68}Ge-nuclide by solvent extraction. The radioactivity was back-extracted into dilute hydrochloric acid (HCl), which was further processed to an imaging agent (Hnatowich, 1977).

A year afterwards, an improved generator was developed based-on *an aluminium oxide (Al$_2$O$_3$) matrix column*, loaded with ^{68}Ge, from which ^{68}Ga was extracted with a sodium ethylene-diamine-N,N,N',N'-tetraacetic acid (Na-EDTA) solution (Greene and Tucker, 1961). *The next generation's ^{68}Ge/^{68}Ga-generators*, introduced by Kopecky and Mudrova (1974), made possible the elution of ^{68}Ga^{3+} based-on ion-exchange with HCl. Improved versions of Kopecky's and Mudrova's generators are today

commercially available. Also other matrix materials and eluates can be used; for example titanium dioxide (TiO_2), pyrogallol-formaldehyde copolymer, alpha ferrous oxide, tin oxide and styrene-divinyl-benzene copolymer containing N-methylglucamine matrixes (Meyer *et al.*, 2004). *TiO_2-based generator* (Cyclotron Co., Obninsk, Russia) is used all around the world. ^{68}Ga yield is ≥ 60 % during the first year, decreasing to 25 % after three years or 200 elutions (Fani *et al.*, 2008).

Improvements are still needed, because the ^{68}Ga solutions obtained from the generators are usually too acidic and too diluted for use in direct labeling procedures (which utilize the chelating ability of the macromolecule itself, like lactoferrin), and may contain some impurities, which may be a problem for labeling on a small scale (Meyer *et al.*, 2004, Velikyan, 2005; Fani *et al.*, 2008). Before ^{68}Ga-labeled compounds become standard radio-pharmaceuticals in daily nuclear medicine, the requirements of pharmaceutical legislation must be clarified (Breeman and Verbruggen, 2007). Indeed, the first draft of the pharmacopeia for the production of [^{68}Ga-DOTA, Tyr^3]octreotide (*^{68}Ga-DOTA-TOC*) is under process.

2.2. Imaging of Cancer and Inflammation

2.2.1. PET Imaging of Cancer

When determining the outcome of a disease, prevention and early diagnosis are as important as treatment. The success of early diagnosis relies upon finding tumors at a curable stage, before they have had a chance to spread from their site of origin. This can be achieved by PET imaging of people with expected malignancy, in the hope of detecting very early lesions (Underwood, 2004a).

The utilization of ^{18}F-FDG for PET is possible, because glucose consumption is increased in tumors due to rapid cell proliferation. As a glucose analogue, ^{18}F-FDG reflects the level of glucose metabolism. Glucose and ^{18}F-FDG use cell surface transporters, glucose transporter-1 and -3 in particular, which are expressed at a high level in cancer cells (Younes *et al.*, 1997). ^{18}F-FDG, like glucose, is phosphorylated by *hexokinases* (particularly by *hexokinase* II) into ^{18}F-FDG 6-phosphate. Subsequently, ^{18}F-FDG 6-phosphate is trapped inside the cell, because it is not metabolized any further. Specific tumor imaging agents are warranted, because ^{18}F-FDG is specific merely for glucose consumption.

In addition to i) glucose metabolism, other well-known targets for tumor cell imaging are ii) synthesis of membrane lipids, iii) amino acid transport and iv) synthesis of DNA (reflecting the activity of *thymidine kinase 1*) (van Waarde and Elsinga, 2008). Markers of the synthesis of membrane lipids are, for example, carbon-11(^{11}C)-labeled acetate and [methyl-^{11}C]choline (^{11}C-choline). The exact uptake mechanism of ^{11}C-acetate into tumor cells is still unknown (Oyama *et al.*, 2002; Song *et al.*, 2009), whereas ^{11}C-choline is a radiolabeled analog of choline that is a choline-phospholipid precursor. Choline-phospholipids are needed for the lipid synthesis of cell membranes and in the modulation of transmembrane signaling. The malignant transformation of

cells is associated with enhanced synthesis of the cell membrane, and thus also with the induction of *choline kinase* activity. In rapidly proliferating cells (such as tumor cells), higher *choline kinase* activity induces an increase of choline phosphorylation leading to large amounts of phosphocholine converted to phosphatidylcholine. Subsequently, intravenously administered ^{11}C-choline is taken into cells by specific transporters, phosphorylated into ^{11}C-phosphocholine by *choline kinase,* and trapped inside the cell (Hara *et al.*, 1997; Hara, 2002; Roivainen *et al.*, 2000).

In turn, examples of amino acid transport markers are [^{11}C-methyl]methionine (^{11}C-MET), O-2-^{18}F-fluoroethyl-L-tyrosine (^{18}F-FET), ^{11}C-tyrosine (^{11}C-TYR), [N-methyl-^{11}C]α-methylaminoisobutyric acid (^{11}C-MeAIB) (Lindholm *et al.*, 1993; Heiss *et al.*, 1999; Bolster *et al.*, 1986; Sutinen *et al.*, 2003). In addition, as examples of the markers for synthesis of deoxyribonucleic acid (DNA), i.e. radiolabeled nucleosides, are worth mentioning [^{11}C-methyl]thymidine and 3'-deoxy-3'-[^{18}F]fluorothymidine (^{18}F-FLT) (Shields *et al.*, 1998; Halter *et al.*, 2004).

2.2.1.1. ^{68}Ga-Based PET Imaging Agents of Cancer

To my current knowledge six DOTA-conjugated and subsequently ^{68}Ga-labeled peptide based radiopharmaceuticals for imaging of cancer are in clinical trials: [^{68}Ga-DOTA, Tyr³]octreotide (*[68]Ga-DOTA-TOC*), [^{68}Ga-DOTA, 1-Nal³]-octreotide (*[68]Ga-DOTA-NOC*), [^{68}Ga-DOTA-2-Nal,Tyr³,ThrNH₂⁸]octreotide (*[68]Ga-DOTA-Lanreotide*) and [^{68}Ga-DOTA,Tyr³,Thr⁸]octreotide (*[68]Ga-DOTA-TATE*) bind differently to subtypes of somatostatin receptors, and are studied especially for the imaging of neuroendocrine tumors (NETs) (Pool *et al.*, 2010; Fani *et al.*, 2008). ^{68}Ga-DOTA-PEG₂-[D-Tyr⁶, β-Ala¹¹, Thi¹³, Nle¹⁴] BN(6-14) amide (*[68]Ga-DOTA-BZH₃*) (Dimitrakopoulos-Strauss *et. al.*, 2007) is a bombesin analog. It binds to bombesin receptors [including e.g. neuromedin B and gastrin-releasing peptide (GRP) receptors]. ^{68}Ga-DOTA-BZH₃ is studied for the imaging of gastrointestinal tumors and prostate cancer. *[^{68}Ga-DOTA-D-Glu]gastrin*, binding to gastrin receptors [i.e. cholecystokinin-2 (CCK-2 receptors)], is studied for the imaging of medullary thyroid cancer (Mäcke and André, 2007, Fani *et al.*, 2008, Pool *et al.*, 2010).

^{68}Ga-DOTA-TOC is the first ^{68}Ga-based PET-imaging agent widely studied (Mäcke and André, 2007). It is convenient in the diagnosis of neuroendocrine tumors (NETs), a rare and heterogenous group of neoplasms, which originate from the neural crest. The majority of NETs arises in the gastrointestinal tract, pancreas or the lungs. NETs are rare in any other location (Haug *et al.*, 2009). ^{68}Ga-DOTA-TOC enables fast diagnosis within one hour in 94 % of the cases, and when compared to the available SPECT-methods, the radiation dose for a patient is remarkably lower and visualization of bone metastases is better (Mäcke and André, 2007), however, it is not FDA or European Medicines Agency (EMEA) approved. ^{68}Ga-DOTA-NOC is a modification, which may have some advantage over the original ^{68}Ga-DOTA-TOC, because ^{68}Ga-DOTA-NOC has a broader somatostatin receptor subtype profile and 2.5 fold higher tumor uptake, but also higher uptake in some healthy organs (Mäcke and André, 2007). ^{68}Ga-DOTA-NOC has been suggested for the new golden standardad for imaging of NETs

(Gotthardt *et al.*, 2004; Mäcke and André, 2007; Ambrosini *et al.*, 2010). ^{68}Ga-DOTA-TATE is better in the evaluation of well-differentiated metastatic NETs, compared to ^{18}F-fluorodihydroxyphenyl-L-alanine (^{18}F-DOPA), which is known to visualize NETs with high sensitivity. According to Haug and colleagues (2009), ^{68}Ga-DOTA-TATE PET should be employed as the first choice of diagnostic method for this class of tumors, however, it is not approved by either the FDA or EMEA.

Bombesin is a peptide isolated from frog skin. Corresponding mammalian peptides include GRP and neuromedin B, while endogenous mammalian bombesin is not identified. GRP and neuromedin B target G-protein coupled receptors at the cell membrane; bombesin receptor, GRP receptor (with a high affinity imparticular for GRP) and neuromedin B receptor (with a high affinity for neuromedin B) (Maina *et al.*, 2006).

Gastrin is a hormone that stimulates the secretion of gastric acid (HCl) and aids in gastric motility. It is released from the stomach and secreted into the bloodstream. Gastrin is found primarily in three forms: big, little and minigastrin, which are composed of 34, 17 or 14 amino acids, respectively. The release of gastrin is controlled by stomach distension, vagus stimulation (mediated by the bombesin-like peptides), proteins of food, gastric acid (negative feed-back) and local or circulating hormones (Nicholl *et al.*, 1985). The gastrin receptor is over-expressed in certain cancers. More than 90 % of medullary thyroid cancers show an elevated level of gastrin receptors. Radiolabeled CCK analogs, as well as analogs of gastrin and minigastrin have showed promising targeting for gastrin receptors (Pool *et al.*, 2010).

2.2.2. Imaging of Inflammation

Inflammation is a nonspecific tissue's response to any kind of injury, regardless of the cause. If the injury is caused by microbes or involves microbes, it leads to infection. Inflammation can be divided into acute and chronic inflammation based on the duration of the inflammatory reaction. *Acute inflammation* is an immediate response lasting for 8-10 days. In the early stages, edema fluid, fibrin and white blood cells (WBCs) i.e. leukocytes, especially neutrophils, accumulate in the extracellular spaces of the damaged tissue. The neutrophil polymorphism is essential for the histological diagnosis of inflammation (Stephenson, 2004). Within 48 hours of the initiation, monocytes and macrophages become the dominant cell types (Blankenberg and Strauss, 2002). If the immuno response of the body fails to heal, the inflammation becomes chronic. The *chronic inflammation* is characterized by the infiltration of lymphocytes, plasma cells and macrophages. The chronic phase may last for even years (Stephenson, 2004; Goldsmith and Vallabhajosula, 2009).

The locally changed conditions, such as enhanced blood flow, enhanced vascular permeability and influx of WBCs, promote the accumulation of imaging agents to the site of inflammation (Boerman *et al*, 2001). *[67]Ga-citrate, radiolabeled WBCs* and Indium-111(^{111}In)- or Technetium-99m(^{99m}Tc)-*labeled antibodies* are used for SPECT imaging of inflammation. Because during inflammation glucose consumption is raised due to active inflammatory cells, such as macrohages, and rapidly proliferating healing

tissues, ^{18}F-FDG can be used for PET imaging of the inflammation (Goldsmith and Vallabhajosula, 2009).

^{67}Ga-citrate and ^{18}F-FDG are useful to identify both acute and chronic inflammation, but neither of them is an inflammation specific imaging agent. The use of ^{67}Ga as a metabolic imaging agent is based-on its intravenous administration as a salt of citric acid (Moerlein and Welch, 1981; Goldsmith and Vallabhajosula, 2009). ^{67}Ga^{3+} is rapidly released from the weak chelator citrate *in vivo*, hydrolyzed and/or bound to transferrin, distributed in blood and accumulated in blood-rich tissues, like inflamed sites and tumors. Because the citrate is able to prevent the precipitation of ^{67}Ga(OH)$_3$, only soluble ^{67}Ga(OH)$_4^-$ is formed (Green and Welch, 1989). The acidic microenvironment causes the release of ^{67}Ga from transferrin and binding to other iron-binding molecules, such as lactoferrin, ferritin or bacteria-produced sideophores (Vallabhajosula *et al.*, 1980; Weiner *et al.*, 1981). The use of ^{67}Ga-citrate has been characterized by its slow accumulation, which makes the imaging of tumors by SPECT possible only after several hours, even days (Even-Sapir and Israel, 2003). On the other hand, according to a recent preliminary clinical study concerning ^{68}Ga-citrate PET, a good vizualisation of inflammation was obtained already at 1.5 hours after injection (Rizzello *et al.*, 2009).

Radiolabeled leukocytes are the golden standard to image inflammation (Boerman *et al*, 2001). The benefit of using radiolabeled WBCs is their specificity for infection imaging. Unfortunately, their use is limited to the detection of acute inflammation. The reason is that during acute inflammation WBCs (mainly neutrophils), and some macrophages, extravasate at the injured site. When inflammation becomes chronic the amount of neutrophils reduces. The radiolabeled WBCs consist mainly from radiolabeled neutrophils, since during the quite demanding preparation procedure, including the isolation of WBCs from the patient's own blood (normally includes 59 % neutrophils, 34 % lymphocytes and 2 % monocytes) and *in vitro* labeling of the cells, lymphocytes are usually damaged by radiation. Because in chronic inflammation the accumulation of neutrophils at the inflamed site is limited, radiolabed WBCs are not suitable for the imaging of chronic inflammation (Goldsmith and Vallabhajosula, 2009).

The radiolabeling of WBCs is performed by using ^{111}In-labeled oxine-chelator or ^{99m}Tc-labeled hexamethylpropylene-amineoxime (HMPAO)-chelator. Also ^{67}Ga-labeled WBCs have been studied in patients with promising results in 1975 (Burleson *et al.*, 1975). However, it appears that ^{111}In-labeled WBCs have proven to be better in the long run, since literature about ^{67}Ga-labeled WBCs after this initial report is limited. Recent *in vitro* study reports that ^{66}Ga-labeled WBCs would be a potential imaging agent for inflammation imaging by PET, because ^{66}Ga has a suitable half-life of 9.4 hours for cell kinetic studies (Ellis and Sharma, 1999). ^{68}Ga-labeled platelets have been studied in patients for the visualization of blood clots by PET imaging with poor results due to a high blood background at early time points (Goodwin *et al*, 1993).

Even if there is in the market some imaging agents based on labeling WBCs in the circulation ("WBC labeling *in vivo*"), they are not used for clinical routines. These

include several monoclonal antibodies against the surface antigens of granulocytes. One of them, ^{99m}Tc-labeled antistage specific embryonic antigen-1 monoclonal immunoglobulin M class antibodies (^{99m}Tc-anti-SSEA-1 IgM, market name is LeuTech) is approved and marketed in many European countries (Boerman *et al*, 2001; Goldsmith and Vallabhajosula., 2009). Also, nonspecific human polyclonal immunoglobulins (HIGs), labeled with ^{111}In or ^{99m}Tc, can be used. Furthermore, ^{99m}Tc-labeled interleukins seem to be potential for inflammation imaging. They are of human origin, non immunogenic, have low molecular weight (<25 g/mol) and clear rapidly from blood circulation. In addition, labeled antibiotics are in the market. ^{99m}Tc-labeled ciprofloxacin (market name Infecton) is suitable for inflammation imaging, but it is unable to differentiate between infection and sterile inflammation (Goldsmith and Vallabhajosula, 2009).

2.2.3. Relationship Between Inflammation and Cancer

Long-lasting inflammatory reaction around tumor tissue is common and reminds one of chronic inflammation. Inflammation is sustained by cytokines excreted by tumor cells, or released by tissue destruction (Vihinen *et. al*., 2005). Normally, inflammation is a beneficial response to injury, but it may also promote cancer-cell survival, implantation and growth (Mantovani *et al.*, 2008). At least in 15 % of cancer cases the origin can be found from prolonged inflammation (Marx, 2004). Tissues proliferate rapidly during inflammation making them vulnerable to mutations predisposing for cancer (van Waarde and Elsinga, 2008).

Immune surveillance can control or eliminate some cancer preceeding changes, but otherwise inflammation may promote carcinogenesis (Mantovani *et al.*, 2008). It has been suggested that the immune system recognises cancer and yet cannot control malignant growth. Indeed, the human body develops antibodies and T cells against tumor-specific antigens. The inability to resist cancer can be a consequence of immunodeficiency associated with modulatory properties or the tumor-bearing status of cancerous or bystander cells. In other words, immune surveillance causes the ability of tumor cells to resist the defence mechanisms (Dunn *et al.*, 2004; Mantovani *et al.*, 2008).

Furthermore, the mechanism of inflammation induced by cancer may lay in the function of macrophages as well. Normally macrophages destroy harmful subjects or injured cells by producing toxic agents. These toxic components may also cause carcinogenic mutations. Also at later stages of cancer, macrophages may promote cancer my helping the transformed cells to escape from the primary tumor site (Marx, 2004). Tumor-associated macrophages and B cells can interact and consequently cause tissue remodelling and neoangiogenesis (van Waarde and Elsinga, 2008).

When developing imaging agents for cancer, the fast proliferation of cells is being exploited. On the other hand, because during inflammation also healing tissues proliferate rapidly, the differentiation of cancer from inflammation is demanding. ^{18}F-FDG is the most used PET imaging agent for cancer, even if it causes false-positive

tumor findings. ^{18}F-FDG is not specific for cancerous growth or inflammation, but for glucose metabolism (Halter *et al.*, 2004; van Waarde and Elsinga, 2008).

When estimating the differentiation capacity of new imaging agents, the imaging agents are defined in the following way: The formula for *specificity* is: true negative (TN)/[TN + false positive (FP)] (Halter *et al.*, 2004). The goal is that the imaging agent would not accumulate in non-target tissues and its specificity i.e. proportion of TN of all negatives (TN and FP), would approach 100 %. The accumulation of an imaging agent to non-target tissues would a cause wrong finding, called FP. Usual FP happens when ^{18}F-FDG is used for scanning, and instead of tumors it accumulates to inflammation. Later on, FP findings are revealed to be non-target tissue, e.g. after the examination of a biopsy.

The formula for *sensitivity* is: true positive (TP)/[(TP + false negative (FN)] (Halter *et al.*, 2004). The objective is that sensitivity, i.e. proportion of TP of all positives (TP+ FN), would approach 100 %. TP is an imaging finding that is afterwards confirmed to be a correct finding. FN means that the target was not visualized by the imaging agent.

Selectivity can be expressed with a selectivity index: (target uptake - background)/(non-target uptake - background). Tumor selectivity, for instance, expresses the tumor-to-inflammation ratio corrected for background activity (van Waarde *et al.*, 2004).

Various techniques have been proposed to increase the tumor specificity of ^{18}F-FDG, e.g. improvements of data acquisition (delayed, dual time point or dynamic imaging) and improvements of data analysis, but still discrimination between tumor and inflammation is not always possible. Proliferation markers may allow an improved differential diagnosis of tumor and inflammation. These tumor imaging agents include i) radiolabeled lipid precursors, ii) amino acids, iii) nucleosides and iv) receptor ligands (van Waarde and Elsinga, 2008).

A radiolabeled *lipid precursor* choline, as well as aminoacids and nucleosides, have been reported to show greater tumor-specificity than ^{18}F-FDG. Reports of ^{11}C-choline for differentiation are contradictory. According to some studies, ^{11}C-choline is more tumor-specific than ^{18}F-FDG (van Waarde and Elsinga, 2008), but it has been also reported to accumulate to inflammatory sites (Roivainen *et al.*, 2003; Roivainen and Yli-Kerttula, 2006; Laitinen *et al.*, 2010). Other promising imaging agents for differentiation are a radiolabeled artificial *amino acid*, ^{18}F-FET, and a radiolabeled *nucleoside*, ^{18}F-FLT. They are more tumor-specific than ^{18}F-FDG, but their tumor uptake is lower resulting in relatively low sensitivity. Only radiolabeled nucleosides are true/direct markers for accelerated proliferation; the rest are surrogate markers and linked to increased proliferation indirectly. Each radiolabeled proliferation marker has high physiological uptake in some areas of the body, and for that reason they should not be considered as a replacement for ^{18}F-FDG, but rather providing additional diagnostic specificity (van Waarde and Elsinga, 2008). It has been reported that radiolabeled *receptor ligands*, especially sigma-ligands (σ-ligands), are more tumor selective than ^{18}F-FDG and ^{11}C-choline (van Waarde *et al.*, 2006).

2.2.4. Potential PET Targets and Imaging Agents

2.2.4.1. ^{68}Ga-Chloride

Recently, we have been able to establish a relationship between the ^{68}Ga-chloride uptake with PET at the site of a local bone infection, and underlying structural changes determined with peripheral quantitative computed tomography (pQCT) (Mäkinen *et al*, 2005). Rapid localization of radioactivity was observed in the inflamed leg of rats. In addition, when using ^{68}Ga-chloride as a control in ^{68}Ga-oligonucleotide studies, Roivainen *et al.* (2004) noticed uptake in tumors during two hours of dynamic PET imaging. The advantage of ^{68}Ga-chloride is the fast and simple production, i.e. the cyclotron-free and labeling-free production. ^{68}Ga-chloride is readily available at a PET-laboratory. Compared with the use of ^{67}Ga in SPECT, ^{68}Ga-chloride PET would have the following advantages: better spatial resolution, higher sensitivity, the possibility for quantitative assessment of the imaging agent accumulation in tissues and a lower absorbed radiation dose for the study subject, although the the expenses of using PET vs. SPECT are higher.

When reviewing the uptake mechanisms of radiogallium, one must begin with the elution of ^{68}Ga-chloride, because the formulation affects the uptake mechanism. After the elution from [68]Ge/^{68}Ga generator with 0.1 M HCl, ^{68}Ga is in the form of ^{68}Ga-chloride ($^{68}GaCl_3$) (Mäkinen *et al*, 2005). A soluble anion $^{68}Ga(OH)_4^-$ (gallate) is stable under acidic conditions (pH 3-7), but if its concentration exceeds to a nanomolar level, it can form insoluble colloids, $^{68}Ga(OH)_3$. In an aqueous solution, the only stable oxidation state is +3. (Mäcke and André, 2007; Fani *et al.*, 2008). Also, when neutralized the ionic Ga tend to precipitate (Bernstein, 1998).

Different isotopes behave in a similar fashion chemically and physiologically (in some cases the effect of differences in isotope weights may have an influence on biological properties). They differ only in physical properties (Saha, 2004b). For that reason some assumptions of the *in vivo* behavior of ^{68}Ga can be made from ^{67}Ga, which has been extensively studied after an intravenous injection of ^{67}Ga-citrate. Still, there might be some difference in ^{68}Ga behavior when administered as ^{68}Ga-chloride. ^{67}Ga-citrate can be classified as a nonspecific tumor/inflammation imaging agent (Vallabhajosula *et al.*, 1980; Goldsmith and Vallabhajosula, 2009). Since Ga^{3+} is chemically very similar to iron (Fe^{3+}), they behave physiologically in a similar fashion (Bernstein, 1998). In blood (pH 7.4), the solubility of Ga^{3+} is high and Ga^{3+} is bound to an iron-binding protein transferrin (Vallabhajosula *et al.*, 1980; Green and Welch, 1989; Weiner, 1996; Bernstein, 1998; Mäcke and André, 2007; Fani *et al.*, 2008). In tumorous or inflammatory tissue, Ga-transferrin leaks from arterioles and new capillaries (formed due to angiogenesis) into the extracellular fluid space (Tsan and Scheffel, 1986, Love and Palestro, 2004; Goldsmith and Vallabhajosula, 2009). Ga-transferrin binds to a transferrin receptor on the cell membrane, the complex is taken into a cell by endocytosis, and Ga is released as a consequence of the acidification of the endosome. Also, cell debris and relative anaerobic conditions result in acidic conditions (in tumorous and inflamed tissues), dissociation of Ga from transferrin, and

further binding to other iron-binding molecules (such as lactoferrin, ferritin, or bacteria-produced siderophores) (Vallabhajosula *et al.*, 1981; Weiner *et al*, 1981; Tsan and Scheffel, 1986; Bernstein 1998, Goldsmith and Vallabhajosula, 2009). The sideorophore-Ga complex is presumably transported into bacterium, where it remains until phagocyted by macrophages. Some Ga^{3+} may also be transported to the inflammation site bound by leukocytes (Weiner *et al.*, 1981; Bernstein, 1998; Love and Palestro, 2004).

In almost all cases, the accumulation of Ga^{3+} in malignant tissue correlates with level of transferrin receptor (cluster of differentiation 71, CD71) expression. In physiological conditions, all nucleated cells of the body express transferrin receptors, which are needed for iron metabolism, for example during DNA synthesis. The increased metabolic activity of tumor cells requires a high iron uptake, and this requirement leads to an increased number of transferrin receptors. However, Ga^{3+} can enter tumor cells also by a transferrin independent mechanism. In the proposed transferrin independent mechanism gallate plays a role. Due to its small size it may easily penetrate cellular membranes (Larson *et al*., 1980; Chitambar and Civkovic, 1987; Weiner, 1996, Bernstein, 1998). Also, Ga^{3+} uptake by macrophages, and more particularly in the lysosome-like structures has been reported (Swartzendruber *et al.*, 1971). The uptake mechanisms of radiogallium into tumors are not fully understood, and a wide variety of factors can be involved.

2.2.4.2. Targeting of Vascular Adhesion Protein-1

Vascular adhesion protein-1 (VAP-1) is an endothelial glycoprotein playing a critical role in cellular trafficking by recruiting lymphocytes, CD8+ T lymphocytes in particular, from the blood into the lymphoid organs and inflamed tissues (Salmi and Jalkanen, 1992; Salmi *et al*., 1997; Salmi and Jalkanen, 2001; Merinen *et al*., 2005). VAP-1 is practically absent from the endothelial surface of normal tissues, but upon infection/inflammation it is translocated from intracellular granules to the endothelial surface (Salmi *et al.*, 1997). For instance, in various skin inflammatory diseases (e.g. psoriasis), inflammatory bowel diseases (e.g. Crohn's disease) and inflamed joints (e.g. rheumatoid arthritis), blood vessels start to express VAP-1 on their endothelial surface (Salmi *et al*., 1993; Marttila-Ichihara *et al*., 2006). In addition to endothelial cells, VAP-1 is present in smooth muscle cells, adipocytes, and in follicular dendritic cells to some extent (Salmi *et al*., 2001). Besides being an adhesion molecule, VAP-1 is also an enzyme having semicarbazide-sensitive amine oxidase (SSAO) activity. The VAP-1/SSAO molecule is expressed both in a membrane-associated and a soluble form, circulating in the blood stream with elevated levels during inflammation (Kurkijärvi *et al.*, 2000; Zorzano *et al.*, 2003; Bono *et al.*, 1998; Salmi and Jalkanen, 2005; Gokturk *et al.*, 2003).

The structure of the VAP-1 molecule was discovered by X-ray crystallography. Then peptides fitting to the enzymatic groove of VAP-1 were searched by molecular modeling. The discovered peptides were tested *in vitro*, and one of them showed a long lasting inhibitory effect (Yegutkin *et al*., 2004). It was selected for PET imaging agent development. When ^{68}Ga-labeled and DOTA-conjugated, this peptide is a potential

inflammation imaging agent for PET. Our recent studies suggest that VAP-1 can be used as a molecular target for demonstrating the phase of inflammation in healing bones and the progress of infection in osteomyelitic bones (Lankinen *et al.*, 2008). The first VAP-1 targeting candidate peptide (VAP-P1) for PET imaging is named ^{68}Ga-DOTAVAP-P1.

2.2.4.3. Targeting of Matrix Metalloproteinase-9

Since matrix metalloproteinase-9 (MMP-9) is over-expressed in most tumor types and it is known to be associated with tumor growth, metastasis and angiogenesis (Bloomston *et al.*, 2002), it is a potential target for the development of PET imaging agents.

MMP-9 belongs to a MMP family of zinc-dependent proteolytic enzymes of 26 MMP variants (Li and Xu, 2005). In normal physiology and pathophysiology matrix metalloproteinases (MMPs) play a major role in tissue modeling and remodeling by being capable of degrading extracellular matrix (ECM) proteins. For example, MMPs are associated with morphogenesis, wound healing, and tissue resorption (Benbow and Brinckerhoff, 1997). MMP-9 expression is normally low and mainly found in keratinocytes, neutrophils and eosinophils (Ståhle-Bäckdahl and Parks, 1993). Over-expression has been associated with tumorigenesis in many malignancies, like sarcomas, carcinomas, gliomas, lymphomas and malignant melanomas (Raithatha *et al.*, 2000; Sakata *et al.*, 2004; Vihinen *et al.*, 2005). Elevated MMP-9 serum levels of melanoma patients are associated with rapid tumor progression (Nikkola *et al.*, 2005). In tumors MMP-9, also known as gelatinase B, degrades the gelatin of the ECM and thus promotes tumor cell migration and invasion into blood vessels and surrounding tissues (Bloomston *et. al.*, 2002, Sternlicht and Werb, 2001). MMP-9 is also expressed in the endothelial cells of the tumor blood vessels as part of their growth process (Koivunen *et al.*, 1999; Wikström *et al.*, 2003; Phillips and Birnby, 2004; Del Bufalo *et al.*, 2004).

MMP-9 is synthesized as an inactive pro-enzyme and transported in vesicles to the cell surface. Then MMP-9 becomes activated on the cell surface, or after secretion from the cell by its own activity, other MMPs or serine proteases, or by dissociation of complex partners or inhibitors (e.g. tissue inhibitors of metalloproteinases, TIMPs) (Sato *et al.*, 1994; Brooks *et al.*, 1996; Hofman *et al.*, 2000; Deryugina *et al.*, 2001; Sternlicht and Werb, 2001; Schnaeker *et al.*, 2004).

The enthusiasm to develop MMP targeting drugs, MMP inhibitors in particular, failed to bring new therapeutics to the market in the past decade. The main reasons for this may lay in the fact that most of the inhibitors were broad-spectrum drugs, and thus their selectivity was poor, they had side effects, they were administered in the wrong time and not-depending on the expression level of MMPs that varies during the course of tumorigenesis, the therapeutic index was small, or they did not show a clinical endpoint (Vihinen *et. al.* 2005; Vartak and Gemeinhart, 2007). Even if these compounds failed as therapeutics, they may serve as leads for developing imaging agents, since the lack of functionality caused by binding to the target is not a

requirement for imaging, and when administered as a tracer dose the possibility of side effects are minimized. The development of MMP targeted agents for imaging is a relatively new field, as the first report of a MMP (in particular MMP-2) targeting imaging agent for the optical imaging of tumors *in vivo* was published in 2001 by Bremer and colleagues. MMPs are potential targets for *in vivo* imaging, because of their pericellular location without the need to penetrate the cell membrane (Yang *et al.*, 2009). The special advantage is the possibility to amplify the signal with the enzymatic activity of MMPs. Most of these applications are for optical imaging (Randy *et al.*, 2008). MMP inhibitors are designed to recoginize the active site of MMPs, and thus it is possible to identify active MMPs from latent MMPs (proMMP and inhibited MMPs) (Scherer *et. al.*, 2008). MMP-9 targeting imaging agents could be useful, in addition to cancer, also in inflammatory diseases with an elevated MMP-9 level, such as atherosclerosis and Alzheimer's disease (Backstrom *et al.,* 1992; Robertson *et al.*, 2007). They would be valuable for drug development as well, since during the development of therapeutic MMP inhibitors it is important to be able to show the therapeutic action (Yang *et al.*, 2009).

MMP-9 expression has been previously targeted with several synthetic compounds radiolabeled with ^{11}C, ^{18}F, copper-64 (^{64}Cu), ^{111}In, iodine-123 (^{123}I) or ^{99m}Tc. There were many reasons why these SPECT or PET agents did not proceed any further. The studies showed no correlation between MMP-9 and the imaging results, high nonspecific binding was noticed, resulting from poor *in vivo* stability, the radiochemical yields were low, radiolabeling reaction times were long and/or the purification methods in their radiochemical synthesis were complicated (Zheng *et. al.*, 2002; Zheng *et. al.*, 2004; Wagner *et. al.*, 2009; Spraque *et. al.*, 2006; Hanaoka *et. al.*, 2007; Oltenfreiter *et. al.*, 2004; Kuhnast *et. al.*, 2004; Medina *et. al.*, 2005; Yang *et. al.*, 2009).

Koivunen *et al*. (1994) have identified potential MMP-9 targeting peptides using phage display. In 1999, Koivunen and collegues found peptide inhibitors specific for gelatinases, MMP-2 and MMP-9. In this thesis work, we DOTA-conjugated and ^{68}Ga-labeled one of the peptides and tested it for visualizing tumors (Paper III).

2.3. Preclinical PET in Drug Development

Molecular imaging is expected to have an increasing role in drug discovery and development (Agdeppa and Spilker, 2009). As mentioned earlier, imaging is part of the biomarker concept. A biomarker is, in general, a substance or characteristic used as an indicator of a biological state or pharmacological responses. A good PET imaging agent serves as a biomarker. The aim of a biomarker strategy is to confirm the targeting property of the candidate molecule, give early information of the safety and efficacy of the compound, as well as facilitate dose selection (Beckmann *et al.*, 2007). Biomarkers as early indicators could diminish the number of human subjects being exposed to experimental drugs with little or no therapeutic potential.

Preclinical PET has been particularly useful in monitoring intra- or extracellular receptor expression (Berger and Gambhir, 2001; Dzik-Jurasz, 2004). The advantage of

the PET imaging of animal models of human diseases is that it may facilitate the translation from preclinical to clinical research, meaning that preclinical study designs can be utilized in a similar concept for humans. This can strengthen the bridge between preclinical and clinical research (Beckmann *et al.*, 2007). PET can be utilized in several steps in the drug discovery process, starting from preclinical imaging in target identification (Fig. 2) and validation, e.g. when phenotyping transgenic animals. Imaging is used most intensively in the preclinical phase for the *in vivo* testing of pharmacokinetic properties [absorption, distribution, metabolism and excretion studies (ADME studies)] and the efficacy of compounds. The kinetics can be obtained from a single animal, which reduces biological variability, as the same animal can be used as its own control and imaged several times. In safety studies, PET imaging has received little attention, but it could be utilized more widely to reduce the amount of animals and costs. This would require changes in the requirements of regulatory authorities. In the clinical phases, *in vivo* imaging can be used as well in a cost-effective and patient number diminishing manner (Beckmann *et al.*, 2007).

In the future, more imaging studies with small animal PET will be performed with awake animals to avoid the effect of anesthesia on the results. High-resolution imaging of fully awake animals is only possible when motion correction is applied. This is possible when motion tracking systems and the recorded spatial transformations are used to list mode events to create a motion-corrected sinogram. However, at the moment the use of the software is limited to groups with a strong engineering team (Dupont *et al.*, 2009).
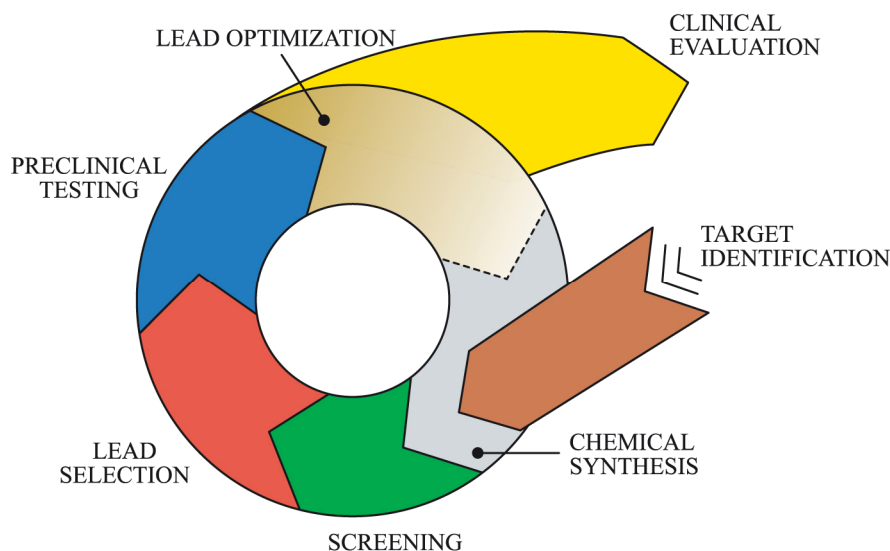

Figure 2. Simplified view of the drug/imaging agent discovery process. The screening method of labeled compounds can be utilized using biochemical or cellular assays, tissue sections and at the whole body level both *ex vivo* and *in vivo*. Modified from the figures presented by Beckmann and collegues (2007) and Agdeppa and Spilker (2009).

2.4. Imaging Agent Development

The process of imaging agent development is very similar to standard drug discovery and development. The process of drug/imaging agent development proceeds from target identification and validation to finding a lead with high affinity (Section 2.4.1.1., Table 1), uptake at the target site, adequate clearance, and low toxicity. The major difference between imaging agent and standard drug development is that a therapeutic drug, usually by inhibiting the target, induces a functional impact, while the only criteria for an imaging agent is that it must bind to the target (Blankenberg and Strauss, 2002; Agdeppa and Spilker, 2009). Almost any molecule can be chosen for radiolabeling and further evaluation (Berger and Gambhir, 2001). Target validation for imaging agents also presumes that the amount of target molecules can be quantitatively detected (concentration of receptors or transporters (B_{max}) = 50 000 – 100 000/cell) (Blankenberg and Strauss, 2002; Agdeppa and Spilker, 2009). Furthermore, the synthesis of an imaging agent is different from the synthesis of a therapeutic drug, because a signaling moiety is incorporated into the targeting molecule for imaging purposes. The signaling moiety may also affect the delivery, retention, binding and clearance (Agdeppa and Spilker, 2009). A requirement for the imaging agent is also high specific radioactivity in order to target the typically low-concentration markers of disease, especially in preclinical studies to sustain tracer quantities, where the injected dose can lead to much greater receptor occupancy than in humans. Imaging agents usually have limited toxicity due to the small (tracer) dose. Since PET imaging agents do not have pharmacological effects, the response cannot be directly measured. Instead, the proof of the mechanism is shown by correlation between imaging agent uptake and modulated target density. Modulation can be induced by using therapeutics or genetically modified mice. In addition, competition and inhibition studies can be used to demonstrate specific binding. To solve the precise location of an imaging agent, autoradiography and radiologic-histologic correlates are used (Beckmann *et al.*, 2007; Agdeppa and Spilker, 2009).

The validation of PET imaging agents, in an early phase is important to cut lost efforts and costs, as well as to diminish the failure of the agent in the later steps of drug discovery. Imaging biomarkers can interact with physiological biomarkers to determine the expression level in a quantitative manner and the location of potential therapeutic drug targets, and thus imaging biomarkers can be used to estimate the potential of therapeutic drug candidates (Agdeppa and Spilker, 2009).

2.4.1.   Qualifications for PET Imaging Agents

The positron signalling isotope, allowing PET imaging, set certain requirements for an imaging agent. PET detects the γ-emission released when the positron coincidence with an electron of the tissue. An ideal signaling isotope is a nuclide that is a pure positron emitter, but unfortunately many nuclides used emit also γ-radiation. γ-emission of nuclides is falsely detected as γ-emission released as a result of

coincidence. Ideal signaling isotopes possess also fairly low positron energy. PET detects the γ-emission released at the place where the emitted positron coincides with an electron. The higher is the positron energy, the longer is the range from the actual site of the nuclide, and the lower is the resolution (Lundqvist and Tolmachev, 2002).

Furthermore, an imaging agent for PET must have high specific radioactivity [SRA (Bq/mol or Bq/kg)] (de Goeij *et al*., 2005, Velikyan, 2005). High SRA is important, because imaging agents are administered as tracer doses. A tracer dose is such a small dose that it does not affect any pharmacological effects, meaning in a receptor system that the ligand binds typically to only less than one percent of the receptors. In practice, a tracer dose means nanomolar amounts (Meikle *et al*., 2001). A tracer dose is the requirement for a quantitative analysis of PET data and *ex vivo* measurements. High SRA might be also critical for providing a sufficient contrast of a PET image. SRA of ^{68}Ga-labeled molecules, in particular, is affected by the used bifunctional chelator's ability to bind ^{68}Ga^{3+}, and the labeling conditions, such as the temperature, ^{68}Ga^{3+}-concentration and possibly impurities in the labeling reaction (Velikyan, 2005).

The charge, lipophilicity and protein binding are crucial properties affecting to diffusion, clearance and localization of an imaging agent. The charge of an imaging agent, determines its solubility, i.e. hydro/lipophilicity. The greater the charge, the higher is the hydrophilicity. On the contrary, uncharged and nonpolar agents are lipophilic, i.e. more soluble in organic solvents and lipids. Whereas, the higher the lipophilicity, the greater is the diffusion through the cell membrane causing (usually) the higher accumulation to intracellular targets. Although, many agents use transporters for internalization and diffusion is not essential. The lipophilicity enhances binding to plasma proteins as well. Agents bound to plasma proteins are not free and consequently not effective. Binding to blood proteins reduces lipid solubility and diffusion, and to some extent also blood clearance, causing a higher background signal. For this reason the binding to blood proteins should be low. Almost all agents tend to bind to plasma proteins to some extent. Many metals, including Ga, bind to blood protein transferrin. Protein binding has a major role affecting on distribution, clearance and localization to the target. Other important requirements are chemical, radiochemical, radionuclidic and microbial purity, as well as the ability to resist radiolysis and affect the minimal radioactivity burden. The intravenous administration of a PET imaging agent sets also certain requirements. The agents should have proper pH, ionic strength and osmolality, properties that are measured, especially prior to administration to humans (Young *et al*., 1986; Lundqvist and Tolmachev, 2002; Gotthardt *et al*., 2004; Okarvi, 2004; Saha, 2004b).

2.4.1.1. Qualifications for Radio-Peptides

During a disease, the expression pattern of different receptors in pathogenic tissues change, creating several possibilities for targeting, e.g. cell surface receptors on morbid cells (Fischman, 1989; Okarvi, 2004). The ability to pass cell membranes is required when the target is intracellular (Phelps, 2002). Also intracellular retention is essential

when receptor mediated internalization is taken for the advantage of signal amplification. Extracellular degradation or internalization-followed degradation causing excretion will result in a low target-to-background ratio. Intracellular retention is possible for radiometal chelator conjugated amino acids, like ^{68}Ga-DOTA-peptides, which are trapped inside lysosomes and they do not have any transport pathway out of the cells. In addition to radiometal-chelator-conjugated amino acids, also radiolabeled antibody fragments are potential imaging agents (Gotthardt *et al.*, 2004). The properties and special requirements of radio-peptides are discussed below.

When designing a new radio-peptide it is important to choose the right nuclide for labeling, decide how to attach it to the peptide, and then examine the radio-peptide's biological properties, especially, particularly in the *in vivo* stability and the distribution in the body (Lundqvist and Tolmachev, 2002). The common way to label peptides for diagnostics is the attachment of a "foreign" element to the peptide structure by halogenation or by metal ion labeling through a chelator. It is important to select a radionuclide with a suitable half-life, matching with the biokinetics of the peptide and allowing the correct "time window" for PET imaging. Otherwise, selecting a too late or long time window causes a weak signal in the target (the SRA decreases with time) and thus low target-to-background ratios are obtained. On the other hand, if the radioactivity from the blood is incompletely cleared, a late time window must be selected (Lundqvist and Tolmachev, 2002). The half-life of the radionuclide should not be longer than the time window, i.e. the necessary time to complete the study, in order to diminish the radioactivity burden (Saha, 2004b). The proper time window for ^{68}Ga-isotope is immediately after injection, lasting for around 3.5 hours (Lundqvist and Tolmachev, 2002).

The synthesis by attaching a chelator and the radio-labeling of peptides is easy, and peptides tolerate well the harsh synthesis conditions. In many cases, the peptides retain their specific binding after this modification (Lundqvist and Tolmachev, 2002; Okarvi, 2004). The biological properties of peptides are not usually remarkably affected by ^{68}Ga-labeling. The 68-min half-life of ^{68}Ga-isotope is suitable for the biokinetics of most peptides (Lundqvist and Tolmachev, 2002; Reubi and Mäcke, 2008). In general, labeling through a DOTA-chelator is widely used, since the binding between DOTA and a broad range of metallic ions demonstrates sufficient *in vivo* stability (Gotthardt *et al.*, 2004). The main requirements for ^{68}Ga^{3+} chelators are rapid and sufficient linking to the targeting molecule, stability against demetallation in pH 4-8 during preparation and in *in vivo* -circumstances, stability in the presence of serum cations (Ca^{2+}, Zn^{2+}, Mg^{2+}), and the ability to avoid ligand exchange with the blood serum protein transferrin. The ^{68}Ga-chelator-complex should be inert or more stable than the ^{68}Ga^{3+}-transferrin complex in order to not donate ^{68}Ga^{3+} for transferrin, which would result in liver and lung accumulation (Fani *et al.*, 2008).

Many biological properties of radio-peptides are beneficial for imaging due to their relatively small size, compared with the size of traditionally used antibodies in clinical imaging. In general, small lipophilic molecules are diffusible through lipid-containing membranes resulting in fast biokinetics. They penetrate rapidly to tissues, bind quickly to the target, as well as are cleared fast from the blood and non-target tissues. For this

reason a biological half-life, even only a few minutes, may be long enough to allow early imaging acquisition (Fischman, 1989, Lundqvist and Tolmachev, 2002; Gotthardt *et al.*, 2004; Okarvi, 2004; Baum *et al.*, 2008). When the target is intracellular, diffusion through the cell membrane is essential. Although, radio-peptides can be internalized by a receptor-mediated mechanism (Gotthardt *et al.*, 2004), which is not dependent on the lipophilicity.

The properties of peptides can be easily optimized. Native peptides have a high binding affinity and specificity to their targets, but they tend to break down in the blood circulation by peptidases and proteases. For that reason their structure has to be optimized (Okarvi, 2004). The properties of size, charge, polarity and hydrophobicity are modifiable (Fischman, 1989).

Usually radio-peptides are quickly eliminated after transformation, mainly by the liver, to a more hydrophilic form, causing elimination through the kidneys into the urine. The rapid biokinetics allow imaging soon after injection and the use of short-lived isotopes. Large molecules (M > 60 000 g/mol) are not eliminated by the glomerular filtration in the kidney (Saha, 2004b). The solubility can be modified by introducing hydro- or lipophilic amino acids, and in this manner the rate and route of excretion can be affected. Lipophilic peptides are usually cleared by the hepatobiliary route and hydrophilic peptides via the kidneys. The urinary excretion is preferred, because the hepatobiliary excretion causes accumulation of radioactivity in the liver and the guts, leading to an increased background signal in the lower abdomen and complicates the imaging of the targets in the area (Lundqvist and Tolmachev, 2002; Okarvi, 2004). In any case, the faster the excretion is (urinary or fecal), the lower is the radioactivity burden (Saha, 2004b). Radio-labeled peptides are also usually well-tolerated (low toxicity and antigenicity) (Fischman, 1989, Lundqvist and Tolmachev, 2002; Gotthardt *et al.*, 2004; Okarvi, 2004; Saha, 2004b; Baum *et al.*, 2008).

The biological half-life of peptides can be raised in many ways. In order to elevate stability, the peptide sequence can be modified, peptide bonds can be substituted, amino groups can be replaced by imino groups, foreign molecules with familiar structures can be used, the amino- or carboxyl-terminus can be modified and the functional groups can be changed, or it is possible to add appropriate D-amino acids, unusual amino acids or side chains. In addition, cyclization can be used to stiffen the conformational mobility and this way to raise the biological stability, as well as, to enhance the affinity. Also, by changing the radiolabel or the manner how it is attached to the peptide, distribution times of even hours can be achieved. A linker/spacer between the label and binding site, such as polyethyleneglycol (PEG, PEG_3 and PEG_4 etc.), can be used to raise the stability or to avoid the label to interfering with the binding site. Although, modification with a linker may affect also the other biological properties (de Jong *et al.*, 1998; Lundqvist and Tolmachev, 2002, Okarvi, 2004; Autio *et. al.*, 2008).

In practice, it is difficult for an imaging agent to meet all the mentioned criteria and usually established imaging agents are the best of many compromises (Saha, 2004b).

Table 1. Normative Values for Essential Properties of a Good PET Imaging Agent

Property	Target value	Reference
Fast plasma clearance	Mins-hours	Phelps, 2002
High target-to-background ratio	> 1.5	Gulec, 2007
Sufficient amount of targets	B_{max} = 50 000 -1 000 000 / cell	Blankenberg and Strauss, 2002; Agdeppa and Spilker, 2009
High affinity	$K_d \leq 10$ nM *	Blankenberg and Strauss, 2002
Lipophilic [acceptable octanol/buffer partition coefficient (log P or log D **)] or ability to advance a carrier system, when the target is intracellular	Log P = 1 – 2 allows diffusion through the cell membrane	John and Green, 1990; Phelps, 2002; Packard *et al.*, 2002
Low plasma protein binding	A sufficient amount has to be free to bind the target	Young *et al.*, 1986
Fast renal excretion	→ Low radiation dose	Okarvi, 2004; Saha, 2004b
High metabolic stability	Ability to avoid metabolism during the imaging procedure	Green and Welch, 1989
High specific radioactivity	SRA ≥ 100 MBq/nmol resulting in 0.1–10 nmoles per dose ***	Hume *et al.*, 1998; Blankenberg and Strauss, 2002

* K_d is an equilibrium dissociation constant. ** Lipophilicity of uncharged compounds is determined as a ratio of the compound between octanol and water, expressed as partition coefficient (P). Lipophilicity of charged compounds is expressed as distribution coefficient (D), which is determined between octanol and a buffered water solution. The values are given according to practice in logarithmic values. *** SRA is a prerequisite for a tracer dose and depends on B_{max}, K_d and possibly toxicity (Velikyan, 2005).

2.4.2. Development of ^{68}Ga-Labeled Imaging Agents

2.4.2.1. Attachment of ^{68}Ga-Radionuclide

[68]Ga-radionuclide can be attached through *a bifuctional chelator*, which is a ligand able to covalently bind a targeting molecule and a metal cation (Fani *et al.*, 2008). Other possibilities to attach a signaling isotope are an *isotope exchange* reaction, in which one or more atoms of the targeting molecule are replaced by the isotopes of the same element having different mass numbers (e.g. by halogenation), or *direct labeling*, where the imaging agent itself serves as the chelator. The advantage of the isotope exchange reaction is that the chemical and biological properties of the molecule remain the same. Although, in some exceptions the different weight of the surrogate isotope may have an influence on the biological properties (Lundqvist and Tolmachev, 2002; Saha, 2004b; Velikyan, 2005). Direct labeling and attachment through a chelator are used when a radiometal, such as ^{68}Ga, is used for tagging. The attachment of a chelator may affect the binding property and other biological properties, which for that reason must be carefully examined. On the other hand, the synthesis by attaching a chelator and then labeling are usually simple compared to modifying the targeting molecule by changing an isotope in the structure.

Ga^{3+} is attached to a chelator most often with coordination number of 6. During preparation hydrolysis and formation of the $Ga(OH)_3$ can be avoided in the presence of stabilizing weak ligands, such as acetate or citrate (Fani *et al.*, 2008). Available chelators are e.g. DOTA, desferrioxamine-B (DFO), mercapto amino ligands [e.g. triaza triacetic acid (NOTA)], tripodal ligands, triazacyclononane-1-succinic acid-4,7-

diacetic acid (NODASA) and 1-(1-carboxy-3-carbo-*tert*-butoxypropyl)-4,7-(carbo-*tert*-butoxy-methyl)-1,4,7-triazacyclononane (NODAGATOC) (Fani *et al.*, 2008). Also, a linker between the targeting molecule and chelator can be used (See section 2.4.1.1., Qualifications of Radio-Peptides).

2.4.2.2. Pancreatic Cancer and Modeling *In Vivo* Xenografts

Prognosis of pancretic cancer is poor since metastases are often present at the time of diagnosis. In addition, surgery involves a high risk of operative complications and death (Underwood, 2004b). The exocrine pancreas can be investigated by endoscopic retrograde cholangiopancreatography (ERCP), which is an x-ray technique based on imaging agents. The method is invasive and for that reason it involves some risks. In addition to ERCP, the detection of pancretic cancer includes the collection of pancretic juice for examination for enzymes or abnormal cells fuctioning as markers of cancer, and taking biopsies to confirm the findings (Underwood, 2004b). Noninvasive MR, CT, ultrasound and PET are safer techniques for detecting pancretic cancer (Shah and Mortele, 2007).

Solid tumors in the pancreas may originate from the primary pancreatic cell types or metastasis from nonpancretic primary lesions. Primary pancreatic tissue can be subdivided into epithelial and mesenchymal compartments. Epithelial neoplasms include *tumors arising from the exocrine* (*ductal* or acinar) *cells or endocrine* (islet) *cells*. *Ductal adenocarcinoma/pancreatic adenocarcinoma*, which accounts for approximately 85 % of all pancreatic tumors, arises from epithelial cells of the exocrine gland. The other epithelial tumors, as well as tumors originating from mesenchymal cells, are less common (Shah and Mortele, 2007).

Tumors originating in *exocrine pancreas, pancreatic adenocarcinomas* in particular, can be imaged with somatostatin receptors targeting ^{111}*In-DOTA-lanreotide* by SPECT (Baum *et al.*, 2008) and ^{68}*Ga-DOTA-lanreotide* by PET (Mäcke and André, 2007), or with vasoactive intestinal peptide (VIP) receptors targeting ^{123}*I-VIP* and ^{99m}*Tc-VIP* by SPECT (Okarvi, 2004). Lanreotide has proved to be clinically successful in *islet cell tumors* too (Heppeler *et al.*, 2000).

Tumors originating in *exocrine pancreas, pancreatic acinar cells* in particular, express also bombesin receptor subtype 2 (BB2; also called i.e. GRP receptor) and they can thus be imaged with *[^{68}Ga-DOTA]bombesin* (Reubi *et al.*, 2002; Shuhmacher *et al.*, 2005; Mäcke and André, 2007; Jensen *et al.*, 2008).

Neuroendocrine tumors (NETs), including pancreatic endocrine tumors, are a heterogenous group of neoplasms which are characterized by the peptide hormones and growth factors/cytokines that they produce and by histology. ^{68}*Ga-DOTA-TOC* and ^{68}*Ga-DOTA-NOC* targeting somatostatin receptors expressing NETs have been used to a growing extent (Baum *et al.*, 2008). VIP receptor targeting imaging agents can also be used for imaging pancreatic NET (Okarvi, 2004)

Because pancreatic cancer is still one of the most challenging diseases, finding an accurate diagnosis method is the basis for adequate treatment. A xenograft model of

human pancretic adenocarcinoma cells can be used as a model of pancreatic cancer. The *BxPC-3 pancreatic cancer cell line* originates in primary adenocarcinoma, and it is well-characterized and moderately-differentiated (Tan *et al.*, 1986; Sipos *et al.*, 2003). The cell line is capable of forming tumors in athymic mice and rats. The rat BxPC-3 xenograft model has been used for testing imaging agents (Roivainen *et al.*, 2004; Wack *et al.*, 2003; von Forstner *et al.*, 2008).

2.4.2.3. Melanoma and Modeling *In Vivo* Xenografts

Another serious cancer in addition to pancreatic cancer is malignant melanoma. It is the most severe form of skin cancer and the most common one in young adults. The incidence is increasing in western countries. Without early detection, the prognosis is poor. In addition to visual assessment, imaging tecniques of dermoscopy and computed dermoscopy are used for the diagnosis of cutaneous melanoma. Other imaging techniques, such as CT, MRI, SPECT and in particular PET-CT, improve identification of patients suitable for surgical metastectomy. ^{18}F-FDG is the mostly frequently used PET agent for diagnosis and staging, although it has limitations when detecting the melanoma cells, which do not use glucose as an energy source or when the size of the tumors is small. Melanoma-targeting antibodies or antibody fragments have also been developed for imaging (McQuade *et. al.*, 2005, Wei *et. al.*, 2007; Garbe and Eigentler, 2007). Several ^{18}F-labeled PET and ^{123}I-labeled SPECT agents have been examined clinically for the imaging of melanoma.

Melanoma is known to over-express, for instance, melanocortin-1 receptors (MC1R) and MMP-9, which could be suitable targets for imaging purposes. The first ^{68}Ga-DOTA-peptide for imaging melanoma is ^{68}Ga-DOTA-α-melanocyte-stimulating hormone (α-MSH) analogue, ^{68}Ga-DOTA-ReCCMSH(Arg^{11}) targeting MC1R (Wei *et. al.*, 2007).

2.4.2.4. Osteomyelitis and Modeling Bone Infection

The diagnosis of bacterial induced infection of bone, osteomyelitis, is difficult. Osteomyelitis is divided into acute and chronic. The symptoms of osteomyelitis are fever and localized bone pain. For diagnosis, one of the most commonly used imaging techniques is SPECT after injection of technetium(^{99m}Tc)-labeled diphosphonates (i.e. bone scintigraphy), ^{67}Ga-citrate, ^{111}In-labeled WBC or *in vivo* labeled WBC (^{99m}Tc-labeled monoclonal murine M class immunoglobulin, named ^{99m}Tc-Fanolesomab). Also ^{18}F-FDG PET is used (De Winter *et al.*, 2002; Love and Palestro, 2004; Jones-Jackson *et al.*, 2005).

To diagnose especially *acute osteomyelitis*, conventional radiography, SPECT with ^{99m}Tc-labeled diphosphonates or MRI is performed (Peters, 1998). When complicating factors are present incurring false positive findings with MRI and bone scintigraphy, ^{18}F-FDG PET is more suitable. Any form of osteomyelitis can progress to a cronic state. The use of bone scintigraphy in combination with a WBC scan has good clinical accuracy to detect *chronic osteomyelitis* in the peripheral skeleton. The usefulness of

WBC scanning in the central skeleton is low due to presence of bone marrow, which takes up labeled WBC. The problem can be overcome by performing complementary bone marrow imaging with ^{99m}Tc-sulfur colloid. Thus, an all-in-one method ^{18}F-FDG PET is more suitable. The radionuclide procedure of choice for vertebral infections has been ^{99m}Tc-labeled diphophonates SPECT in combination with ^{67}Ga-citrate SPECT. A specific and sensitive all-in-one method for diagnosis of osteomyelitis is warranted (De Winter *et al.*, 2002; Love and Palestro, 2004).

An osteomyelitis model in rats was developed by O'Reilly and Mader (1999) and it was used for the first time for PET imaging by Mäkinen *et al.* (2005). Shortly, the model was developed by drilling a cortical defect into the proximal tibial metaphysic and removing the bone marrow. Sodium morrhuate was injected into the medullary cavity and bacterial inoculum was injected.

2.4.2.5. Biokinetics

The focus in small animal imaging is shifting from detection of the imaging agent uptake and distribution towards the quantitation of the physiological parameters (Dupont *et al.*, 2009). Biokinetics (or kinetics) can be obtained by measuring the radioactivity concentration (concentration of the imaging agent) as a function of time from excised organs *ex vivo*, or by PET imaging *in vivo* from a single animal. Dynamic PET provides a sequence of "snapshot" images of a tissue's radioactivity concentration, allowing the calculation of regional time-activity curves (TACs). Biokinetics describes the alteration in the time course of radioactivity as it travels from the blood to the organ of interest (Laforest *et al.*, 2005). The preclinical imaging is important for validation of new imaging agents before human studies. After the dynamic PET imaging of animals, the correlation between the amount of target and the imaging results is clarified. The amount of the target can be measured with *ex vivo* techniques. The binding potential (BP) values obtained *in vivo* and *ex vivo* are consequently compared.

The uptake and clearance of the imaging agent are influenced by the delivery in the blood to the tissue, by plasma concentration and by the rate of transfer between the plasma and extracellular space, by the rate of transfer across the cell membrane, by the rate of metabolism, by the amount of targeted molecules, receptors or enzymes and by the affinity of binding between the radioligand and the target (Young *et al*, 1986; Meikle *et al.*, 2001). To obtain the physiological parameters of interest from the regional TACs, mathematical modeling of observed biokinetics of the imaging agent is required (Meikle *et al.*, 2001). The aim of kinetic modeling (also called tracer kinetic modeling or simply modeling) is to estimate the physiological parameters obtained from TACs. The modeling requires the measurement of radioactivity in the arterial blood (input function) and in the organ of interest. Arterial blood radioactivity is corrected for radioactive metabolites. In brief, organ TAC is normalized with the cumulative input function (Dupont *et al.*, 2009).

There are five methods to obtain blood input functions in rodent experiments: direct blood sampling, direct measurement of blood activity by a beta-detecting probe, an arterial-venous shunt, image-based factor analysis and region of interest (ROI) analysis of dynamic PET-images. Direct blood sampling is the current reference standard, having the limitations of being invasive and having limited temporal resolution. Factor analysis successfully extracts the blood input function for mice and rats. In this method, the blood input function is derived from dynamic PET-images without the need for drawing ROIs (Laforest *et al.,* 2005). The ROI-based method is less accurate due to the limited image resolution of the PET system, which results in a partial volume effect and spillover. The other mentioned methods are somewhat difficult to use. The measurement of blood input function can be avoided by using reference tissue as the input function, which is a method used in brain research (Meikle *et al.*, 2001). Reference tissue is an organ, which does not have any specific uptake of the imaging agent, but unfortunately there is no reference tissue for many imaging agents.

The models require that the physiological state; including anesthesia, heart rate and blood pressure; should remain constant during imaging. Careful selection of the anesthetic is required to ensure that it does not interfere with the distribution and biokinetics of the imaging agent. The imaging agent used must be well-established and validated, otherwise no conclusions of the biochemical processes can be drawn (Young *et al.*, 1986, Meikle *et al.*, 2001). PET and biokinetic *ex vivo* studies are based on the presumption that the imaging agent, by specific binding, allowes administration as a tracer dose and keeps receptor occupancy virtually unchanged. The tracer dose is usually evaluated by saturation experiments before the biokinetic tests, or directly *in vivo* with a recently introduced small animal imaging technique. This highlights the need for an agent with high specific radioactivity, and results to limitate the amount of radioactivity administered to small animals (Young *et al.*, 1986; Meikle *et al.*, 2001).

PET data can be analyzed visually or on a semiquantitative or quantitative level. Quantitation can be acquired from model calculations. Alternatives are compartment models, spectral analysis, graphical analysis (Logan and Patlak plots), ratios, fractional uptake rate (FUR) and standardized uptake values (SUV). Modeling reversible binding is usually expressed as BP, which reflects both the densities of receptors or transporters (B_{max}) and equilibrium dissociation constant (KD), which are traditionally found by *in vitro* radioligand assays; in theory, $BP=B_{max}/K_d$ (Mintun *et al.*, 1984). Ligands that have low K_d dissociate slowly and have high affinity (Ichice *et al*., 2001).

Biokinetic *ex vivo* studies in healthy small animals represent quantitation on a semiquantitative level, where results are expressed as SUV, target-to-nontarget ratios, or as percent of injected dose per gram of tissue (%ID/g). After a bolus injection, radioligands reach a relatively steady state after a certain time according to the organ in question. In healthy subjects the nonspecific accumulation can be studied.

Similar models for animals and humans can be used in many cases (Dupont *et al.*, 2009). The described new modeling and noninvasive blood input function techniques will enable the *in vivo* obtaining of the basic parameters (see above) for potential imaging agents or offer information on the target function.

2.5. Why to Use ^{68}Ga-Based PET?

The production of PET isotopes by using a [68]Ge/^{68}Ga-generetor is attractive for several reasons: i) The PET radionuclide is continuously available at a reasonable cost from a generator, including centers without a cyclotron, ii) the half-life of 270.8 days of the parent nuclide allows the use of the generator for a long period, up to 1 year or longer, iii) the 68-min half-life of ^{68}Ga matches the biokinetics of many molecules (e.g. peptides) owing to their relatively small size (Breeman and Verbruggen, 2007; Reubi and Mäcke, 2008), and iv) ^{68}Ga-chemistry by using chelator-conjugated molecules is simple (Lundqvist and Tolmachev, 2002).

[68]Ga has a sufficiently long half-life to allow for chemical manipulation in imaging agent development (Hnatowich, 1977). The application of ^{68}Ga-labeled peptides has attracted much attention because of the availability of the cost-effective generator and the simple chemistry. Furthermore, ^{68}Ga-labeling of kit formulations could be convenient in clinical use analogous to ^{111}In and ^{99m}Tc kits, which have been on the market for decades (Baum *et al.*, 2008). Additionally, after diagnosis with a chelator conjugated and accordingly ^{68}Ga-labeled molecule, the same molecule can be labeled with another isotope [e.g. yttrium-90 (^{90}Y), Lutetium-177 (^{177}Lu)], and used for peptide receptor radionuclide therapy. This is possible because many chelators are able to bind different metal nuclides (Pool *et al*., 2010).

The disadvantages of ^{68}Ga are the breakthrough of other metal ion impurities from the [68]Ge/^{68}Ga-generator, low SRA of many ^{68}Ga-labeled molecules and the relatively high positron energy of [68]Ga ($E\beta$+max 1.9 MeV). The impurities in the ^{68}Ga-eluate may complicate the labeling and thus reduce the SRA (Velikyan, 2005). In any case, since to my knowledge, there are no available [68]Ge/^{68}Ga-generators of GMP-quality in the markets, the purification may be needed anyway to abolish even minor metal impurities prior to administration to humans (Breeman and Verbruggen, 2007). [68]Ga possess higher positron energy compared to ^{18}F, which is almost an ideal PET nuclide. The positrons emitted from ^{68}Ga travel a longer distance before annihilation, and this decreases the spatial resolution. Although, it has been reported that practically ^{68}Ga-based PET and ^{18}F-based PET have no remarkable difference in clinical imaging (Sanchez-Crespo, *et al.*, 2004; Lundqvist and Tolmachev, 2002).

Clinicians have reported the advantages of ^{68}Ga-labeled imaging agents in diagnosis. On the other hand, there are already SPECT facilities in many hospitals and therefore SPECT may be the cheapest choice at the moment. The breakthrough of new technologies does not occur immediately. Work and patience are needed to develop the best possible technology.

3. OBJECTIVES OF THE STUDY

The main objective was to study new agents, ^{68}Ga-chloride targeting tumors, ^{68}Ga-labeled peptide targeting inflammation expressing vascular adhesion protein 1 (VAP-1) and ^{68}Ga-labeled tumor cell targeting peptides (TCTPs) for PET imaging.

The specific aims were:

1) To study the properties of generator produced ^{68}Ga-based PET imaging agents *in vitro*

2) Evaluate new ^{68}Ga-based imaging agents for inflammation and cancer in *in vivo* models

4. METHODS

4.1. Synthesis of Potential Tumor or Inflammation Targeting Peptides

Peptides were synthesized using standard chemistry and a 9-fluorenylmethoxycarbonyl (fmoc)-strategy. The 4th carboxyl group of DOTA-chelator was used to form a stable amide bond between the DOTA and the peptide. Linear peptide targeting VAP-1 was composed of nine amino acids (Gly-Gly-Gly-Gly-Lys-Gly-Gly-Gly-Gly), attached to DOTA with a linker and named as *DOTAVAP-P1* (Paper II). Linear peptide, composed of nine amino acids in a random amino acid sequence (Pro-His-Glu-Pro-Thr-Tyr-Pro-Asp-Phe) and attached to DOTA, was used as a negative control for DOTAVAP-P1. Also three DOTA-conjugated tumor cell targeting peptides TCTPs (*DOTA-TCTPs*) were synthesized (Paper III):

- DOTA-TCTP-1, (Cys3-10; H-Gly-Ala-Cys-Leu-Arg-Ser-Gly-Arg-Gly-Cys-Gly-(3,6-dioxaoctane-1,8-diamine)-DOTA),
- DOTA-lactam-TCTP-1 [Glu^8-Ala^1 5.8-2.1 lactam; D-Ala-Leu-Arg-Ser-Gly-Arg-Gly-Glu-(11-amino-3,6,9-trioxaundecanoyl)-δ-D-Orn(2-N-DOTA)-NH$_2$] and
- DOTA-lin-TCTP-1 (Gly-Ala-Ala-Leu-Arg-Ser-Gly-Arg-Gly-Ala-Gly-(3,6-dioxaoctane-1,8-diamine)-NH-DOTA) (Section 4.2, Fig. 3).

The six amino acid motif (Leu-Arg-Ser-Gly-Arg-Gly) is essential for the selective binding of DOTA-TCTPs. The first of the TCTPs was the original cyclic peptide and the others were a cyclic and a linear modification. Polyethylene glycol, triethylene glycol [PEG(3)] inparticular, was used as a linker.

The peptides were purified using high-performance liquid chromatography (HPLC). The identities of the peptides were verified with a mass spectrometry. Detailed descriptions can be found from the original papers (II and III).

4.2. Preparation of ^{68}Ga-Based Imaging Agents

For the preparation of ^{68}Ga-chloride (GaCl$_3$, Table 3), ^{68}Ga was obtained from a TiO$_2$-based ^{68}Ge/^{68}Ga-generator (Cyclotron Co., Obninsk, Russia) by elution with 0.1 M HCl. Elution of the ^{68}Ge/^{68}Ga generator was monitored on-line with a positron sensitive photodiode detector (Hamamatsu S5591, Hamamatsu Photonics K.K. Solid State Division, Hamamatsu City, Japan). The radioactive elution peak was collected and thereafter neutralized with 1.0 M NaOH (Paper I) or used for the ^{68}Ga-labeling of peptides (Papers II and III).

^{18}F-FDG and ^{11}C-choline were prepared as described earlier (Hamacher *et al*., 1986; Roivainen *et al*., 2000). ^{18}F-FDG (Paper I and II) and ^{11}C-choline (unpublished data) were used as positive controls.

To ^{68}Ga-label the DOTA-peptides, 0.5 mL of ^{68}GaCl$_3$ was mixed with sodium acetate (18 mg; Sigma-Aldrich Chemie, Germany). 30 nmol of peptide (except 65 nmol in the case of the negative control peptide for DOTAVAP-P1) was added. The reaction mixture was incubated at 100°C for 20 min, 90°C for 10 min or 95°C for 25

min when labeling DOTAVAP-P1, the negative control peptide for DOTAVAP-P1 or TCTPs, respectively (Table 3). TCTP-1 without a DOTA-chelator was used as a negative labeling control for TCTPs. No further purification was needed. The radiochemical purity was determined by radio-HPLC with a reversed-phase column (μBondapak C_{18}, 7.8 × 300 mm, pore size 125 Å, 10 μm; Waters Corporation, Milford, MA, USA) (Table 2). The radio-HPLC system consisted of LaChrom instruments (Hitachi; Merck Darmstadt, Germany), including a pump L7100, UV detector L-7400 and interface D-7000; an on-line radioisotope detector (Radiomatic 150 TR, Flow Scintillation Analyzer; Packard, Meriden, CT, USA) and a computerized data acquisition system. The quantity of ^{68}Ga-radioactivity retained on the column was controlled.

Table 2. The A/B/C gradients for HPLC when checking the purity of ^{68}Ga-labeled peptides. The flow rate was 6 mL/min and λ = 215 nm. For DOTAVAP-P1 and its negative control peptide A = water, B = acetonitrile and C = 50 mM phosphoric acid. For ^{68}Ga-DOTA-TCTPs, A = 50 mM phosphoric acid, B = 50 mM ammonium acetate/acetonitrile 1:1, C = 50 mM ammonium acetate.

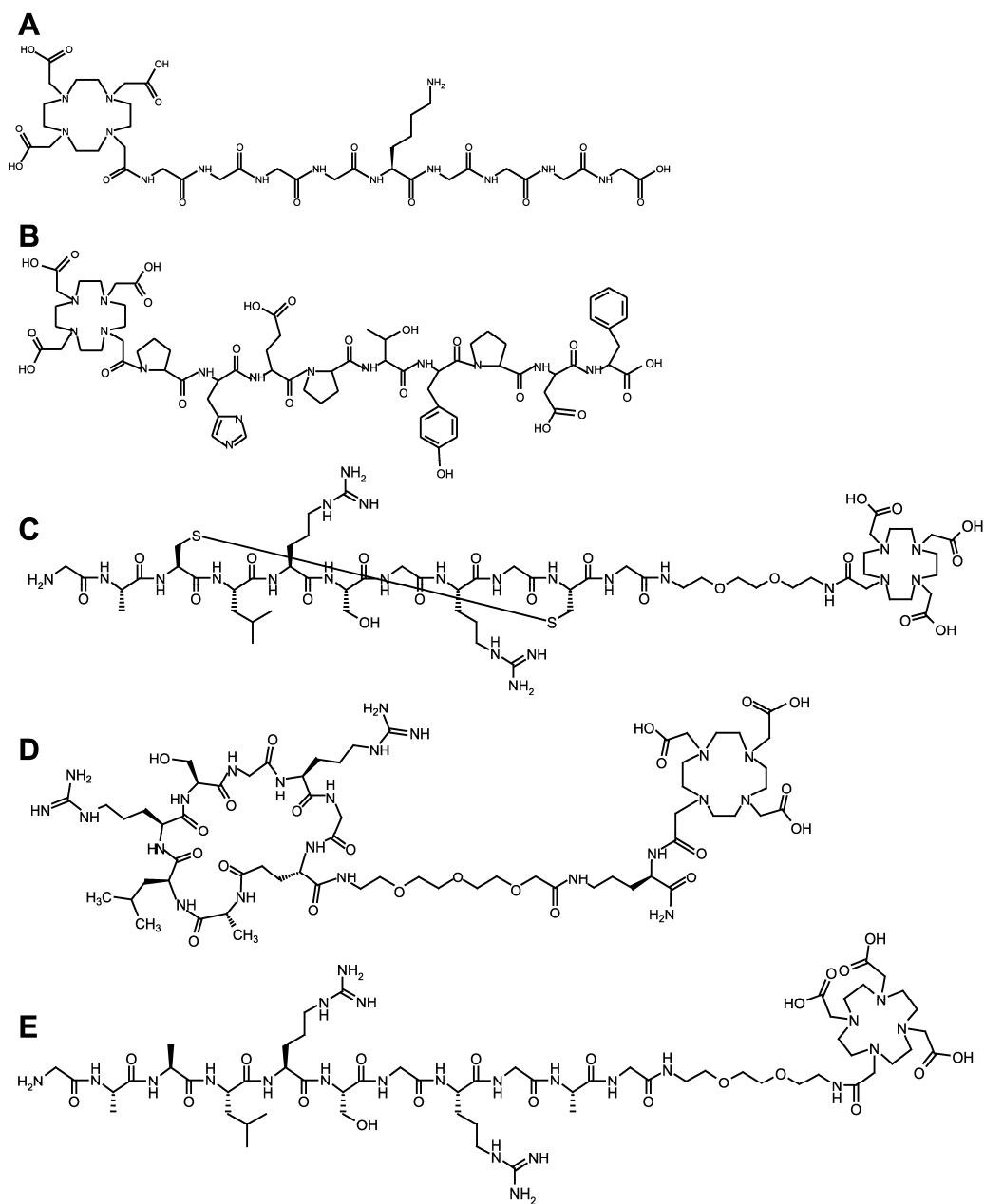| ^{68}Ga-DOTAVAP-P1		The negative control peptide for ^{68}Ga-DOTAVAP-P1		^{68}Ga-DOTA-TCTPs	
0-5 min	100/0/0	0-3 min	100/0/0	0-3 min	0/15/85
5-6 min	100/0/0 → 0/0/100	3-4 min	100/0/0 → 50/50/0	3-4 min	0/30/70
6-10 min	0/0/100	4-7 min	50/50/0	4-5 min	0/60/40
		7-8 min	50/50/0 → 0/0/100	5-8 min	0/70/30
		8-15 min	0/0/100	9-13 min	100/0/0

Figure 3. Structural formulas of the studied peptides. A) DOTAVAP-P1, B) the negative control peptide for DOTAVAP-P1, C) DOTA-TCTP-1, D) DOTA-lactam-TCTP-1 and E) DOTA-lin-TCTP-1.

Table 3. Characteristics of the DOTA-chelator and prepared ^{68}Ga-based imaging agents.

	Linker	Molecular Weight (g/mol)	Formula
DOTA	-	404.42	$C_{16}H_{28}N_4O_8$
^{68}Ga (administered as ^{68}Ga-chloride)	-	69.72	$^{68}Ga^{3+}$
DOTAVAP-P1	-	989.011	$C_{38}H_{64}N_{14}O_{17}$
Negative control peptide for DOTAVAP-P1	-	1488.6	$C_{68}H_{93}N_{15}O_{23}$
DOTA-TCTP-1	Gly+polyethyleneglycol [PEG(3)]; chain length 12 atoms	1550.79	$C_{60}H_{107}N_{23}O_{21}S_2$
DOTA-lactam-TCTP-1	PEG(3)+Orn; chain length 15 atoms	1514.79	$C_{62}H_{110}N_{22}O_{22}$
DOTA-lin-TCTP-1	Gly+PEG(3)	1488.8	$C_{60}H_{109}N_{23}O_{21}$

4.3. *In Vitro* Evaluation

4.3.1. Competitive Enzyme Assay

To examine whether DOTA modification would affect the inhibitory potency of VAP-P1 (Paper II), competitive enzyme assays were performed with phenylmethanamine (benzylamine), which is the preferred test substrate for VAP-1/SSAO (Salmi *et al.*, 2001). Chinese hamster ovary (CHO) cells, stably transfected with full-length human VAP-1 cDNA in pcDNA3 vector (Smith *et al.*, 1998), and human serum samples from healthy volunteers were used as sources of VAP-1/SSAO. Amine oxidase activity was assayed radiochemically using 7-^{14}C-benzylamine hydrochloride (Amersham, UK) as a tracer substrate as described earlier (Salmi *et al.*, 2001). In brief, human serum or sonicated CHO-VAP-1 lysates were preincubated 30 min with various concentrations of DOTAVAP-P1 or VAP-1/SSAO inhibitor, and semicarbazide prior to the addition of ^{14}C-benzylamine. VAP-1 converts ^{14}C-benzylamine to ^{14}C-benzaldehyde and hydrogen peroxide. The aldehydes were extracted using a toluene-containing mixture and the formation of ^{14}C-benzaldehyde was quantified by scintillation counting. The test was repeated twice. (For more details see original Paper II).

4.3.2. Lipophilicity Test

The lipophilicity of ^{68}Ga-DOTAVAP-P1 (Paper II) and ^{68}Ga-DOTA-TCTP-1 (Paper III) was determined using the following procedure: Approximately 5 kBq of ^{68}Ga-DOTAVAP-P1 in 500 µl of phosphate buffered saline (PBS) pH 7.4 was added to 500 µl of 1-octanol. After being vortexed for 3 min, the mixture was centrifuged at 12,000 g for 6 min and 100-µl aliquots of both layers were counted in an automatic

gamma counter cross-calibrated with a dose calibrator (VDC-202, Veenstra Instruments, Joure, Netherlands) (1480 Wizard 3" Gamma Counter; EG & G Wallac, Turku, Finland) (n=4 for ^{68}Ga-DOTAVAP-P1 and n=8 for ^{68}Ga-DOTA-TCTP-1). The lipophilicity was given as a distribution coefficient (D), which is given according to practise in logarithmic value (log D).

4.3.3. Testing of Cells

Suspensions of approximately 10^7 VAP-1 transfected CHO-cells and their mock transfected controls (CHO-cells transfected with the vector only) (Smith *et al.*, 1998) were incubated in a culture medium with 5 MBq (250 μL) of ^{68}Ga-DOTAVAP-P1 at +37°C (Paper II). After 20 min, cells were harvested from the culture dishes by treatment with trypsin, and resuspended in a fresh medium. The cells were collected by centrifugation and washed three times with 1 mL of cold phosphate buffered saline (PBS). The supernatant was removed and the cellular binding of radioactivity was measured using a gamma counter (1480 Wizard 3" Gamma Counter), and corrected by the number of viable cells calculated under the microscope after the incubation experiment. The test was repeated five times.

4.3.4. *In Vitro* Tests for Stability and Binding to Plasma Proteins

The *in vitro* stability of the ^{68}Ga-DOTA-peptides was tested during a 4 h incubation i) in physiological saline, ii) in rat plasma (^{68}Ga-DOTAVAP-P1) and iii) in human plasma at RT or 37°C. Plasma proteins were precipitated with acetonitrile, centrifuged at 3,900 *g* for 5 min at 4°C and removed before the radio-HPLC analyses.

Protein binding of ^{68}Ga-DOTA-TCTP-1 was tested *in vitro* in human plasma (n=4) during a 2 h incubation. Plasma proteins were precipitated with acetonitrile, centrifuged, and the radioactivity in the supernatant and sediment were measured using a well-type gamma counter (Bicron, Newbury, OH). The percentages of radioactivity bound to plasma proteins were calculated thereafter.

4.4. *In Vivo* and *Ex Vivo* Evaluation

4.4.1. Animal Models

Three different animal models were used: Human pancreatic ductal adenocarcinoma cell (BxPC-3) xenografts in rats (Paper I), human melanoma (C8161T/M1) xenografts in rats (Paper III) and osteomyelitic rats (Paper II). Also healthy rats were used to study biodistribution to non-target organs (Paper II). All animal care and experiments were approved by the Lab-Animal Care & Use Committee of the University of Turku and carried out in compliance with the Finnish laws relating to the conduct of animal experimentation. The animals were allowed food and water *ad libitum* and they were kept in the Central Animal Laboratory of the University of Turku.

The animals were anesthetized before the experiments with sodium pentobarbital (Mebunat, Orion, Finland), with a mixture of fentanyl citrate plus fluanisone (Hypnorm® = fentanyl citrate 0.315 mg/mL and fluanisone 10 mg/mL, Janssen Pharmaceutica, Beerse, Belgium) and midazolam (Dormicum 5 mg/mL, Roche, Espoo, Finland/Midazolam Hameln 5 mg/mL, Hameln Pharmaceuticals GmbH, Hameln, Germany), or with isoflurane inhalation (Isofluran Baxter®, Baxter Oy, Helsinki, Finland) (Papers II and III). (See more details from the original papers). Prior to the injection of the tested imaging agents, the rats fasted for at least 2 h.

4.4.1.1. Xenografts in Rats

Athymic male Hsd:RH-rnu/rnu rats were obtained from Harlan (The Netherlands) at the age of 6 weeks. Due to immunodeficiency, the rats needed special filter-top cages. To develop a pancreatic cancer xenograft model a human BxPC-3 cell line was purchased from the American Type Culture Collection (Rockville, MD). Also, a melanoma xenograft model, capable of over-expressing MMP-9, was developed for testing ^{68}Ga-DOTA-TCTPs targeting MMP-9 (Paper III). A C8161T/M1 cell line was established from the human cutaneous malignant melanoma cell line, C8161 (Welch *et al.*, 1991), by growing the cells in mice. C8161T/M1 represents a highly invasive subpopulation of the original cell line, isolated from a lung metastatic tumor (Karyon-CTT Ltd, Helsinki, Finland). The BxPC-3 cells were grown in a RPMI 1640 culture medium and C8161T/M1 cells in a DMEM medium. The medium was supplemented (10 %) with heat-inactivated fetal bovine serum (iFBS), 2 mM L-glutamine, 100 U/mL penicillin and streptomycin (100 µg/mL) in a humidified atmosphere of 5 % CO_2 at 37°. The cells were detached from the culture bottle by trypsin-EDTA and resuspended in a medium for implantation.

Tumor cells (1-50 x 10^6 / rat) were injected subcutaneously into the neck. The time for tumor growth was based on different criteria. All BxPC-3 tumors were allowed to grow to a similar size of 1 cm in diameter, whereas the effect of different time periods for tumor growth was tested in 1-6 -week old C8161T/M1 tumors.

4.4.1.2. Osteomyelitic Rats

The bones of the hind legs (tibias) of Sprague-Dawley rats were operated to induce an infection that would express VAP-1. The unoperated contralateral leg served as the negative control. The osteomyelitis was allowed to develop for 2 weeks before the experiments. Briefly, the induction of deep bone infection was accomplished by injecting 0.05 mL of 5 % wt/vol of sodium morrhuate (Scleromate™, Glenwood, Englewood, N.J) and a bacterial inoculum in a 0.05 mL volume (3×10^8 colony-forming units/mL of *Staphylococcus aureus*, strain 52/52A/80) into the medullary cavity (O'Reilly and Mader, 1999).

4.4.2. *In Vivo* and *Ex Vivo* Tests for Stability and Binding to Plasma Proteins

The *in vivo* stability of ^{68}Ga-DOTA-peptides in plasma, urine and the tumor were studied. 24 ± 7 MBq (36 ± 7.9 µg, 36 ± 8.0 nmol) of ^{68}Ga-DOTAVAP-P1 was i.v. administered to healthy mature Sprague-Dawley rats (weight 280 ± 69 g; 12 male, 12 female). The radio-peptide was allowed to circulate and samples of blood and urine were collected during 2 h (15, 30, 60 and 120 min) p.i. The rats were terminated by intracardiac sodium pentobarbital (Mebunat®, Orion, Finland). Proteins were separated by Microcon YM-30 filters (Microcon, Pori, Finland) at RT from the plasma, which remained after centrifugation (n=5-6 for each time point), and the urine (n=4 for each time point). The filtrates were analyzed by radio-HPLC as described above (Section 4.2).

In vivo plasma stability and *ex vivo* stability in urine and tumor tissue of ^{68}Ga-DOTA-TCTPs was tested in athymic male Hsd:RH-rnu/rnu Harlan rats (9 healthy and 9 tumor-bearing) anesthetized with isoflurane inhalation (Isofluran Baxter®, Baxter Oy, Helsinki, Finland). The rats were i.v. administered with 32 ± 14 MBq of ^{68}Ga-DOTA-TCTP-1 (n=9), ^{68}Ga-DOTA-lactam-TCTP-1 (n=6), or ^{68}Ga-DOTA-lin-TCTP-1 (n=3). (Dose contained all of the peptide used for labeling, i.e. 30 nmol, which is approx. 40-50 µg depending on the molecular mass of the peptide in question). Plasma, urine and tumor samples were taken up to 2 h (15, 30, 60 and 120 min) p.i. Tumor samples were homogenized (Ultra–Turrax T8 homogenizer; IKA® Werke GmbH & Co. KG, Staufen, Germany) in acetonitrile, centrifuged and filtered through a 0.45 µm Acrodisc syringe filter (Waters Corporation, Milford, MA, USA). For all tissue samples, plasma proteins were precipitated and supernatants were analyzed with radio-HPLC, as described above (Section 4.2).

The protein binding of ^{68}Ga-DOTA-VAP-P1 was tested in rat circulation (n=1) 30 min p.i. The samples were handled as described above (Section 4.3.4.). The radioactivity bound to blood cells (blood-plasma ratio of radioactivity) and percentage of radioactivity bound to plasma proteins were calculated thereafter.

4.4.3. PET Imaging

Two hours of dynamic PET imaging was performed to detect and quantify distribution and biokinetics in the target (tumor or infection) and major organs. PET was performed either with a GE Advance scanner (General Electric Healthcare, Milwaukee, WI) (DeGrado *et al.*, 1994) or with a high-resolution research tomography (HRRT) camera, designed for human brain and small animal imaging (Siemens Medical Solutions, Knoxville, TN) (Table 4) (Wienhard *et al.*, 2002). The rats were placed in the centre of the scanner gantry to obtain the best resolution for small objects, and kept on a warm pallet during the procedure. After the transmission scan for attenuation correction, 19 rats (weight 336 ± 50 g) bearing BxPC-3 pancreatic cancer tumors received a ^{68}Ga-chloride, ^{18}F-FDG or ^{11}C-choline intravenous (i.v.) bolus

injection via a tail vein (Table 4). ^{68}Ga-DOTAVAP-P1 or ^{68}Ga-labeled negative control peptides for ^{68}Ga-DOTAVAP-P1 were injected into 6 rats having osteomyelitis or into 12 healthy rats (280 ± 40 g) (Table 4). Twelve melanoma tumors bearing rats (234 ± 20 g) were inoculated with C8161T/M1 cells 1-2 weeks (1 week *n*=8, 2 weeks *n*=4) prior to the injection of ^{68}Ga-DOTA-TCTPs and imaging (Table 4). The imaging started at the time of the injection. Some of the rats were imaged with multiple imaging agents on subsequent days (Papers I and II). At least 6 half-lives of nuclides separated the imaging of 2 agents.

The data acquired were iteratively reconstructed with the ordered-subsets expectation maximization three-dimensional algorithm (OS-EM3D). The imaging agent uptake was analyzed semi-quantitatively by drawing circular ROI in the tumor, osteomyelitic foci, heart, kidney, liver, lung or urinary bladder areas. The average radioactivity concentration in ROI (kBq/mL) was used for further analyses. The uptake was reported as standardized uptake value (SUV, the radioactivity of the ROI divided by the relative injected dose expressed per animal body weight). The images were reviewed on the computer screen in the transaxial, coronal, and sagittal planes. In addition, uptake ratios (target-to-background) were calculated thereafter. Biokinetic curves / time-activity curves (TAC), representing the relative radioactivity concentration in the organ of interest (kBq/mL or SUV) versus time after injection, were determined accordingly. The TACs were decay corrected to the time of injection.

Table 4. Two hour dynamic PET imaging. For more details see the original papers.

Study	Camera	Imaging agent	Rat model	*n* (experiments)	Dose	Anesthetic
I	Advance, HRRT	^{68}Ga-Chloride	Human pancreatic cancer xenograft (BxPC-3 cells)	13	16 ± 3 MBq	Mebunat, an anaesthetic mixture*
	- " -	^{18}F-FDG	- " -	11	16 ± 9 MBq	- " -
Unpub-lished data	- " -	^{11}C-Choline	- " -	10	86 ± 28 MBq	- " -
II	Advance, HRRT	^{68}Ga-DOTAVAP-P1	Healthy (Sprague-Dawley)	12 (1:1 ♂ and ♀)	29 ± 3 MBq, 43 ± 4.9 µg, 43 ± 4.9 nmol	an anaesthetic mixture
	- " -	- " -	Osteomyelitis	16	22 ± 4 MBq, 15 ± 10 µg, 16 ± 10 nmol	an anaesthetic mixture, isoflurane
	- " -	^{18}F-FDG	- " -	2	29 ± 0.3 MBq	an anaesthetic mixture
	- " -	^{68}Ga-labeled negative control peptide for ^{68}Ga-DOTAVAP-P1	- " -	4	20 ± 1 MBq, 55 ± 12 µg, 83 ± 18 nmol	- " -
III	HRRT	^{68}Ga-DOTA-TCTP-1	Human melanoma xenograft (C8161T/M1 cells)	6	19±3.0 MBq, ≈47 µg, ≈30 nmol**	- " -
	- " -	^{68}Ga-DOTA-lactam- TCTP-1	- " -	3	18±0.5 MBq, ≈45 µg, ≈30 nmol**	- " -
	- " -	^{68}Ga-DOTA-lin-TCTP-1	- " -	3	18±0.9 MBq, ≈45 µg, ≈30 nmol**	- " -

*An anaesthetic mixture of fentanyl citrate plus fluanisone and midazolam. **Dose contained all of the peptide used for labeling, i.e. approx. 30 nmol.

4.4.3.1. Competitive Binding with PET

Competitive imaging experiments were performed to show that the uptake of imaging agents was due to specific accumulation. First the rats were imaged normally p.i. of the imaging agent, and thereafter the imaging procedure was replicated in the presence of competitive ligands. Experiments were performed along with ^{68}Ga-DOTAVAP-P1 and 1) aminourea hydrochloride (Semicarbazide hydrochloride; Sigma-Aldrich Chemie GmbH, Steinheim, Germany), which is an inhibitor of VAP-1/SSAO,

or 2) unlabeled DOTAVAP-P1. Three rats were first imaged with ^{68}Ga-DOTAVAP-P1 alone, and after six half-lives of ^{68}Ga with ^{68}Ga-DOTAVAP-P1 plus 900-fold molar excess of semicarbazide (for more details see the original paper). Semicarbazide was injected i.v. 10 min before the ^{68}Ga-DOTAVAP-P1 injection. Analogously, three rats were first imaged with ^{68}Ga-DOTAVAP-P1 alone and then with ^{68}Ga-DOTAVAP-P1 plus a 700-fold molar excess of unlabeled DOTAVAP-P1.

4.4.4. *Ex Vivo* Biodistribution Studies

The findings measured by PET were confirmed by *ex vivo* experiments. *Ex vivo* experiments were performed immediately after PET imaging, or without prior PET recording. The rats were kept on a warm pallet. Tumor bearing rats (BxPC-3 tumor bearing rats weighted 280 ± 69 g and C8161T/M1 tumor bearing rats 263 ± 30 g) or healthy rats (280 ± 69 g) were i.v. injected with ^{68}Ga-based imaging agents (Table 5). ^{68}Ga-chloride and ^{18}F-FDG was studied at 90 min p.i. and ^{11}C-choline at 10 min p.i. The time point for each agent was selected based on the steady state in the target tissue and optimal tumor-to-muscle ratio measured by PET. In the case of ^{11}C-choline a short time point was selected, since ^{11}C-choline is rapidly metabolized *in vivo* (Roivainen *et al*., 2000). After a certain blood circulation time, the rats were terminated in the selected time-points by intracardiac sodium pentobarbital (Mebunat[®], Orion, Finland) and samples of the blood, urine (p.i. of ^{68}Ga-DOTAVAP-P1 in Paper II), tumor (p.i. of ^{68}Ga-chloride and ^{68}Ga-DOTA-TCTPs in Papers I and III, respectively) and various organs were excised, weighed, and measured for radioactivity in a gamma counter (1480 Wizard 3" Gamma Counter). The radioactivity concentration was decay corrected to the time of injection. The results were presented as SUV (organ radioactivity/organ weight) / (total given radioactivity/rat body weight), %ID/g (percentage of injected dose per gram of tissue) or target-to-background ratios.

Table 5. *Ex vivo* **Biodistribution Studies.**

Study	^{68}Ga-Based Imaging Agent	Blood Circulation Time	Rat Model	*n* (animals)	Dose	Anesthetic
I	^{68}Ga-Chloride	90 min	Human pancreatic cancer xenografts (BxPC-3 cells)	4	12±3 MBq	an anaesthetic mixture*
	^{18}F-FDG	90 min	- " -	4	15±3 MBq	- " -
Unpub-lished data	^{11}C-Choline	10 min	- " -	4	151±71 MBq	- " -
II	^{68}Ga-DOTAVAP-P1	15, 30, 60 and 120 min	Healthy (Sprague-Dawley)	6/time point (1:1 ♂ and ♀)	24±7 MBq, 36±7.9 µg, 36±8.0 nmol	- " -
III	^{68}Ga-DOTA-TCTP-1	2, 30, 60 and 120 min	Human melanoma xenografts (C8161T/M1 cells)	27	15±2.6 MBq**	- " -
	^{68}Ga-DOTA-lactam- TCTP-1	120 min	- " -	3	18±0.9 MBq**	- " -
	^{68}Ga-DOTA-lin-TCTP-1	120 min	- " -	3	18±0.5 MBq**	- " -

*An anaesthetic mixture of fentanyl citrate plus fluanisone and midazolam. **This dose contained all of the peptide used for labeling, i.e. 30 nmol (approx. 40-50 µg, depending on the peptide in question).

4.4.5. Targeting at the Microscopical Level and Target Validation

4.4.5.1. Autoradiography Combined with Histological Examination

Tumor targeting of ^{68}Ga-chloride was studied in more detail with an autoradiography of the tumor samples and by following histological and immunohistochemical staining. The rats (weight 238 ± 34 g) were injected with 19 MBq of ^{68}Ga-chloride and for comparison with 24 MBq or 252 MBq of ^{18}F-FDG (Paper I) or ^{11}C-choline (unpublished data), respectively (*n*=1 for each tracer). After the distribution of the imaging agent (90 min for ^{68}Ga-chloride and ^{18}F-FDG, 10 min for ^{11}C-choline) the tumors were excised, frozen in dry ice and cut with a cryomicrotome into 10-20 µm sections. The tumor sections were thaw-mounted onto microscope slides, briefly air-dried and exposed to an imaging plate (Fujifilm BAS TR, Fuji Photo Film Co, Japan) for 2 half-lives of the radioisotope in question. The

distribution of the radioactivity in the sections was digitally scanned using a Fuji BAS-5000 device (Fuji Tokyo, Japan) with an image resolution of 25 μm.

To obtain the corresponding histological information for the distribution of radioactivity, the same sections were stained with hematoxylin and eosin (HE), or using an immunohistochemical method for light microscopy. In addition, some tumor samples were fixed with 4 % formaldehyde, embedded in paraffin, cut into 10 μm sections and stained with HE. For immunohistochemical staining, the DakoCytomation EnVision-system-HRP (K4001, Dako, Glostrup, Denmark) two-step immunohistochemical technique was used.

After ^{68}Ga-chloride autoradiography, the sections were stained with mouse anti-rat CD68 monoclonal antibody (MCA341GA; AbD Serotec, Oxford, UK; optimal dilution 1:2000) to examine if the radioactivity originates from macrophage uptake. The antibody was located with 3,3'-diaminobenzidine tetrahydrochloride (Liquid DAB Substrate, K3468; Dako, Glostrup, Denmark).

The digital autoradiographs were combined with digital histological and immunohistological images using GIMP 2.4.5 (GNU Image Manipulation Program, authored by Peter Mattis and Spencer Kimball; http://www.gimp.org/) and Hugin 0.7 beta 3 hugin (Hugin, authored by Andrew Mihal, Pablo d'Angelo, Max Lyons, Erik Krause, Konstantin Rotkvich and Christoph Spiel; http://hugin.sourceforge.net/) softwares.

4.4.5.2. Microbiological and Histological Analysis of Osteomyelitic Bones

The presence of osteomyelitis was confirmed as previously described (Lankinen *et al.*, 2008; Mäkinen *et al.*, 2005) (Paper II). Using sterile techniques the rat tibia was harvested, the bone defect area was cross-sectioned and quantitative bacterial analysis of the section performed.

To confirm the expression of VAP-1, bone tissue samples from osteomyelitic rats were decalcified, paraffin embedded and stained using an immunohistochemical method. The polyclonal rabbit antiserum used in immunoperoxidase stainings was raised against recombinant human VAP-1, but it recognizes well rat VAP-1 also. The staining of the paraffin sections was done with this primary antibody, followed by peroxidase-conjugated anti-rabbit Ig as the secondary antibody, using the Vectastain kit (Vector Laboratories, Inc., Burlingame, CA) according to the manufacturer's instructions. Normal rabbit serum was used as a negative control. The sections were counter-stained with Mayer's hematoxylin.

4.4.5.3. Zymography and Histology of Melanoma Tumors

For the determination of MMP-9 expression levels, the melanoma xenografts (*n*=39) were examined after different growth times (2–4 weeks) (Paper III). The tumor samples were weighed and homogenized in a lysis buffer (10 mM Tris-HCl pH 7.4, 10 mM NaCl, 3 mM MgCl$_2$, 1 % Triton X-100). The protein concentrations of lysates were determined using the Bradford method. Equal amounts of proteins were loaded

on zymogram gels (Bio-Rad). The samples were separated at 30 mA for 15 min and 15 mA for 2 h. The gel was incubated in a renaturation buffer (0.25 % Triton X-100) for 1 h and in a development buffer (5 mM Tris-HCl pH 7.4, 20 mM NaCl, 0.5 mM CaCl$_2$, 0.002 % Triton X-100) at + 37°C overnight. The gel was stained with PageBlue Protein Staining Solution (Fermentas, Helsinki, Finland) for 1 h and destained in milli-Q H$_2$O. Recombinant human MMP-9 (R&D Systems, MN, USA) was used as a positive control. For the quantification of MMP-9, the digital images of the gels were scanned and analyzed using the ImageJ software (National Institute of Mental Health, Bethesda, MD, USA).

To confirm the expression of MMP-9 in the tumor tissue MMP-9 immunohistochemistry of melanoma xenografts were performed. The tumors after different periods for tumor growth were dissected from the rats and fixed in 10 % paraformaldehyde. The samples were embedded in paraffin and sectioned with a microtome in 5 or 7 µm sections, and put on slides. The slides were de-paraffinized and stained with the anti-MMP-9 antibody (C-20, Santa Cruz Biotechnology, Inc., Santa Cruz, CA, USA). The primary antibody was detected with a biotinylated secondary antibody (Biotinylated anti-goat IgG, Vector Laboratories, Burlingame, CA, USA). The signal was amplified using the TSA Biotin System (PerkinElmer, Boston, MA, USA). The presence of MMP-9 was revealed by the stain from 3,3'-diaminobenzidine (Vector Laboratories, Inc.).

4.5. Statistical Methods

All the results are expressed as mean ± standard deviation. After the testing of normality and variance, an ANOVA test was applied to study the significance of the differences between ^{68}Ga-chloride, ^{18}F-FDG (Paper I) and ^{11}C-choline (unpublished data). A t-test was used for the comparison of PET and *ex vivo* data (Paper I). The findings were expected to originate from a normally distributed population (a possibility of type II error). A *P* value of less than 0.05 was considered statistically significant. Statistical analyses were conducted using SAS 9.1.3 statistical software (SAS Institute Inc., Cary, NC, USA). A Mann-Whitney U-test was applied to study the significance of differences observed in cellular binding between the VAP-1 transfected and mock transfected cells (Paper II).

5. RESULTS

5.1. Identification of the Synthesized ^{68}Ga-DOTA-Peptides

The radiochemical purity of ^{68}Ga-DOTA-peptides was >95 % throughout the study as analyzed by radio-HPLC. The specific activity was 0.8 ± 0.04 and 2.0 ± 0.8, 3.3 ± 0.8 and 1.5 ± 0.6 MBq/nmol (mean±SEM) for ^{68}Ga-DOTAVAP-P1 (Paper I), ^{68}Ga-DOTA- TCTP-1, ^{68}Ga-DOTA-lactam-TCTP-1 and ^{68}Ga-DOTA-lin-TCTP-1 (Paper III).

Incubation of the TCTP-1 peptide without a DOTA-chelator with a ^{68}Ga-labeling mixture revealed no ^{68}Ga binding to the peptide.

5.2. DOTA-Conjugation Did Not Hamper the Enzymatic Activity of VAP-P1

The DOTA-derivative of the VAP-P1 inhibited dose-dependently SSAO activity in human serum and sonicated CHO-VAP-1 lysates with corresponding half-inhibition concentration (IC_{50}) values of 430 µM and 260 µM.

5.3. The ^{68}Ga-DOTA-Peptides Were Hydrophilic

The log D value was -4.5 ± 0.6 and -3.6 ± 0.8 of ^{68}Ga-DOTAVAP-P1 and ^{68}Ga-DOTA-TCTP-1, respectively. The results indicate very high hydrophilicity for both imaging agents.

5.4. ^{68}Ga-DOTAVAP-P1 Bound to Human VAP-1 *In Vitro*

^{68}Ga-DOTAVAP-P1 bound more efficiently to human VAP-1-transfected CHO-cells than to mock transfected cells (4000 ± 790 counts/30 s/10^6 cells vs. 2800 ± 340 counts/30 s/10^6 cells, *P*=0.0159).

5.5. Stability and Binding to Plasma Proteins *In Vitro* and *In Vivo*

The biological half-lives (i.e. when 50 % of total radioactivity is still bound to the unmetabolised/intact peptide) of ^{68}Ga-DOTA-peptides *in vitro* and *in vivo* is presented in Table 6 (and more precisely in the original papers). ^{68}Ga-DOTA-TCTPs did not degrade during the 4 h incubation in saline. Neither in human plasma ^{68}Ga-DOTA-lactam-TCTP-1 did not degrade during the 4 h incubation, whereas the half-lives of ^{68}Ga-DOTA-TCTP-1 and ^{68}Ga-DOTA-lin-TCTP-1 were approximately 2.5 h and 1 h, respectively (Paper III). The amount of intact ^{68}Ga-DOTAVAP-P1 *in vitro* after 4 h incubation in saline, human or rat plasma was 93 %, 88 % and 87 %, respectively (Paper II).

The *in vivo* half-life in rat plasma was 26 ± 2.3 min extrapolated from the amount of unchanged ^{68}Ga-DOTAVAP-P1 during 2 h p.i.

Analyses of rat plasma, urine and tumor homogenates p.i. of ^{68}Ga-DOTA-TCTPs showed that ^{68}Ga-DOTA-lactam-TCTP-1 was the most stable *in vivo*, whereas ^{68}Ga-DOTA-lin-TCTP-1 degraded very rapidly (Tables 6 and 7). The ^{68}Ga-DOTA-TCTP-1 showed moderate *in vivo* stability. The extraction efficiency of ^{68}Ga-radioactivity from blood and tumor homogenates (control samples) was between 65 % and 80 %. The analysis of urine samples, taken 2 h p.i., revealed 81 %, 5.3 % and 97 % of intact ^{68}Ga-DOTAVAP-P1, ^{68}Ga-DOTA-TCTP-1 and ^{68}Ga-DOTA-lactam-TCTP-1, respectively. More than 80 % of the injected radioactivity of ^{68}Ga-DOTAVAP-P1 was detected in the urine as soon as 15 min p.i. and the amount remained constant during the whole 2 h examination.

Table 6. Stability given as biological half-lives (i.e. when 50 % of total radioactivity is still bound to the intact peptide) of ^{68}Ga-DOTA-peptides.

	In Vitro		*In Vivo*
	Physiological Saline, RT	**Human Plasma, 37ºC**	**Rat Blood Circulation**
^{68}Ga-DOTAVAP-P1	>4 h	2.5 h	26 min
^{68}Ga-DOTA-TCTP-1	>4 h	2.5 h	$1\ h < T_{1/2} < 2\ h$**
^{68}Ga-DOTA-lactam-TCTP-1	>4 h	>4 h	< 2 h**
^{68}Ga-DOTA-lin-TCTP-1	>4 h	1 h	<<15 min

*Estimation of *in vivo* half-lives is based to the results shown in Table 7. **Rough estimate based on a limited number of time points.

The quantity of intact ^{68}Ga-DOTA-TCTP-1 in the tumor tissue was quite low (Table 7), even though the plasma stability was moderate. Because the plasma stability of ^{68}Ga-DOTA-lin-TCTP-1 was very low, its tumor stability was not studied.

The blood-plasma radioactivity of ^{68}Ga-DOTAVAP-P1 in rat plasma remained at ratio of 1.4 during 30 min *in vivo*, indicating that 29 % of the radioactivity was bound to blood cells, while 39 % of the radioactivity was bound to rat plasma proteins *in vivo* [corresponding to a plasma free fraction (f_P) of 0.61]. Whereas, 35 % of ^{68}Ga-DOTA-TCTP-1 radioactivity was bound to human plasma proteins *in vitro* ($f_P = 0.65$).

Table 7. Percentage of intact ^{68}Ga-DOTA-peptides *in vivo* in rat plasma and *ex vivo* in urine and tumor homogenates.

Tracer	Plasma				Tumor		Urine
	15 min	30 min	60 min	120 min	15 min	120 min	120 min
^{68}Ga-DOTAVAP-P1	62 ± 1.3	46 ± 3.2	31 ± 9.2	16±19	-	-	81±21
^{68}Ga-DOTA-TCTP-1	72±4.4	-	58±4.2	35±18	45±1.2	9.5±2.6	5.3±2.7
^{68}Ga-DOTA-lactam-TCTP-1	91±2.0	-	-	23±6.2	-	59±4.2	97±2.6
^{68}Ga-DOTA-lin-TCTP-1	0.2±0.4[a]	-	-	-	-	-	-

5.6. *In Vivo* Visualization of Tumors and Inflammation Foci and the Biokinetics of ^{68}Ga-Based Imaging Agents

A comparison of the tumor uptake of ^{68}Ga-chloride, ^{11}C-choline and ^{18}F-FDG (Paper I and previously unpublished data) revealed that all of them were capable of visualizing BxPC-3 tumor xenografts (Fig. 4a-c). The uptake of ^{68}Ga-chloride and ^{11}C-choline showed a very fast initial tumor uptake and a moderate decline with a plateau at 10 min p.i. In contrast, the uptake of ^{18}F-FDG accumulated slowly and reached a plateau at 60 min p.i. (Fig. 4d). The tumor uptake expressed as SUV was 0.9 ± 0.3, 1.1 ± 0.3 and 1.8 ± 1.2 for ^{68}Ga-chloride, ^{11}C-choline and ^{18}F-FDG, respectively. ^{18}F-FDG showed higher tumor accumulation than ^{68}Ga-chloride ($P = 0.003$). The tumor accumulation of ^{68}Ga-chloride compared to that of ^{11}C-choline showed no statistical difference ($P > 0.05$).

The excess of ^{68}Ga-chloride was distributed into the heart, liver, urinary bladder and small intestine (Fig. 4a). The excretion of ^{68}Ga-chloride into the urine was remarkably lower than that of ^{18}F-FDG. The corresponding tissue TACs are shown in Figure 5.
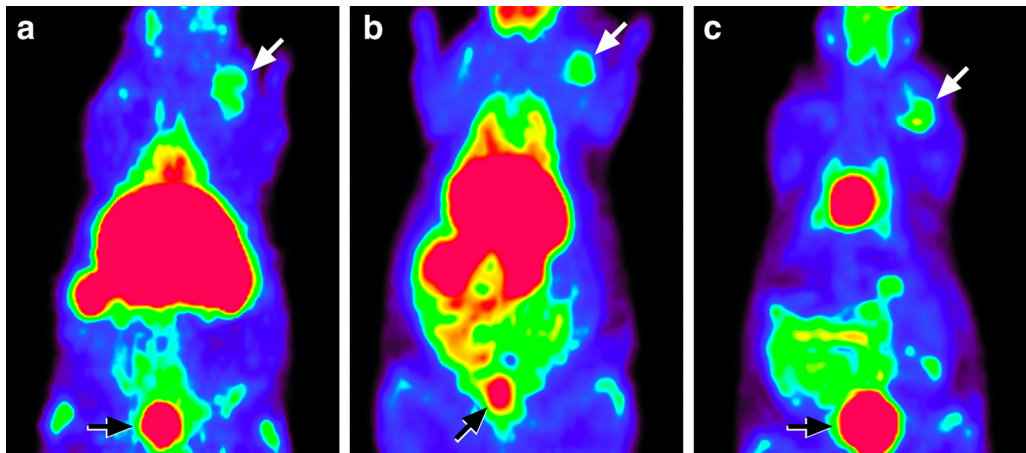
Figure 4. Coronal PET images of a rat injected with a) ^{68}Ga-chloride, b) ^{11}C-choline and c) ^{18}F-FDG on separate days. The tumor formed by subcutaneously implanted BxPC-3 human pancreatic adenocarcinoma cells is marked with a white arrow. The urinary bladder is marked with a black arrow. Images (a summation of a 60 to 70-min period after injection) are color-coded according to the level of radioactivity, from dark blue (the lowest) to hot red (the highest). **d)** The tumor uptake (SUV) of ^{68}Ga-chloride, ^{11}C-choline and ^{18}F-FDG as a function of time. The images concerning ^{68}Ga-chloride and ^{18}F-FDG reprinted with permission from Springer New York (Paper I).
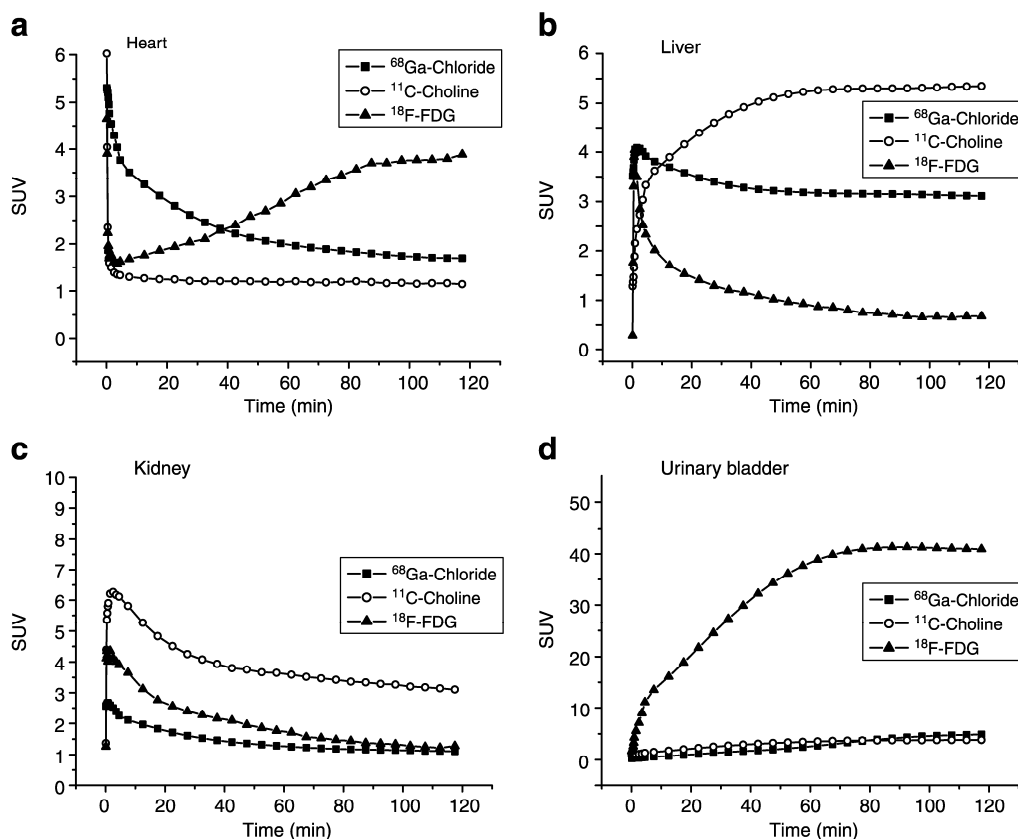
Figure 5. In vivo biokinetics (amount of radioactivity vs. time after injection) of intravenously administered ^{68}Ga-chloride, ^{11}C-choline and ^{18}F-FDG in a rat a) heart, b) liver, c) kidney, and d) urinary bladder. Radioactivity concentrations are expressed as standardized uptake values (SUV) vs. time after injection (min). A mean value of 10-13 rats. The results concerning ^{68}Ga-chloride and ^{18}F-FDG have been presented also in Paper I.

To visualize and quantify the nonspecific accumulation of ^{68}Ga-DOTAVAP-P1 *in vivo*, healthy rats were imaged by a dynamic PET (Paper II: Fig. 3). The highest radioactivity uptake was detected in the urinary bladder, kidneys and liver. Also the lymphoid organs (the thymus, spleen, lymph nodes, and mucosal area of the rat snout) showed a clear uptake (Paper II: Fig. 3A), which is in accordance with the prominent expression of VAP-1 (Salmi and Jalkanen, 2001; Smith *et al.*, 1998). ^{68}Ga-DOTAVAP-P1 had a very fast renal vs. low hepatobiliary excretion, revealed by the time-activity curves of the heart, liver, kidney and urinary bladder (Paper II: Fig. 3B-E).

Infection imaging with ^{68}Ga-DOTAVAP-P1 PET was demonstrated with an experimental model of osteomyelitis (Paper II). There was a clear visualization of the infection focus in the right tibia, although the uptake remained modest with a SUV of 1.2 ± 0.3. ^{18}F-FDG was used as a positive control and showed a higher uptake with a SUV of 1.4 ± 0.03. Also, the target-to-background ratio of ^{18}F-FDG was better. PET-imaging revealed the fast uptake of ^{68}Ga-DOTAVAP-P1 and a plateau at 10 min p.i. at the site of the infection, while the uptake of ^{18}F-FDG reached a plateau approximately

at 50 min p.i. (Paper II: Fig.4). The SUV-ratios between the infected and contralateral healthy tibias at 40-60 min p.i. were 2.3 ± 0.7 (range 1.4 - 3.4; n=6) and 3.1 ± 0.6 (range 2.7 - 3.5; n=2) for ^{68}Ga-DOTAVAP-P1 and ^{18}F-FDG, respectively.

Comparative and competitive imaging experiments indicated the specific accumulation of ^{68}Ga-DOTAVAP-P1 at the infected site. Statistically significant differences were observed between 1) ^{68}Ga-DOTAVAP-P1 and the negative control peptide (2.9 ± 0.8 vs. 1.6 ± 0.4; $P = 0.0211$), 2) ^{68}Ga-DOTAVAP-P1 alone and ^{68}Ga-DOTAVAP-P1 plus competition with semicarbazide (2.0 ± 0.7 vs. 1.3 ± 0.6; $P = 0.0076$), and 3) ^{68}Ga-DOTAVAP-P1 alone and ^{68}Ga-DOTAVAP-P1 plus competition with unlabeled DOTAVAP-P1 (2.6 ± 0.3 vs. 1.8 ± 0.2; $P = 0.0289$). The results are expressed as SUV-ratios, i.e. uptake in the infected bone versus uptake in the contralateral normal bone (Paper II: Table 2).

The tumors were clearly visualized by ^{68}Ga-DOTA-TCTP-1 (Paper III: Fig. 3) and ^{68}Ga-DOTA-lactam-TCTP-1. The tumor uptake of ^{68}Ga-DOTA-TCTP-1 was 60 kBq/mL and the corresponding SUV of 0.6. All 3 peptide conjugates were rapidly taken up by the tumors, but with slightly different biokinetics. Among the ^{68}Ga-DOTA-TCTPs, ^{68}Ga-DOTA-lactam-TCTP-1 showed the slowest uptake and longer retention in the tumor (data not shown).

Nonspecific biodistribution of ^{68}Ga-DOTA-TCTPs was seen in the heart, liver, kidney and urinary bladder. All ^{68}Ga-DOTA-TCTPs showed fairly equal kidney uptake and very high activity in the urine. The kidney uptake of ^{68}Ga-DOTA-TCTP-1 was 490 kBq/mL and the corresponding SUV of 5.1. The activity of ^{68}Ga-DOTA-TCTP-1 in the urine was 11 000 kBq/mL and the corresponding SUV was 91. A representative figure can be seen in Paper III: Fig. 3D. Most of the radioactivity of ^{68}Ga-DOTA-TCTPs was excreted rapidly by the kidneys into the urine, showing the highest accumulation in the urinary bladder after 1 h of injection. The slowest excretion was shown by ^{68}Ga-DOTA-TCTP-1. ^{68}Ga-DOTA-lin-TCTP-1 showed the highest heart uptake with a plateau at 50 min p.i. (31 kBq/mL, SUV of 0.3), as well as a strong overall background and liver signal. ^{68}Ga-DOTA-lin-TCTP-1 had the highest (260 kBq/mL, SUV of 3.0) and ^{68}Ga-DOTA-lactam-TCTP-1 the lowest liver activity (58 kBq/mL, SUV of 0.7).

5.7. *Ex Vivo* Biodistribution

The uptake to BxPC-3-tumors, expressed as %ID/g, was 0.3 ± 0.07, 0.4 ± 0.3 and 0.8 ± 0.4 for ^{68}Ga-chloride, ^{11}C-choline and ^{18}F-FDG, respectively (Table 8). The comparison of the *ex vivo* biodistribution results with the *in vivo* PET results, showed that they were mainly in accordance, with an exception of the tumor uptake of ^{11}C-choline showing higher values when measured by PET ($P < 0.05$) (Fig. 6).

Table 8. %ID/g of ^{68}Ga-chloride, ^{18}F-FDG or ^{11}C-choline at 90 min, 90 min and 10 min p.i, respectively.

Organ	^{68}Ga-chloride	^{11}C-choline	^{18}F-FDG
Blood	1.0±0.07	0.1±0.06	0.1±0.03
Liver	2.1±1.2	1.0±1.0	0.2±0.03
Lung	0.7±0.3	1.1±0.8	0.4±0.02
Muscle	0.1±0.01	0.1±0.06	0.1±0.02
Skin	0.2±0.04	0.1±0.1	0.4±0.08
Tumor	0.3±0.07	0.4±0.3	0.8±0.4
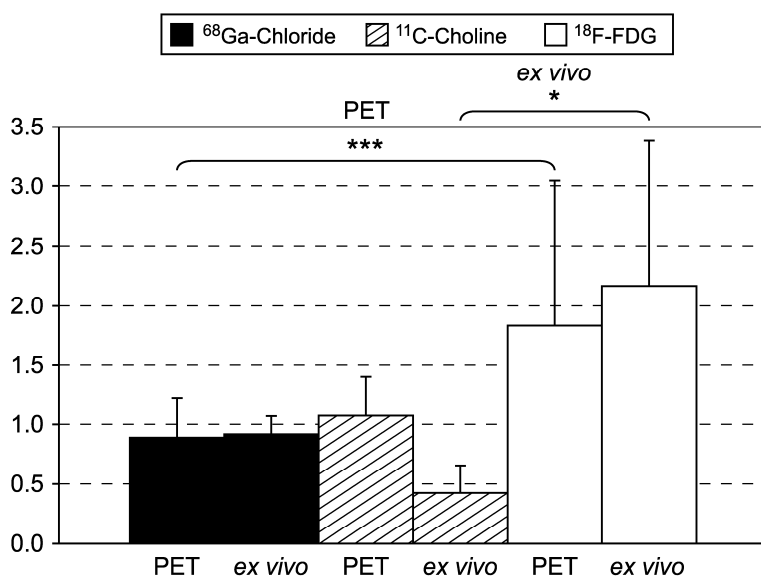
Figure 6. SUV at the tumor site calculated from PET and *ex vivo* biodistribution data. The results of the *ex vivo* measurements were in accordance with the results of the *in vivo* PET imaging, except for ^{11}C-choline. * P < 0.05, *** P < 0.005. The results concerning ^{68}Ga-chloride and ^{18}F-FDG have been presented also in Paper I.

^{68}Ga-chloride had slow blood clearance. The blood radioactivity of ^{68}Ga-chloride was 10 times higher, when compared with ^{18}F-FDG and ^{11}C-choline. All 3 imaging agents gave tumor-to-muscle ratios high enough to differentiate the tumor from the surrounding tissues (4.0 ± 0.3, 3.5 ± 1.0 and 7.9±3.2 for ^{68}Ga-chloride, ^{11}C-choline and ^{18}F-FDG, Table 9). The tumor-to-muscle ratio of ^{68}Ga-chloride was slightly higher than that of ^{11}C-choline, although without statistical significance (Fig. 7). The other target-to-nontarget ratios; i.e. tumor-to-blood, tumor-to-liver, tumor-to-lung and tumor-to-skin ratios; showed lower values for ^{68}Ga-chloride than for ^{18}F-FDG and ^{11}C-choline

(even though there was no statistical significance between tumor-to-skin ratios between ^{68}Ga-chloride and ^{18}F-FDG and tumor-to-lung between ^{68}Ga-chloride and ^{11}C-choline, $P > 0.05$).
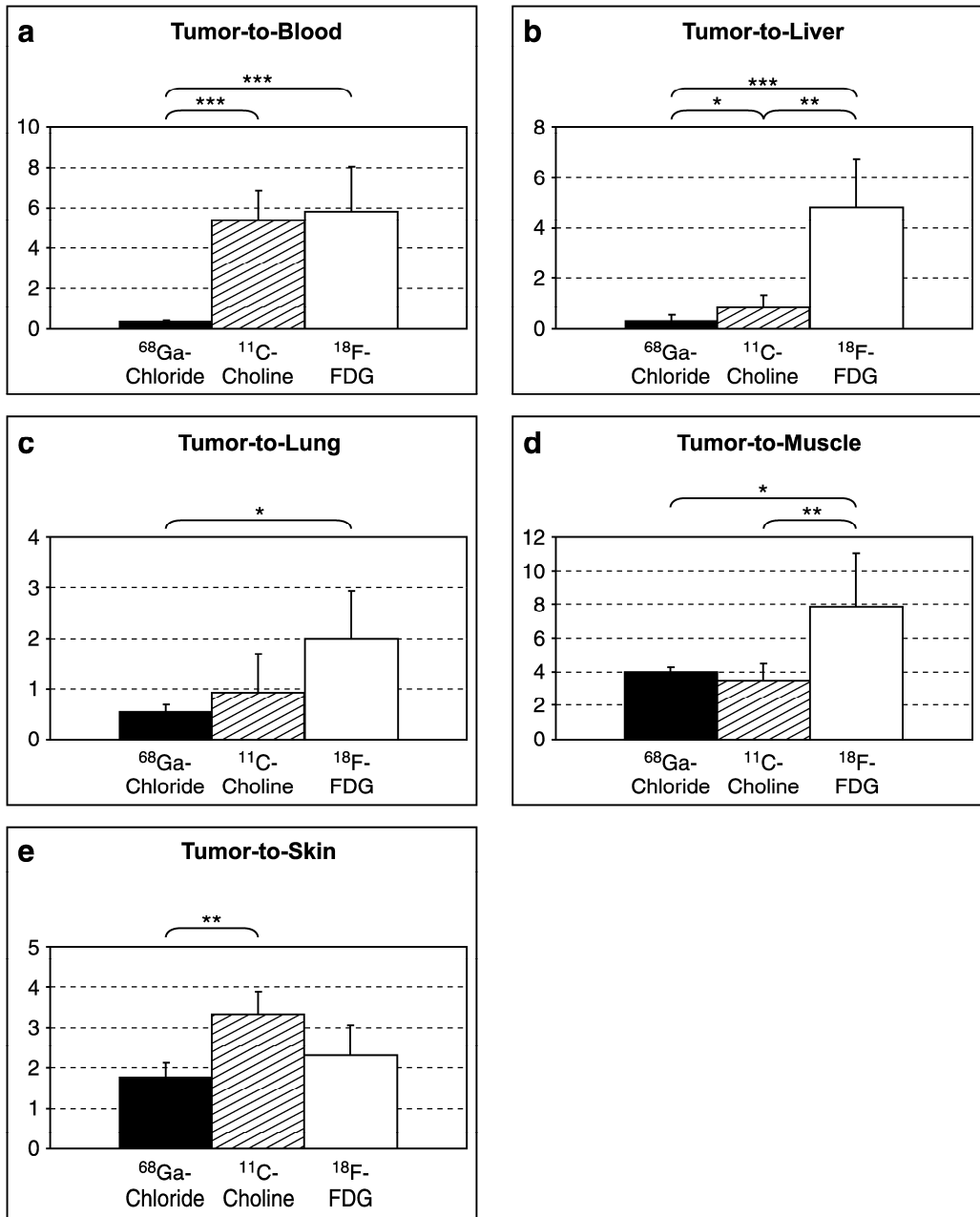

Figure 7. Target-to-nontarget ratios. a) Tumor-to-blood, **b)** tumor-to-liver, **c)** tumor-to-lung, **d)** tumor-to-muscle and **e)** tumor-to-skin ratios calculated from the *ex vivo* measurements of ^{68}Ga-chloride at 90 min, ^{11}C-choline at 10 min and ^{18}F-FDG at 90 min and after injection in tumor-bearing nude rats. * $P < 0.05$, ** $P < 0.01$, *** $P < 0.005$. The results concerning ^{68}Ga-chloride and ^{18}F-FDG have been presented also in Paper I.

The non-target accumulation of ^{68}Ga-DOTAVAP-P1 was demonstrated in healthy rats (Paper II). The measurement of organ-specific radioactivities showed the highest values in the urine (the mean %ID/g of all 4 time points was 22.0), followed by the kidneys (0.8), urinary bladder (0.4), liver (0.3), lung (0.3), spleen (0.3) and blood (0.1). For the rest of the organs, the radioactivity uptake was below 0.1. The lowest uptake of ^{68}Ga-DOTAVAP-P1 was seen in the brain with a mean %ID/g of 0.004. The *ex vivo* biodistribution showed that i.v. administered ^{68}Ga-DOTAVAP-P1 was rapidly cleared from the blood circulation. The agent was excreted quickly through the kidneys into the urine with lower activity in the liver, thus verifying the fast renal vs. low hepatobiliary excretion, noticed by PET. The intestine showed no accumulation (Paper II: Table 1). *Ex vivo* biodistribution results (Paper II: Table 1) are in conformity with PET-imaging (Paper II: Fig. 3).

From the tested ^{68}Ga-DOTA-TCTPs, ^{68}Ga-DOTA-TCTP-1 had the highest *ex vivo* tumor-to-muscle ratio of 5.5 ± 1.3 at 2 h p.i. (Paper III: Fig. 4; Section 5.7.: Table 9). The corresponding values for ^{68}Ga-DOTA-lactam-TCTP-1 and ^{68}Ga-DOTA-lin-TCTP-1 were 3.2 ± 0.2 and 3.2 ± 0.6, respectively. ^{68}Ga-DOTA-TCTP-1 had a tumor-to-blood ratio of 1.2 ± 0.3. As regards tumor-to-lung and tumor-to-liver ratios, there was not much difference between the 3 tested compounds.

The follow-up series revealed the effect of tumor growth (2-4 weeks) on the ^{68}Ga-DOTA-TCTP-1 uptake (Paper III: Tables 2-3). The 3-week-old developed tumors, measured 1 h p.i., showed the highest uptake (0.2 ± 0.03 %ID/g), as well as tumor-to-muscle (4.8 ± 0.4) and tumor-to-blood ratios (0.9 ± 0.3) (n=3-4 at each time point). A weak correlation between MMP-9 levels and the biodistribution results was seen (the correlation coefficient between the MMP-9 level and tumor-to-muscle ratio = 0.33).

The summary of the target-to-background ratios of all the tested imaging agents are presented in Table 9.

Table 9. Target-to-background ratios of the studied imaging agents. ^{68}Ga-DOTA-TCTP-1 was found the most promising of the tested ^{68}Ga-DOTA-TCTPs, and for that reason the effect of different length for tumor growth was further examined for this particular radio-peptide and the results of optimal tumor growth time (three weeks) are shown.

Agent	Time-point	Ex Vivo					In Vivo	n
		T/Blood	T/Liver	T/Lung	T/Muscle	T/Skin	O/ Healthy Leg	(rats)
[68]GaCl₃ (I)	90 min	0.4±0.08	0.3±0.3	0.5±0.1	4.0±0.3	1.8±0.4	-	4
^{18}F-FDG (I)	- " -	5.8±2.2	4.8±1.9	2.0±0.9	7.9±3.2	2.3±0.7	-	4
[11]C-choline (unpub-lished data)	10 min	5.3±1.5	0.9±0.4	0.9±0.8	3.5±1.0	3.3±0.6	-	4
^{68}Ga-DOTA-VAP-P1 (II)	40-60 min	-	-	-	-	-	2.3±0.7	6
^{18}F-FDG (II)	- " -	-	-	-	-	-	3.1±0.6	2
^{68}Ga-DOTA-TCTP-1 (III)	2 h	1.2±0.3	0.2±0.1	0.4±0.03	5.5±1.3	-		2
^{68}Ga-DOTA-lactam-TCTP-1 (III)	2 h	0.6±0.1	0.4±0.02	0.4±0.003	3.2±0.2	-		3
^{68}Ga-DOTA-lin-TCTP-1 (III)	2 h	1.5±1.0.	0.3±0.2	0.7±0.4	3.2±0.6	-		3
^{68}Ga-DOTA-TCTP-1, follow-up series (III)	1 h*	0.9±0.03	0.5±0.2	0.3±0.03	4.8±0.4	-	-	3

T=Tumor, O=Osteomyelitis. *The one hour time-point is presented for the three-week-old developed tumors, since it showed the most promising tumor accumulation in the follow-up series.

5.8. Closer Examination of the Uptake and Targets

5.8.1. Homogenous Distribution of ^{68}Ga-Chloride in Tumor Tissue

Representative digital autoradiographs of ^{68}Ga-chloride, ^{11}C-choline and ^{18}F-FDG biodistribution in the tumor tissue are shown in Figure 8. Each of the imaging agents showed a different biodistribution in tumor tissue. The ^{68}Ga-radioactivity was quite homogeneously distributed within the tumor tissue, while distribution of ^{18}F-FDG and ^{11}C-choline was more heterogenous.
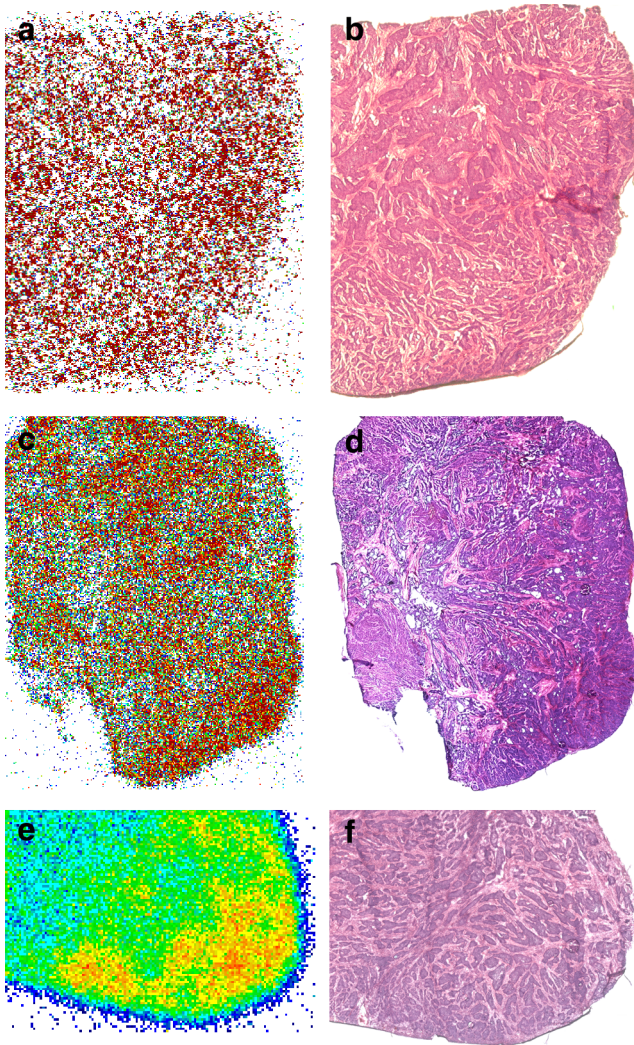
Figure 8. Representative digital autoradiographs of BxPC-3 tumor cryosections and corresponding haematoxylin and eosin (HE) stainings. a) ^{68}Ga-chloride autoradiography at 90 min post injection (p.i.) and **b)** the HE-staining of the same section. **c)** ^{11}C-choline autoradiography at 10 min p.i. and **d)** the corresponding HE-staining. **e)** ^{18}F-FDG autoradiography at 90 min p.i. and **f)** the corresponding HE-staining. The dark blue represents the lowest and hot red the highest amount of radioactivity. The images concerning ^{68}Ga-chloride and ^{18}F-FDG reprinted with permission from Springer New York (Paper I).

The histological sections of BxPC-3 tumors showed mainly homogenous, viable tumor tissue without major necrotic areas (Paper I: Fig. 6). ^{68}Ga-chloride uptake by the tumor was mostly by viable cancer cell islets. Immunohistochemical staining with mouse anti-rat CD68 recognising rat macrophages, revealed a homogenous distribution in the tumor tissue (Paper I: Fig. 7a-c). However, the CD68-staining was even more prominent in the surrounding stroma than in the tumor tissue.

5.8.2. Successful Induction of Osteomyelitis

The presence of infection and expression of VAP-1 in the osteomyelitic rat model was confirmed by microbiological and histological analysis (Paper II). The inoculated pathogen (*S. aureus*) was cultured from the bone specimens of all osteomyelitic rats. Whereas, the expression of VAP-1 was depicted in all of the immunohistochemically analyzed osteomyelitic bone samples (Paper II: Fig. 5). Positive staining of VAP-1 was seen in the endothelium of blood vessels and surrounding adipose cells.

5.8.3. Expression of MMP-9 in Melanoma Xenografts

Zymography demonstrated that the expression level of MMP-9 in 3-week-old developed rat xenografts was on an average of 0.5 ng/mg of tumor tissue (Paper III: Table 4).

MMP-9 was clearly detected immunohistochemically at 2 and 6 weeks after inoculation of the C8161T/M1 cells. The signal was located both in the endothelium layer of the blood vessels and in the ECM (Paper III: Fig. 5).

6. DISCUSSION

The aim was to preliminarily evaluate new PET agents for imaging cancer and inflammation using experimental models. ^{68}Ga-chloride was prepared by elution and neutralization and two lead peptides, VAP-P1 targeting VAP-1 and TCTP-1 targeting MMP-9, were synthesized and modified for PET imaging purposes by conjugation with DOTA and labeling with ^{68}Ga. Consequently, the aim was to assess the essential properties needed in physiological circumstances using *in vitro* assays and preclinical tests in rats, such as stability against radiolysis, resistance to proteolysis and binding to proteins in the blood, as well as lipophilicity and the ability to bind to the target *in vitro*, *in vivo* stability in the blood and *ex vivo* stability in the target tissue, as well as tissue distribution and biokinetics.

The studied ^{68}Ga-based imaging agents showed their potential features by passing the essential *in vitro* tests, proceeding further to preclinical *in vivo* evaluation and being able to visualize the target. The target uptake and target-to-background ratios of these agents, however, were not optimal and resulted, in case of ^{68}Ga-chloride, due to slow clearance caused by binding to blood transferrin, and in the case of ^{68}Ga-DOTA-peptides, from low *in vivo* stability and/or low lipophilicity leading to a too rapid blood clearance and urinary excretion. Further optimization is recommended to improve the properties towards better stability in the target (^{68}Ga-DOTA-TCTP-1), slower excretion by the kidneys (^{68}Ga-DOTA-peptides), higher specific activity (all ^{68}Ga-DOTA-peptides) and possibly better affinity. It was shown here with MMP-9 targeting ligands, that the properties of ^{68}Ga-labeled peptides are modifiable.

6.1. The Hypothesis and Search for Leads

Gallium has been used since the 1960s for SPECT imaging (Anger H. O. and Gottschalk, 1963; Shealy *et al.*, 1964). In SPECT, gallium is used in the form of ^{67}Ga-citrate, which is a salt of citric acid. We hypothesized that ^{68}Ga could be used for the PET imaging of tumors in a similar fashion as ^{67}Ga is used for SPECT. Our research group has previously reported that ^{68}Ga-chloride can be used for the PET imaging of inflammation (Mäkinen *et. al.*, 2005) and also is taken up by tumors (Roivainen *et. al.*, 2004). Here the suitability of this salt of ^{68}Ga and HCl and simply neutralized eluate from the ^{68}Ge/^{68}Ga-generator was examined in more detail for the PET imaging of tumors.

VAP-1 was chosen as the target for developing inflammation imaging agents, because it is an inflammation inducible enzyme. VAP-1 is rapidly translocated from intracellular sources to the endothelial cell surface during inflammation (Salmi *et al.*, 1997). A molecule targeting VAP-1 was found by Yegutkin and collegues (2004). This molecule, containing the peptide sequence of GGGGKGGGG, was the most efficient one found capable to interact with VAP-1 in competitive enzyme assays *in vitro*. These inhibitory effects were specific for VAP-1, but not for other related amine oxidases such as diamine oxidase, monoamine oxidases A and B, and retina-specific amine oxidase. The ability of this peptide to fit into the active-site of VAP-1 was further

confirmed by the modeling results done with computer docking stimulations (Yegutkin *et. al.*, 2004). Also a negative control peptide was chosen based on computer docking stimulations. A bulky and rigid peptide without a central lysine residue (PHEPTYPDF) cannot fit properly into the substrate channel of VAP-1, and thus is not capable of modulating the enzyme activity (Yegutkin *et. al.*, 2004). However, peptides GGGGGGGGGK and KGGGGGGGG, which only differ from P1 with respect to the position of the lysine residue in the polypeptide chain, are also weak inhibitors of SSAO activity. For these reasons, the PHEPTYPDF peptide was chosen to be the negative control peptide for PET studies.

MMP inhibitors may be convenient for imaging purposes, although they have not shown to be proper as therapeutics, mainly due to poor selectivity (Section 2.2.4.3; Blankenberg and Strauss, 2002; Agdeppa and Spilker, 2009). Koivunen and coworkers (1999) found a particular MMP inhibitor, specific for gelatinases (MMP-2 and -9), through the biopanning (phage display) (Smith, 1985) of living malignantly-transformed human cells. The most intensively studied MMP inhibitor is a peptide called CTT. This MMP-2/MMP-9 inhibitor has been radiolabeled and preclinically evaluated by four distinct groups (Sprague *et. al.*, 2006; Hanaoka *et al.*, 2007; Kuhnast *et. al*, 2004; Medina *et. al.*, 2005). However, selective binding to MMP-2/MMP-9 was not demonstrated, and all modifications of this peptide exhibited poor *in vivo* stability resulting in low tumor uptake. The present results with another MMP inhibitor compound, named TCTP-1, are quite similar.

6.2. Evaluation of ^{68}Ga-Based PET Imaging Agents for Cancer and Inflammation

6.2.1. The Structure-Function-Relationship

Some conclusions about the biological properties can be made already from the aimed structure of the imaging agent, and this should lead to the designing of the structure. In this content it is beneficial to understand the basic chemical properties of the agent, which rule out the diffusion, internalization, localization, clearance and elimination.

^{68}Ga-chloride was the first tested imaging agent in this study. Once eluted from the ^{68}Ge/^{68}Ga-generator with 0.1 M HCl, ^{68}Ga is in the form of ^{68}Ga-chloride (^{68}GaCl$_3$). In an aqueous solution, ^{68}Ga is rapidly hydrolyzed. A soluble anion ^{68}Ga(OH)$_4^-$ (gallate) is stable under acidic conditions (pH 3-7), but if its concentration exceeds the nanomolar level, it can form insoluble ^{68}Ga(OH)$_3$ colloids (Mäkinen *et al*, 2005; Mäcke and André, 2007; Fani *et al.*, 2008). ^{68}Ga-chloride was neutralized with NaOH prior to intravenous administration. It is known that in the pH of 7.4 (pH in the blood) most of the Ga is soluble, and in the blood Ga^{3+} is bound to an iron-binding protein transferrin (Vallabhajosula *et al.*, 1980; Green and Welch, 1989; Weiner, 1996; Bernstein, 1998; Love and Palestro, 2004; Mäcke and André, 2007; Fani *et al.*, 2008).

The form of Ga may affect the uptake mechanism into the tumor. It is known that (when administered in the form of ^{67}Ga-citrate) Ga is bound to tumors by transferrin receptors, and for that reason it can be used for the imaging of the increased iron

metabolism of tumor cells. The accumulation of Ga^{3+} in malignant tissue correlates with the level of transferrin receptor expression in almost all cases (Larson *et al*., 1980; Chitambar and Civkovic, 1987; Weiner, 1996, Bernstein, 1998). However, Ga^{3+} can enter tumor cells also by a transferrin independent mechanism. In this proposed transferrin independent mechanism, $Ga(OH)_4^-$ penetrates through cellular membranes due to its small size (Larson *et al*., 1980; Chitambar and Civkovic, 1987; Weiner, 1996, Bernstein, 1998). Also, Ga^{3+} uptake by macrophages has been reported (Bernstein, 1998; Swartzendruber *et al.*, 1971). Accordingly, it is possible that Ga-chloride accumulates mainly by macrophage phagocytosis, if it is neutralized prior to injection due to the formation of colloids. Also the size of hydroxide colloids, depending on the base used for neutralization, may affect the accumulation (Hnatowich, 1977). A wide variety of factors can affect the uptake of radio-gallium into tumors. In order to clarify the uptake mechanism, we did not study the solubility of ^{68}Ga, but instead examined the accumulation in more detail on the microscopic level.

The peptides were conjugated to the N-terminus by converting one of the -COOH groups to an active ester, thus making it capable to form an amide bond. A modified version of the original DOTA-TCTP-1 peptide, DOTA-lactam-TCTP-1, was synthesized for the purpose of developing a peptide structure that would be more sustainable against proteolysis in the blood. A cyclic structure was used in the TCTPs, because it is known that cyclization raises the stability in blood circulation and stiffens the conformation, and thus possibly leads to better affinity (Okarvi, 2004). Also, a peptide bond (Cys-Cys) of the original peptide was changed to a lactam bridge (DOTA-lactam-TCTP-1) in order to raise the stability (Section 4.2., Fig. 3C-D). Also a linear control peptide was synthesized (DOTA-lin-TCTP-1) (Fig. 3E). The synthesis and ^{68}Ga-labeling of peptides was straightforward. ^{68}Ga-DOTA-TCTP-1 showed the most promising targeting properties in the *in vivo* PET and *ex vivo* measurement series and for that reason it was studied most intensively.

The selective and efficient labeling of the DOTA-conjugated peptides with ^{68}Ga showed that there were no significant amounts of free radionuclides or the chelate was not detached from the peptide structure during labeling. This is relevant, because ^{68}Ga-chloride itself is also tumor and inflammation (Mäkinen *et. al*., 2005) oriented. There was no need for further purification.

^{68}Ga is a suitable isotope for labeling peptides owing to its fast *in vivo* kinetics. In general, the biokinetics of small peptides is fast. Raising the molecular size affects by slowing down the kinetics. The conjugating and labeling of the studied peptides raised the size (with 472.14 g/mol) and consequently the radio-peptides were rather long peptides (Section 4.2., Table 3) (Lundqvist and Tolmachev, 2002). The properties, including kinetics, of the prepared radio-peptides are reported here.

As a proof of retained functionality after DOTA-conjugation, the *in vitro* competitive enzyme assays were performed for DOTAVAP-P1. DOTAVAP-P1 was capable to bind VAP-1 and even to inhibit the enzymatic activity of VAP-1. These types of imaging agents, affecting to the enzymatic activity of their target, could give the possibility for signal amplification. This option of VAP-1 targeting would be

interesting to examine in the future. Also, MMP-9 targeting imaging agents might be used in this way (Randy *et al.*, 2008).

6.2.2.   Justification of Animal Models

To test the agents *in vivo*, experimental tumor models were established. Experimental models in rats were chosen prior to mice, because the imaging of bigger animals is easier due to the resolution of the PET cameras used, and since while performing these studies we did not have access to a dedicated small animal PET. Human ductal pancreatic adenocarcinoma cells BxPC-3 or MMP-9 expressing human melanoma C8161T/M1 cells were implanted s.c. into athymic rats and the cells were allowed to form tumors. These models were chosen, since imaging and early diagnosis of pancreatic cancer and melanoma remains a challenge (Nakao *et al.*, 2006; Saif *et al.*, 2008; McQuade *et. al.*, 2005, Wei *et. al.*, 2007; Garbe and Eigentler, 2007) and these cells were capable to form s.c. tumors in rats. Melanomas in particular were chosen, because they are one of several cancers over-expressing MMP-9. The MMP-9 expression level of the C8161T/M1 cell line is significant (data not shown). Early diagnosis of pancreatic cancer is often delayed, because PET is not yet the primary method, even though being the most accurate one, and usually only symptomatic patients with suspected malignancy are PET imaged (Saif *et al.*, 2008). Compared to other diagnostic strategies, PET indicates the metabolic activity of the lesions, and thus reveales the metastatic nature of them. The benefit of PET-CT, especially in the diagnosis of melanoma, would be more accurate in staging (particularly in patients with apparent metastasis) and in the facilitation of decision making on surgical treatment strategies (Garbe and Eigentler, 2007).

The inflammation caused by *Staphylococcus aureus* bone infection in rats was used for testing ^{68}Ga-DOTAVAP-P1, because this model was readily available for our studies (Mäkinen *et. al.*, 2005). ^{68}Ga-DOTAVAP-P1 was designed to target inflammation inducible human VAP-1 molecule, but as the VAP-1 molecule is very conserved between different species, we were able to study VAP-1 targeting in rats.

6.2.3.   Targeting of ^{68}Ga-DOTAVAP-P1

The targeting of ^{68}Ga-DOTAVAP-P1 was tested first on the VAP-1 expressing cell model, where the expression of human VAP-1 was modulated (Paper II). The significant difference between human VAP-1 transfected vs. mock transfected cells suggests that ^{68}Ga-DOTAVAP-P1 bind to human VAP-1. The most important evidence of VAP-1 targeting was obtained by *in vivo* PET imaging using osteomyelitic rats. When imaged in the presence of the negative control peptide or competitors (semicarbazide and nonradioactive DOTAVAP-P1) the uptake of ^{68}Ga-DOTAVAP-P1 to inflammation foci was significantly lower ($P < 0.05$). This indicated that the binding of ^{68}Ga-DOTAVAP-P1 to VAP-1 was specific.

6.2.4. Affect of Lipophilicity to Agents Targeting Extracellular Proteins

The distribution of agents is affected by their solubility to water vs. lipid containing tissues and structures. ^{68}Ga-DOTAVAP-P1 is composed of polar glycine and basic lysine in the physiological pH 7.4, while ^{68}Ga-DOTA-TCTP-1 includes mostly polar amino acids, as well as some basic arginine residues and nonpolar aminoacids. The polarity and charge of basic amino acids implies the hydrophilic property for these ^{68}Ga-DOTA-peptides. To clarify this, the octanol-water distribution coefficient was assessed. Indeed, the tested radio-peptides revealed themselves to be very water-soluble as their log D were ≤ –3.6. In general, the polyethylene glycol(PEG)-linker that was used in the structures of TCTPs increases water solubility even more (Harris and Chess, 2003). The introduction of a bifunctional PEG-moiety (MW 3,400) into the peptides is used to protect polypeptides from degradation, which usually enhances pharmacokinetics, pharmacodynamics, limits antigenicity and toxicity. Pegylation slows down renal clearance by making the molecules larger and thus reduces the filtration of them into the urine. The changes in size and structure can affect the biological activity as well (Harris and Chess, 2003). PEG can be introduced between the DOTA and the N-terminal amino acid.

The passive transport through cell membranes is not possible for very hydrophilic agents. In case of the tested ^{68}Ga-DOTA-peptides, the ability to pass cell membranes is not a key question, since the targets for these peptides are extracellular. Both VAP-1 and MMP-9 are translocated at the cell surface from intracellular granules. MMP-9 can also be secreted to ECM (Sato *et al.*, 1994; Brooks *et al.*, 1996; Salmi *et al.*, 1997; Hofman *et al.*, 2000; Deryugina *et al.*, 2001; Sternlicht and Werb, 2001; Schnaeker *et al.*, 2004). Both VAP-1 and MMP-9 can be detected on the luminal endothelial surface of the blood vessels and in the blood in soluble forms, when expressed in elevated levels (Bono *et al.*, 1998; Kurkijärvi *et al.*, 2000; Zorzano *et al.*, 2003; Gokturk *et al.*, 2003; Salmi and Jalkanen, 2005; Koivunen *et al.*, 1999; Wikström *et al.*, 2003; Phillips and Birnby, 2004; Del Bufalo *et al.*, 2004). Indeed, the pericellular location of the target can be considered as a benefit, because there is no need for internalization (Yang *et al.*, 2009).

6.2.5. Estimation of the Amount of Free Ligands

The protein binding of ^{68}Ga-DOTAVAP-P1 (39 %) and ^{68}Ga-DOTA-TCTP-1 (35 %) were moderate, leaving most of the compound free to interact with the desired target and still keeping a pool of molecules potentially protected from degradation. Although, even high plasma protein binding may be acceptable, if the binding is loose and a sufficient amount of the imaging agent is released from the proteins in the capillaries.

6.2.6. Amount of Unmetabolished Ligans

One of the important properties of a PET imaging agent is its metabolic stability. PET measures the total radioactivity concentration in tissues and is not capable of discriminating different radiochemical entities, such as radioactive degradation products or metabolites. For that reason a radio-HPLC analysis method was developed. The pH-gradient HPLC method reported here results in a good separation of different ^{68}Ga compounds, and also a good peak shape of ^{68}Ga-DOTA-peptides (Paper II: Fig. 2; Paper III: Fig. 2). All ^{68}Ga-DOTA-peptides were highly stable in physiological saline. Incubation in human plasma revealed moderate stability *in vitro* for ^{68}Ga-DOTAVAP-P1 and ^{68}Ga-DOTA-TCTP-1. ^{68}Ga-DOTA-lactam-TCTP-1 was not degraded at all by proteolytic enzymes during a 4 h incubation in human plasma. The stability of the ^{68}Ga-DOTA-TCTP structure was raised drastically by the replacement of the cystine bridge by a lactam bridge, as expected (Harris and Chess, 2003; Peräkylä *et al.*, 2007). Instead, the linearized TCTP structure, seemed to be degraded very rapidly in human plasma. A large portion of short peptide fragments was released from it, and the *in vitro* half-life was approximately 1 hour.

The biological half-lifes designated moderate stability in rat circulation for ^{68}Ga-DOTAVAP-P1 (26 min) and ^{68}Ga-DOTA-TCTP-1 (>1 hour). Furthermore, the amount of intact peptide versus radiometabolites in tumors was studied. 45 % ± 1.2 % of ^{68}Ga-DOTA-TCTP-1 was intact in tumor tissue at 15 min p.i. and decreased over time (Paper III: Table 1). Therefore, it is logical that ^{68}Ga-DOTA-TCTP-1 PET imaging revealed a slow decrease of tumor uptake once the maximal uptake was reached. Because ^{68}Ga-DOTA-lactam-TCTP-1 showed a higher level of intact radio-peptide (59 % ± 4.2 % at 2 hours p.i.), also PET showed a slower wash-out from the tumor site. Even with replacing the cystine bridge by a lactam bridge, a strong increase in stability was achieved, and tumor targeting was slightly reduced according to the PET and the *ex vivo* measurements. Fast degradation *in vivo* is known to cause a strong background signal (Yang *et. al*., 2009), which seemed to be the case with ^{68}Ga-DOTA-lin-TCTP-1. The degradation products of ^{68}Ga-DOTA-peptides included most probably a ^{68}Ga-DOTA chelator attached to one to three amino acids, short ^{68}Ga-DOTA-peptide fragments, and a small amount (≤3 %) of [68]Ga. The identification of the degradation sites might aid in the construction of more stable peptides. PEG was used to raise the stability of ^{68}Ga-DOTA-TCTPs. It can be used also to stabilize the structure of ^{68}Ga-DOTAVAP-P1, without affecting the targeting (Autio *et. al*., 2008). Another way to improve the *in vivo* stability is by composing the peptide partially or fully of D-amino acids, the addition of pseudo-peptide bonds, N-terminal pyroglutamic acid or acetylation or C-terminal amidation (Gotthard *et al*., 2004).

6.2.7. PET Imaging of Tumors with ^{68}Ga-Chloride and ^{68}Ga-DOTA-TCTPs

Tumor visualization was possible with ^{68}Ga-chloride PET with a SUV value of 0.9 ± 0.3. Also ^{11}C-choline and ^{18}F-FDG were capable of visualizing subcutaneous human ductal pancreatic cancer tumors in rats. There was no statistical difference between the tumor uptake of ^{68}Ga-chloride and ^{11}C-choline. When compared to ^{18}F-FDG, the tumor uptake of ^{68}Ga-chloride was faster, while the uptake of ^{18}F-FDG was higher and showed greater variation between animals. The critical organs for the nonspecific accumulation of ^{68}Ga-chloride were the the blood rich heart and liver. Pancretic cancer and liver tissue have high levels of transferrin receptors, which is in accordance with Ga accumulation (Bernstein, 1998; Ryschich *et al.*, 2004). A benefit of ^{68}Ga-chloride is the lower liver uptake compared to ^{11}C-choline, even if the lowest liver burden of all was induced by ^{18}F-FDG.

Also ^{68}Ga-DOTA-TCTP-1 and ^{68}Ga-DOTA-lactam-TCTP-1 were capable of visualizing tumors in PET, while ^{68}Ga-DOTA-lin-TCTP-1 control, showed high background signals throughout the body. A comparison of ^{68}Ga-DOTA-TCTPs revealed that ^{68}Ga-DOTA-TCTP-1 had the highest tumor uptake (SUV of 0.6), while the accumulation of all ^{68}Ga-DOTA-TCTPs was roughly at the same level. ^{68}Ga-DOTA-TCTP-1 showed the maximal tumor uptake immediately after injection and a prolonged presence, which slowly decreased during two hours of imaging. ^{68}Ga-DOTA-lactam-TCTP-1 showed a maximal tumor uptake at a slightly later time point (SUV of 0.4 at 10 min p.i.), and it showed a slightly slower wash-out from tumors than ^{68}Ga-DOTA-TCTP-1 did. Most of ^{68}Ga-DOTA-TCTP-1's radioactivity was excreted rapidly into the urine.

6.2.8. Proof of the Results of Tumor PET

The *ex vivo* delineated tumor uptake was 0.3 ± 0.07 %ID/g at 90 min p.i. for ^{68}Ga-chloride. The *ex vivo* tumor-to-muscle ratios were in accordance with PET, showing that ^{68}Ga-chloride (4.0±0.3) seems to be as good as ^{11}C-choline for detecting BxPC-3 tumors ($P > 0.05$), while ^{18}F-FDG was the best ($P < 0.05$). The tumor-to-skin ratio of ^{68}Ga-chloride predicts success when compared to ^{18}F-FDG ($P < 0.05$).

Also the *ex vivo* comparison of ^{68}Ga-DOTA-TCTPs were in accordance with PET, showing the most promising tumor targeting properties for ^{68}Ga-DOTA-TCTP-1 (tumor-to-muscle ratio of 5.5 ± 1.3 at 2 h), and for that reason it was selected to for further studies. The continuation series with ^{68}Ga-DOTA-TCTP-1 showed a modest uptake in the measured organs during 1 h p.i., including the tumor (%ID/g ≤0.2 and tumor-to-blood values <1). As a conclusion, the 2 hour time point showed the best imaging results; clearance from the blood and accumulation in tumor tissue (Section 5.7., Table 9).

6.2.9. PET Imaging of Inflammation with ^{68}Ga-DOTAVAP-P1

The imaging of infection with ^{68}Ga-DOTAVAP-P1 PET was demonstrated in an experimental model of bone infection in rats. PET showed that in this model ^{68}Ga-DOTAVAP-P1 accumulated more to the inflamed leg than the negative control peptide. Also, *in vivo* competition studies indicated that the uptake was a result of specific binding. ^{68}Ga-DOTAVAP-P1 showed a rapid uptake at the site of the inflammation caused by a *S. aureus* infection, although the uptake to the inflammation site was lower (SUV of 1.2 ± 0.3 and target-to-background ratio 2.3 ± 0.7 at 40-60 min p.i.) compared to that of the positive control, ^{18}F-FDG (SUV of 1.4 ± 0.03 and target-to-bkg of 3.1 ± 0.6 at 40-60 min p.i.). The target-to-bkg greater than 1.5 should be enough for the *in vivo* detection of inflammation (Gulec, 2007). The affinity might be improved even by slight changes in the amino acid structure and a more stable structure would reach the target better.

The golden standard for inflammation imaging is SPECT, with *in vitro* labeled leukocytes, although the sensitivity is suboptimal (van Eerd *et. al.*, 2005; Palestro, 2007, Boerman *et al.*, 2001). Inflammation foci can be also SPECT imaged with ^{123}I-labeled anti-VAP-1 antibody SPECT targeting VAP-1 (Jaakkola *et al.*, 2000). Compared to this VAP-1 targeting SPECT approach, the now described ^{68}Ga-DOTAVAP-P1 PET have important advantages; such as the better spatial resolution, faster uptake at the site of infection, and lower radioactive exposure for a patient.

6.2.10. Ability to Visualize Metastases from Lung and Liver

Tumor-to-lung and tumor-to-liver ratios are valuable when evaluating the potential of a new imaging agent to detect metastases from these tissues. For example, pancreatic cancer and melanoma easily send metastases in particular to the liver. Many cancers, like melanoma, are known to send metastases also to the lungs (Nakao *et al.*, 2006; Mohr *et al.*, 2009). ^{18}F-FDG would be clearly superior to differentiate BxPC-3 metastases from the liver and lung tissue (tumor-to-liver and tumor-to-lung ratios were 4.8 ± 1.9 and 2.0 ± 0.9, respectively). Liver and lung metastases could not be detectable with ^{68}Ga-chloride, ^{11}C-choline and ^{68}Ga-DOTA-TCTP-1, since their tumor-to-liver and tumor-to-lung ratios were below 1 (Section 5.7., Fig. 7b-c and Table 9).

6.2.11. Elimination

The blood clearance of ^{68}Ga-chloride was slow (estimated from TAC of the heart), while that of ^{68}Ga-DOTAVAP-P1 and ^{68}Ga-DOTA-TCTPs was fast. The *ex vivo* results, high blood radioactivity (1.0 ± 0.07 %ID/g) and modest tumor-to-blood ratio (0.4 ± 0.08) at 90 min p.i., confirmed the slow clearance of ^{68}Ga-chloride. The slow clearance was most likely caused by Ga^{3+} binding to transferrin, which has been reported also by Breeman *et al.* (2005). Consequently, the excretion of ^{68}Ga-chloride into the urine was relatively low. In opposite, the fast blood clearance of ^{68}Ga-DOTA-TCTP-1 (SUV peak of heart decreased ≤ 1 during 5 min of imaging and *ex vivo*

measurements showed only 1.1 ± 0.04 %ID/g already at 2 min p.i.) was promoted by rapid excretion into the urine. The analysis of urine samples, taken 2 h p.i., revealed that most of of ^{68}Ga-DOTA-TCTP-1 was excreted after degradation (5.3 % was intact). The radioactivity in the blood may have affected the tumor uptake of ^{68}Ga-chloride and ^{68}Ga-DOTA-TCTP-1 to some extent (especially during 1 h p.i. of ^{68}Ga-DOTA-TCTP-1, when the tumor-to-blood ratio was <1), thus comparative studies with a perfusion marker, such as oxygen-15-labeled water, are warranted and should clarify this concern.

PET revealed that the blood radioactivity of ^{68}Ga-DOTAVAP-P1 decreased during 20 min imaging to a SUV under 1. The biodistribution obtained by PET and *ex vivo* measurements showed a rapid blood clearance (the blood radioactivity was only 0.2 ± 0.05 %ID/g at 15 min p.i.), as well as a quick accumulation in the kidneys and urine, but relatively low accumulation in the liver and no accumulation in the intestine. These biodistribution results indicate rapid urinary excretion, which in turn enhanced blood clearance. Over 80 % of the radioactivity was detected in the urine as soon as 15 min p.i. and the radio-HPLC analysis revealed that >80 % of the peptide excreted in unmetabolized form. Also uptake in the urinary bladder wall was detected in *ex vivo* measurements, which is in accordance with the VAP-1 expression in the smooth muscle (Salmi *et al.*, 2001).

PET revealed that all ^{68}Ga-DOTA-TCTPs had a fairly equal kidney uptake and very high activity in the urine. [The uptake of ^{68}Ga-DOTA-TCTP-1 was 490 kBq/mL (SUV of 5.1) and 11 000 kBq/mL (SUV of 91) in the kidney and urinary bladder, respectively]. The liver uptake of ^{68}Ga-DOTA-TCTPs was lower. ^{68}Ga-DOTA-lin-TCTP-1 had the highest (260 kBq/mL, SUV of 3.0) and ^{68}Ga-DOTA-lactam-TCTP-1 the lowest liver activity (58 kBq/mL, SUV of 0.7), which was in accordance with the amount of metabolism of the peptide variants. These distribution results imply that the TCTPs were cleared mainly via the kidneys.

Usually, radio-peptides are eliminated quickly through the kidneys after transformation into a more hydrophilic form, while other substances may prefer excretion through the liver to bile and further to feces. Some foreign substances, such as very hydrophilic or small molecular weight peptides, may be excreted in an intact form into the urine (Lundqvist and Tolmachev, 2002; Okarvi, 2004; Saha, 2004b). The fast clearance, as well as urinary excretion, of ^{68}Ga-DOTA-peptides can be explained by their very high water-solubility. After i.v. administration, some portion of ^{68}Ga-DOTA-peptides may have been degraded by enzymes in the liver, and then the metabolites may have returned to the blood circulation.

The rapid renal excretion is preferred for a PET-imaging agent, due to a lower radioactivity burden for the body, but slower excretion might be beneficial to increase the availability of ligand to the target. In the case of ^{68}Ga-DOTA-peptides, the blood clearance may have been too fast. Renal excretion could be slowed down by modifying the structure to more lipophilic. Also pegylation of ^{68}Ga-DOTAVAP-P1 slowed down renal excretion (Autio *et al.*, 2008; data not shown).

6.2.12. Evaluation and Identification of the Target *Ex Vivo*

To examine closer the uptake of ^{68}Ga-based imaging agents or their targets, different *ex vivo* experiments were performed. The correlation for ^{68}Ga-chloride and transferrin receptors in human BxPC-3 xenografts was not studied, but instead the targeting at a microscopical level (µm) was performed to depict the areas of tissues accumulating [68]Ga. Because the resolution of PET is at a millimeter level, the more focused examination of the ^{68}Ga-chloride accumulation in tumor tissue was performed with autoradiography combined with an histological analysis. The resolution of the method shows certain tissue areas, but it is not able to show the accumulation in individual cells. Autoradiography combined with histological and immunohistochemical macrophage staining was performed, followed with microscopical examination. The analysis revealed that ^{68}Ga-radioactivity was taken up mostly by viable cancer cell islets and possibly partly also by macrophages. In future ^{68}Ga-chloride studies, the correlation for ^{68}Ga-chloride and transferrin receptors in BxPC-3 tumors might be worth clarifying. The presence of targets for ^{68}Ga-labeled peptides was confirmed in the used animal models. The bone infection was verified by microbiological analysis and the expression of VAP-1 by immunohistochemistry. The expression of MMP-9 in the human melanoma xenografts was confirmed also by immunohistochemical staining. Furthermore, the expression level was measured by zymography, even though indicating only low expression of MMP-9.

6.3. Possible Limitations and Development Proposals

[68]Ga-chloride PET revealed radioactivity in addition to the tumor, in the heart, liver, kidneys, urinary bladder and small intestine. The accumulation in the small intestine might be a disadvantage when considering the diagnosis of pancretic cancer. Advantageously, it has been reported that there is no uptake of ^{68}Ga-chloride in a healthy pancreas (Lendvai *et. al.*, 2005). When using a PET-CT camera, the examination of separate organs is possible. In this light, it might be possible to visualize pancretic tumors against the healthy pancretic tissue. Unfortunately, we did not have access to a small-animal PET-CT while performing this study. Another reason why radioactivity in the small intestine might disturb the PET imaging of pancreatic tumors is the range of positrons in the tissue. The mean range in water (giving an estimate of range in tissue) of [68]Ga (2.9 mm) is greater, when compared to that of almost ideal PET-nuclides, [18]F (0.6 mm) or [11]C (1.1 mm) (Vallabhajosula, 2007). For that reason, the radioactivity in the neighboring tissue may mask the radioactivity in the pancreatic tissue. Although, it has been shown that the clinical image qualities of [68]Ga- (β+ decay 89%, $E\beta$+max 1.9 MeV, $T_{1/2}$ 68 min) vs. ^{18}F-labeled agents (β+ decay 97%, $E\beta$+max 0.64 MeV, $T_{1/2}$ 110 min) are not necessarily very much different from each other (Sanchez-Crespo *et al.*, 2004). Even if ^{68}Ga has a shorter half-life than ^{18}F, the significant advantage for ^{18}F-labeled agents is the lower radiation dose due to their lower positron energy.

Quite a small number of animals were used in this study, which may be inadequate to notice statistical significant differences and results in the impression of similarity between the compared agents. The reason for this quite common problem in animal studies, especially in PET imaging, is to cut the costs of these laborious methods. Still, the results of this preliminary study give an estimate of the tested ^{68}Ga-based agents.

Accumulation to kidneys was noticed also after the injection of ^{68}Ga-DOTA-peptides. The high kidney uptake often hinders the *in vivo* application of radiolabeled peptides. The renal accumulation could have been reduced by the administration of certain amino acids (Wei *et. al.*, 2007; Bernard *et. al.*, 1997). This might be worthwhile to consider in future studies.

Comparative imaging experiments and enzyme assays were used to proof the specific binding of ^{68}Ga-DOTAVAP-P1 in the osteomyelitic bones. Still, for the purpose of describing the binding, the assessment of the affinity would have been helpful. In future studies with this model, it would be important to examine also the correlation of the results with the infection/inflammation induced VAP-1 expression in the endothelium. Concerning the targeting of ^{68}Ga-DOTA-TCTPs, it has been previously shown that the *in vivo* tumor accumulation of N,N,N',N'',N''-diethylenetriaminepentaacetate(DTPA)-conjugated and Europium-labeled TCTP-1 can be blocked by the injection of anti-MMP-9 antibody (Peräkylä *et. al.*, 2007; Koivistoinen *et. al.*, 2006). Thus, the *in vivo* blocking studies were not described here.

There is a call for a relevant MMP-9 expressing animal model, since due to lack of a suitable model, many studies may have failed to show the correlation between MMP expression levels and imaging results (Scherer *et al.*, 2008; Van de Wiele and Oltenfreiter, 2006). With a validated model reliable screening of (therapeutic or imaging) agent candidates would be possible. There is also a need for a proper imaging agent to show the real value of therapeutics targeting MMPs. Unfortunately, the rat melanoma model used in the present study showed also quite a low MMP-9 expression level and a poor correlation between MMP-9 expression and imaging results. (The correlation coefficient between the MMP-9 level and tumor-to-muscle ratio p.i. of ^{68}Ga-DOTA-TCTP-1 was 0.33). It is possible that the quantity of MMP-9 was not sufficient to facilitate optimal targeting of the tested ^{68}Ga-DOTA-TCTPs. The explanation for the poor correlation may be that the correlations were searched for between MMP-9 expressed in the whole tumor tissue and the imaging results. Possibly, correlations should be searched for between the extracellular MMP-9 and the imaging results. Although, at least over half of the radioactivity in ^{68}Ga-DOTA-TCTP-1 PET originated from metabolites in the tumor tissue after one hour, it is not necessarily a hindrance if the accumulation has been due to specific binding and the metabolites are not immediately flushed away. In addition, some radiometabolites may also bind to the target. As already mentioned, the structure of ^{68}Ga-DOTA-TCTP-1 still needs some optimization. Another fact, which may also affect the accumulation of ^{68}Ga-DOTA-TCTPs, is that the tumors showed a collapsed morphology with a hollow and necrotic center, especially at the later stages. When the tumor becomes necrotic, its blood circulation decreases and less radio-peptide can reach the target.

However, the relatively weak tumor accumulation of the studied ^{68}Ga-DOTA-TCTPs might also be due to the type of MMP-9 expressed. In rat xenografts, the melanoma cells produce *human* MMP-9 and the growing tumor blood vessels produce *rat* MMP-9. These proteins differ slightly in their amino acid sequence, which is enough to be detected differently by various antibodies. These differences may further affect the ^{68}Ga-DOTA-TCTPs binding to MMP-9. A more detailed characterization of the tumor xenografts with respect to their MMP-9 expression (Western Blot, RNA content) might have been useful. Also the state or conformation of MMP-9 during the progression of melanoma may have complicated finding the correlation between the imaging agent and the MMP-9 level. MMP-9 may be activated at some stages of tumorigenesis and inhibited in others (Sato *et al.*, 1994; Brooks *et al.*, 1996; Hofman *et al.*, 2000; Deryugina *et al.*, 2001; Sternlicht and Werb, 2001; Schnaeker *et al.*, 2004), which may affect the ability of MMP-9 to bind ^{68}Ga-DOTA-TCTP-1.

The target uptakes of ^{68}Ga-chloride and ^{68}Ga-DOTA-peptides revealed to be rather low. This may be partly explained by the SRA of ^{68}Ga-DOTA-peptides. The SRA of ^{68}Ga-DOTA-peptides was low (varying during the course of this study according to the age of the [68]Ge/^{68}Ga-generator from 0.8 MBq/nmol for ^{68}Ga-DOTAVAP-P1 to 3.3 MBq/nmol for ^{68}Ga-DOTA-lactam-TCTP-1), when compared to other radiometal-labeled peptides (Schuhmacher *et al.*, 2005; McQuade *et al.*, 2005; Antunes *et al.*, 2007; Wei *et al.*, 2007). Although, low SRAs of PET imaging agents have been reported also by other groups, e.g., the SRA of ^{68}Ga-DOTA-α-MSH analogue was at the same order of magnitude (104 mCi/μmol = 3.8 MBq/nmol) than that of ^{68}Ga-DOTA-peptides. The low SRA affects by raising the administered dose, which should be kept as a tracer dose as that is a prerequisite for PET. The lower the SRA is, the more the dose contains unlabeled agents competing with the labeled agents. Indeed, it has been reported that the uptake to the target can be affected by a large dose, and that a higher uptake would be expected with a higher SRA (Wei *et. al.*, 2007). The doses of ^{68}Ga-DOTA-peptides were relatively high (36 μg, 36 nmol of ^{68}Ga-DOTAVAP-P1 and 30 nmol, approx. 40-50 μg of ^{68}Ga-DOTA-TCTPs in the *ex vivo* measurements). In general, higher doses are administered prior to PET imaging, regardless of the SRA. The reason for a high radioactive dose prior to PET is that PET is not able to detect such low radioactivity levels than with the *ex vivo* measurements technique. Consequently, it seems that, the *ex vivo* measurements are a more precise method and it should be performed side by side with PET imaging of small animals.

The specific radioactivity of ^{68}Ga-DOTA-peptides decreased together with the age of the generator, due to the decaying of the parent nuclide, [68]Ge. Although, one must keep in mind when estimating different studies side by side that the results of separate studies are not fully comparable. The amount of administered peptide, differences in tumor types and the volumes and status of the tumor cells maintained in each laboratory, affect the results (Wei *et. al.*, 2007). The evaluation of different agents would be easier if there would be an agreed consensus on how to report the values. The best way to report radioactivity is as an IUPAC-unit Bq, SRA as Bq/mol (Velikyan, 2005) and doses as moles, which tells the accurate amount of administered molecules.

It is widely known that ^{68}Ga-based imaging agents often have lower SRA, but they can also be produced with high SRA (Breeman *et al.*, 2005; Velikyan, 2005). It may

not do justice to ^{68}Ga-based imaging agents to evaluate them by comparing their target accumulation with agents, whose production is based on totally different methods, i.e. the production of isotopes by cyclotron and attaching them directly to the targeting molecule, without a chelator. ^{68}Ga-based agents have many other benefits, and the problems associated with a possible low SRA may be overcome by purification or more sophisticated production methods (Velikyan, 2005).

6.4. Feasibility of ^{68}Ga-Based PET

The ^{68}Ga-based PET for the screening of potential imaging agents, described in this thesis work, is promising when aiming at investigating the properties of an interesting molecule, but care must be taken to keep the doses in tracer quantities. For this purpose the SRA can be raised by lowering the amount of the agent in the labeling reaction or by purifying after labeling (Velikyan, 2005). The associated method, *ex vivo* measurements of exciced organs p.i. of DOTA-conjugated and ^{68}Ga-labeled molecules of interest, is an important proof for the PET findings. The technique is more accurate and the lower injected doses advance even more accurate quantification.

[68]Ga-chloride was able to visualize human pancreatic cancer xenografts in rats by PET. Advantageously, when compared to ^{11}C-choline, they showed no statistical difference in the tumor targeting and ^{68}Ga-chloride possessed lower liver uptake. Although, comparison with ^{18}F-FDG showed that the tumor uptake of ^{68}Ga-chloride was lower and ^{18}F-FDG caused the lowest liver burden of all, but also great variation between the animals. It is possible that the tumor uptake of ^{68}Ga-chloride was affected by the high blood pool radioactivity, since the blood clearance was slow due to transferrin binding.

Ostemyelitis-induced VAP-1 can be targeted by ^{68}Ga-DOTAVAP-P1 at the site of inflammation, because the peptide remained the property of specific binding to VAP-1 after DOTA-conjugation and ^{68}Ga-labeling, shown by competitive enzyme assays and comparative imaging experiments. Furthermore, we have shown in another study that ^{68}Ga-DOTAVAP-P1 can differentiate inflammation from pancreatic cancer tumors (Autio *et al.*, 2010). In theory, also [66]Ga-labeled WBCs (Ellis and Sharma, 1999) could be suitable for the differentiation of acute inflammation from cancer, since WBCs accumulate to acute inflammation (as explained above in section 2.2.2), and not in remarkable amounts to the site of the chronic inflammation, which is often present in tumors. Here we showed that ^{68}Ga-DOTAVAP-P1 visualized the inflammation focus, although with somewhat modest targeting properties. In general, inflammation-specific imaging is challenging and the accumulation of imaging agents to the inflammation site is promoted by locally changed conditions, such as enhanced blood flow and vascular permeability (Boerman *et al.*, 2001). ^{68}Ga-DOTAVAP-P1 is the first candidate peptide and an essential opening for developing VAP-1-specific imaging agents. Different modifications of the peptide are currently being explored. In addition, other small molecular inhibitors of VAP-1 and anti-VAP-1 antibodies will also be evaluated in the future.

Synthetic peptides binding to MMP-9 may be useful for the purpose of diagnosing cancers expressing MMP-9 by means of *in vivo* imaging. A DOTA-conjugated and ^{68}Ga-labeled peptide designated as TCTP-1, and two modified versions, were evaluated as imaging agents for PET in a rat melanoma xenograft model. The best visualization of tumor xenografts was obtained with the original cyclic peptide, ^{68}Ga-DOTA-TCTP-1. The replacement of the cystine bridge by a lactam increased the stability drastically, but hindered the tumor targeting slightly. This suggests that there is need for further optimization. This thesis study demonstrated that ^{68}Ga-based technology is feasible for modifying and optimizing potential targeting molecules, such as molecules targeting VAP-1 or MMP-9, to PET imaging agents.

Target-to-background values of the tested ^{68}Ga-based agents (4.0, 2.3 and 5.5 measured for ^{68}Ga-chloride *ex vivo* at 90 min p.i., ^{68}Ga-DOTAVAP-P1 *in vivo* at 40-60 min p.i. and ^{68}Ga-DOTA-TCTP-1 *ex vivo* at 2 h p.i., respectively) fulfilled the criteria for the target-to-bkg being at least 1.5 (Gulec, 2007) and thus they are capable of visualizing targets from the background.

The ^{68}Ga-based method, including PET and *ex vivo* measurements, is attractive for several reasons. The generator-produced ^{68}Ga-isotope is readily available and production with a generator is relatively cheap, compared to production with a cyclotron. The [68]Ge/^{68}Ga-generator possesses a one to two year life span depending on uploaded [68]Ge radioactivity and the utilization capacity. In this study, an inorganic TiO_2-based [68]Ge/^{68}Ga-generator, supplied by Cyclotron Co. was used. The breakthrough of impurities from this generator type is minimal ([68]Ge <0.01 %, Zn^{2+}, Al^{3+}, Ge^{4+}, Ti^{4+}, Cu^{2+} <50 nM) (Meyer *et al*., 2004; Velikyan *et al*., 2004; Breeman *et al*., 2005). Furthermore, ^{68}Ga-nuclide has the suitable characteristics for PET detection. The half-life of 68 min is suitable for PET detection and the testing of relatively small molecules (like peptides) owing to rapid pharmacodynamics and kinetics, and the half-life is long enough for the chemical manipulations in agent development. The ^{68}Ga-chemistry, including the conjugation and labeling of molecules, is simple. In addition, in clinical use molecules attached to certain chelator and then ^{68}Ga-labeled could first be used for PET diagnosis, followed with radiotherapy using the same targeting molecule labeled with another isotope.

7. SUMMARY AND CONCLUSIONS

[68]Ga-based agents for PET are potential candidates to be applied for imaging cancer and inflammation. The ^{68}Ga-based method is attractive for several reasons, as shown in this study. Production of ^{68}Ga-based agents is convenient with a [68]Ge/^{68}Ga-generator, which is relatively cheap and allows for the easy availability of the ^{68}Ga-isotope. The ^{68}Ga-chemistry (conjugation and labeling of molecules) is simple. The half-life of ^{68}Ga is long enough for the chemical manipulations and it matches with the biokinetics of most peptides.

The development and testing of three types of ^{68}Ga-based imaging agents are reported here. ^{68}Ga-chloride for the PET imaging of cancer was produced by simple elution and neutralization. The radio-peptides were first DOTA-conjugated and then ^{68}Ga-labeled. ^{68}Ga-DOTAVAP-P1, targeting VAP-1, was used for the detection of inflammation, and ^{68}Ga-DOTA tumor cell targeting peptides (TCTPs) were designed to selectively target MMP-9. ^{68}Ga-chloride and ^{68}Ga-DOTAVAP-P1 were compared with two clinically used imaging agents, ^{11}C-choline and ^{18}F-FDG. The original lead TCTP, was compared with two of its modifications. All the agents proceeded from *in vitro* tests to preclinical *in vivo* evaluation, and were capable to visualize the target. The tumor uptake, expressed as SUV, was 0.9 and 0.6 for ^{68}Ga-chloride and ^{68}Ga-DOTA-TCTP-1, respectively. The uptake to the inflammatory site was 1.2 for ^{68}Ga-DOTAVAP-P1. Tumor-to-muscle ratios were 4.0 and 5.5 measured for ^{68}Ga-chloride *ex vivo* at 90 min p.i. and for ^{68}Ga-DOTA-TCTP-1 *ex vivo* at 2 h p.i., respectively. The osteomyelitic leg-to-healthy leg ratio was 2.3 measured for ^{68}Ga-DOTAVAP-P1 *in vivo* at 40-60 min p.i. Although, the target uptake of these agents remained modest, resulting from ^{68}Ga-chloride binding to blood transferrin and the rapid clearance of ^{68}Ga-DOTA-peptides, the target-to-background values were high enough for the visualization of targets from the background. The tumor uptake of ^{68}Ga-chloride was at the same level with ^{11}C-choline, but lower than that of ^{18}F-FDG. ^{68}Ga-chloride caused lower liver burden than ^{11}C-choline. The kidney uptake of the tested imaging agents and following excretion is common for radio-peptides and could be avoided by the pre-administering of certain aminoacids. A comparison with control peptides and competitors showed that even after conjugation and labeling, ^{68}Ga-DOTAVAP-P1 remained its specific binding to VAP-1. The competitive measurements were shown to be a convenient method for proofing the specific binding. ^{68}Ga-chloride may also be suitable for the imaging of infection and ^{68}Ga-DOTAVAP-P1 for the differentiation of inflammation from cancer.

This proof-of-principle study demonstrated that ^{68}Ga-based technology is feasible for modifying and optimizing potential targeting molecules, such as molecules targeting VAP-1 or MMP-9, to PET imaging agents. The field of ^{68}Ga-based agents is in progress and under growing interest.

8. ACKNOWLEDGEMENTS

I wish to also thank Pirkko's group. You took me into your warm atmosphere and offered your support. I want to express my particular gratitude to Jani Seppänen, who has taught me a lot about and helped me with cell culturing.
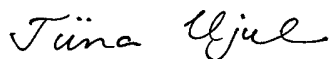
I wish to thank my friends for their support, especially Tiina-Kaisa Kukko-Lukjanov for her valuable advice. Furthermore, I want to thank my dear course mates in Health Biosciences '98 and Professors Markku Koulu, Kalervo Väänänen, Liisa Kanerva and Seppo Salminen, as well as Heli Törmänen, the secretary of Health Biosciences, for being so encouraging. You made my enthusiasm for science even deeper. Also Dr. Hannele Uusitalo-Järvinen was a cheery role model of a young female scientist to me.

I owe my deepest gratitude to my family for their love and patience. My husband Jukka-Pekka Ujula, his parents Tarja and Pertti Ujula, my brother-in-law Hannu Ujula, as well as my parents, Anneli and Pentti Pöyhönen, my sister Paula Pöyhönen and her partner Mattias Gestranius, made this possible with their never-ending support and child-care help. Also, my dear grandmother Kerttu Ollari had a contribution by supporting me and allowing me to live with her for a while. My one-year-old son, Emil, has been my sunshine, when I needed it most.

Turku, December 2010

Tiina Ujula

9. REFERENCES

Agdeppa E. D. and Spilker M. E. (2009). A review of imaging agent development. *AAPS J.* **11**, 286-299.

Ambrosini V., Campana D., Bodei L., Nanni C., Castellucci P., Allegri V., Montini G. C., Tomassetti P., Paganelli G., Fanti S. (2010). ^{68}Ga-DOTANOC PET/CT clinical Impact in Patients with Neuroendocrine Tumors. *J Nucl Med* **51**, 669–673.

Anger H. O. and Gottschalk A, (1963). Localization of brain tumors with the positron scintillation camera. *J Nucl Med* **77**, 326-330.

Antunes P., Ginj M., Zhang H., Waser B., Baum R. P., Reubi J. C., Mäcke H. (2007). Are radiogallium-labelled DOTA-conjugated somatostatin analogues superior to those labelled with other radiometals? *Eur J Nucl Med Mol Imaging* **34**, 982-993.

Autio A., Haukkala J., Henttinen T., Virsu P., Pöyhönen T., Maksimow M., Salomäki S, Jalkanen S., Roivainen A. (2008). Effects of PEGylation to the stability of ^{68}Ga-DOTA-peptides for VAP-1 targeting [abstract P777]. *Eur J Nucl Med Mol Imaging* **35**, Suppl 2, S389.

Autio A., Ujula T., Luoto P., Salomäki S., Jalkanen S., Roivainen A. (2010). PET imaging of inflammation and adenocarcinoma xenografts using vascular adhesion protein 1 targeting peptide ^{68}Ga-DOTAVAP-P1: Comparison with ^{18}F-FDG. *Eur J Nucl Med Mol Imaging* **37**, 1918-1925.

Backstrom J. R., Miller C. A., Tökés Z. A. (1992). Characterization of neutral proteinases from Alzheimer-affected and control brain specimens: identification of calcium-dependent metalloproteinases from the hippocampus. *J Neurochem* **58**, 983-992.

Baum R. P., Prasad V., Hommann M., Hörsch D. (2008). Receptor PET/CT imaging of neuroendocrine tumors. *Recent Results Cancer Res* **170**, 225–242.

Beckmann N., Kneuer R., Gremlich H.-U., Karmouty-Quintana H., Blé F.-X., Müller M. (2007). In vivo mouse imaging and spectroscopy in drug discovery. *NMR Biomed.* **20**, 154-185.

Benbow U. and Brinckerhoff C. E. (1997). The AP-1 site and MMP gene regulation: what is the fuss about? *Matrix Biol* **15**, 519-526.

Berger F. and Gambhir S. S. (2001). Recent advances in imaging endogenous or transferred gene expression utilizing radionuclide technologies in living subjects: applications to breast cancer. *Breast Cancer Res* **3**, 28-35.

Bernard B. F., Krenning E. P., Breeman W. A. P., Rolleman E. J., Bakker W. H., Visser T. J., Mäcke H., de Jong M. (1997). D-Lysine reduction of indium-111 octreotide and yttrium-90 octreotide renal uptake. *J Nucl Med* **38**, 1929-1933.

Bernstein L. R. (1998). Mechanisms of therapeutic activity for gallium. *Pharmacological Reviews* **50**, 665-682.

Blankenberg F. G. and Strauss H. W. (2002). Nuclear medicine applications in molecular imaging. *J. Magn. Reson. Imaging* **16**, 352-361.

Bloomston M., Zervos E. E., Rosemurgy A. S. (2002). Matrix metalloproteinases and their role in pancreatic cancer: A review of preclinical studies and clinical trials. *Ann Surg Oncol* **9**, 668-674.

Boerman O. C., Dams E. T. M., Oyen W. J. G., Corstens F. H. M., Storm G. (2001) Radiopharmaceuticals for scintigraphic imaging of infection and inflammation. *Inflamm res* **50**, 55-64.

Bolster J. M., Vaalburg W., Paans A. M., van Dijk T. H., Elsinga P. H., Zijlstra J. B., Piers D. A., Mulder N. H., Woldring M. G., Wynberg H. (1986). Carbon-11 labelled tyrosine to study tumor metabolism by positron emission tomography (PET). *Eur J Nucl Med* **12**, 321-324.

Bono P., Salmi M., Smith D. J., Jalkanen S. (1998). Cloning and characterization of mouse vascular adhesion protein-1 reveals a novel molecule with enzymatic activity. *J Immunol* **160**, 5563-5571.

Breeman W. A. P., de Jong M., de Blois E., Bernard B. F., Konijnenberg M., Krenning E. P. (2005). Radiolabelling DOTA-peptides with [68]Ga. *Eur J Nucl Med Mol Imaging* **32**, 478-485.

Breeman W. A. P. and Verbruggen A. M. (2007). The [68]Ge/^{68}Ga generator has high potential, but when can we use ^{68}Ga-labelled tracers in clinical routine?. *Eur J Nucl Med Mol Imaging* **34**, 978-981.

Bremer C., Bredow S., Mahmood U., Weissleder R., Ching-Hsuan T. (2001). Optical Imaging of Matrix Metalloproteinase–2 Activity in Tumors: Feasibility Study in a Mouse Model. *Radiology* **221**, 523-529.

Brooks P. C., Stromblad S., Sanders L. C., von Schalscha T. L., Aimes R. T., Stetler-Stevenson W. G., Quigley J. P., Cheresh D. A. (1996). Localization of matrix metalloproteinase MMP-2 to the surface of invasive cells by interaction with integrin alpha(v) beta(3). *Cell* **85**, 683-693.

Burleson R. L., Holman L., Tow D. E. (1975). Scintigraphic demonstration of abscesses with radioactive gallium labeled leukocytes. *Surg Gynecol Obstet* **141**, 379-141.

Chitambar C. R. and Zivkovic Z. (1987). Uptake of gallium-67 by human leucemic cells: Demonstration of transferrin receptor-dependent and transferrin-independent mechanisms. *Cancer Res* **47**, 3929-3934.

de Goeij J. J. M. and Bonardi M. L. (2005). How do we define the concepts specific activity, radioactive concentration, carrier, carrier-free and no-carrier-added? *J Radioanal Nucl Chem* **263**, 13-18.

Deryugina E. I., Ratnikov B., Monosov E., Postnova T. I., DiScipio R., Smith J. W., Strongin A. Y. (2001). MT1-MMP initiates activation of pro-MMP-2 and integrin alpha(v)beta(3) promotes maturation of MMP-

2 in breast carcinoma cells. *Exp Cell Res* **263**, 209-223.

DeGrado T. R., Turkington T. G., Williams J. J., Stearns C. W., Hoffman J. M., Coleman R. E. (1994). Performance characteristics of a whole-body PET scanner. *J Nucl Med* **35**, 1398-1406.

Del Bufalo D., Trisciuoglio D., Scarsella M., D'Amati G., Candiloro A., Iervolino A., Leonetti C., Zupi, G. (2004). Lonidamine causes inhibition of angiogenesis-related endothelial cell functions. *Neoplasia* **6**, 513-522.

De Winter F., Vogelaers D., Gemmel F., Dierckx R.A. (2002). Promising Role of 18-F-Fluoro-D-Deoxyglucose Positron Emission Tomography in Clinical Infectious Diseases. *Eur J Clin Microbiol Infect Di*s **21**, 247-257.

Dimitrapoulou-Strauss A., Hohenberger P., Haberkorn U., Mäcke H. R., Eisenhut M., Strauss L. G. (2007). ^{68}Ga-labeled bombesin studies in patients with gastrointestinal stromal tumors: comparison with ^{18}F-FDG. *J Nucl Med* **48**, 1245-1250.

Dzik-Jurasz A. S. K. (2004). Molecular imaging in oncology. *Cancer Imaging* **4**, 162-173.

Dunn G. P., Old L. J., Schreiber R. D. (2004). The three Es of cancer immunoediting. *Annu Rev Immunol* **22**, 329-60.

Dupont P. and Warwick J. (2009). Kinetic modelling in small animal imaging with PET. *Methods* **48**, 98-103.

Edwards C. L. and Hayes R. L. (1969). Tumor scanning with ^{67}Ga citrate. *J Nucl Med* **10**, 103-105.

Ellis B. L. and Sharma H. L. (1999). Co, Fe and Ga chelates for cell labelling: A potential use in PET imaging? *Nucl Med Commun.* **20**, 1017-1021.

Evans J. W. and Peters A. M. (2002). Gamma camera imaging in malignancy. *Eur J Cancer* **38**, 2157-2172.

Even-Sapir E. and Israel O. (2003). Gallium-67 scintigraphy: a cornerstone in functional imaging of lymphoma. *Eur J Nucl Med Mol Imaging* **30**: S1, S65-81.

Fani M., André J. P., Mäcke H. R. (2008). ^{68}Ga-PET: a powerful generator-based alternative to cyclotron-based PET radiopharmaceuticals. *Contrast Media Mol. Imaging* **3**, 67-77.

Fischman A. J. (1989). Quo Vadis radioimmune imaging. *J Nucl Med* **30**, 1911-1915.

Garbe C. and Eigentler T. K. (2007). Diagnosis and treatment of cutanous melanoma: state of the art 2006. *Melanoma Res* **17**, 117-127.

Gleason G. (1960). A positron cow. *Int J appl Radiat Isotopes* **8**, 90-94.

Gokturk C., Garpenstrand H., Nilsson J., Nordquist J., Oreland L., Forsberg-Nilsson K. (2003). Studies on semicarbazide-sensitive amine oxidase in patients with diabetes mellitus and in transgenic mice. *Biochim Biophys Acta* **1647**, 88-91.

Goldsmith S. J. and Vallabhajosula S. (2009). Clinically proven radiopharmaceuticals for infection imaging: Mechanisms and applications. *Semin Nucl Med*. **39**, 2-10.

Goodwin D. A., Lang E. V., Atwood J. E., Dalman R. L., Ransone C. M., Diamanti C. I., McTigue M. (1993). Viability and biodistribution of ^{68}Ga MPO-labelled human platelets. *Nucl Med Commun.* **14**, 1023-1029.

Gotthardt M., Boermann O. C., Behr T. M., Béhé M. P., Oyen W. J. G. (2004). Development and clinical application of peptide-based radiopharmaceuticals. *Curr Pharm Des* **10**, 2951-2963.

Green M. A. and Welch M. J. (1989). Gallium radiopharmaceutical chemistry. *Nucl Med Biol* **16**, 435-448.

Greene M. W. and Tucker W.D. (1961). An improved gallium-68 cow. *Int J appl Radiat Isotopes* **12**, 62-63.

Gulec S. A. (2007). PET probe-guided surgery. *J Surg Oncol* **96**, 353-357.

Halter G., Buck A. K., Schirrmeister H., Wurziger I., Liewald F.,Glatting G., Neumaier B., Sunder-Plassmann L., Reske S. N., Hetzel M. (2004). [^{18}F]3-deoxy-3'-fluorothymidine positron emission tomography: Alternative or diagnostic adjunct to 2-[^{18}F]-fluoro-2-deoxy-D-glucose positron emission tomography in the workshop of suspicious central focal lesions? *General Thoracic Surgery* **127**, 1093-1099.

Hamacher K, Coenen H. H, Stocklin G. (1986). Efficient stereospecific synthesis of no-carrier-added 2-^{18}F-2-deoxy-D-glucose using aminopolyether supported nucleophilic substitution. *J Nucl Med* **27**, 235-238.

Hanaoka H., Mukai T., Habashita S., Asano D., Ogawa K., Kuroda Y., Akizawa H., Iida Y., Endo K., Saga T., Saji H. (2007). Chemical design of a radiolabeled gelatinase inhibitor peptide for the imaging of gelatinase activity in tumors. *Nucl Med Biol* **34**, 503-510.

Hara T. (2002). [^{11}C]Choline and 2-deoxy-2-[^{18}F]fluoro-D-glucose in tumor imaging with positron emission tomography. *Mol Imaging Biol* **4**, 267-273.

Hara T., Kosaka N., Shinoura N., Kondo T. (1997). PET imaging of brain tumor with (methyl-[^{11}C])choline. *J Nucl Med* **38**, 842-847.

Harris J. M. and Chess R. B. (2003). Effect of pegylation on pharmaceuticals. *Nat Rev Drug Discov* **2**, 214-221.

Haug A., Auernhammer C. J., Wängler B., Tiling R., Schmidt G., Göke B., Bartenstein P., Pöpperl G. (2009). Intraindividual comparison of ^{68}Ga-DOTA-TATE and ^{18}F-DOPA PET in patients with well-differentiated metastatic neuroendocrine tumours. *Eur J Nucl Med Mol Imaging* **36**, 765-770.

Heiss P., Mayer S., Herz M., Wester H. J., Schwaiger M., Senekowitsch-Schmidtke R. (1999). Investigation of transport mechanism and uptake kinetics of O-(2-[^{18}F]fluoroethyl)-L-tyrosine *in vitro* and *in vivo*. *J Nucl Med* **40**, 1367-1373.

Heppeler A., Froidevaux S., Eberle A. N., Mäcke H. R. (2000). Receptor targeting for tumor localization and therapy with radiopeptides. *Curr Med Chem* **7**, 971-994.

Higasi T., Nakayama Y., Murata A., Nakamura K., Sugiyama M., Kawaguchi T., Suzuki S. Clinical evaluation of ^{67}Ga-citrate scanning. (1971). *J Nucl Med* **13**, 196-201.

Hnatowich D. J. (1977). A review of radiopharmaceutical development with short-lived generator-produced radionuclides other than [99m]Tc. *Int J Appl Radiat Isot* **28**, 169-181.

Hofman U. B., Westphal J. R., Waas E. T., Becker J. C., Ruiter D. J., Van Muijen G. N. (2000). Coexpression of integrin alpha(v)beta(3) and matrix metalloproteinase-2 (MMP2) coincides with MMP2 activation: correlation with melanoma progression. *J Invest Dermatol* **115**, 625-632.

Hume S. P., Gunn R. N., Jones T. (1998). Pharmacological constraints associated with positron emission tomographic scanning of small laboratory animals. *Eur J Nucl Med* **25**, 173-176.

Ichise M, Meyer J. H. and Yonekura Y. (2001). An introduction to PET and SPECT Neuroreceptor Quantification Models. *J Nucl Med* **42**, 755-763.

Ito Y., Okuyama S., Sato K., Takahashi K., Sato T., Kanni I. (1971). [67]Ga tumor scanning and its mechanisms studied in rabbits. *Radiology* **100**, 357-362.

Jaakkola K., Nikula T., Holopainen R., Vähäsilta T., Matikainen M. T., Laukkanen M. L., Huupponen R., Halkola L., Nieminen L., Hiltunen J., Parviainen S., Clark M. R., Knuuti J., Savunen T., Kääpä P., Voipio-Pulkki L. M., Jalkanen S. (2000). In vivo detection of vascular adhesion protein-1 in experimental inflammation. *Am J Pathol*. **157**, 463-471.

Jensen R. T., Battey J. F., Spindel E. R., Benya R. V. (2008). International union of pharmacology. LXVIII. Mammalian bombesin receptors: nomenclature, distribution, pharmacology, signaling and functions in normal and disease states. *Pharmacol Rev* **60**, 1-42.

John E. K. and Green M. A. (1990). Structure-activity relationships for metal-labeled blood flow tracers: comparison of keto aldehyde bis(thiosemicarbazonato) copper(II) derivatives. *J Med Chem* **33**, 1764-1770.

Jones-Jackson L., Walker R., Purnell G., McLaren S. G., Skinner R. A., Thomas J. R., Suva L. J., Anaissie E., Miceli M., Nelson C. J., Ferris E. J., Smeltzer M. S. (2005). Early detection of bone infection and differentiation from post-surgical inflammation using (FDG-PET) in an animal model. *J Orthop Res* **23**, 1484-1489.

Koivistoinen A., Taube S., Huttunen M., Sihvo E., Peräkylä H., Salo J., Bergman M. G. (2006). Novel cancer targeting peptides for non-neuroendocrine tumour imaging [abstract P189]. *Eur J Nucl Med Mol Imaging* **33**, S265.

Koivunen E., Wang B., Dickinson CD, Ruoslahti E. (1994). Peptides in cell adhesion research. *Methods Enzymol* **245**, 346-369.

Koivunen E., Arap W., Valtanen H., Rainisalo A., Medina O. P., Heikkilä P., Kantor C, Gahmberg C. G., Salo T., Konttinen Y. T., Sorsa T., Ruoslahti E.,

Pasqualini R. (1999). Tumor targeting with a selective gelatinase inhibitor. *Nature Biotechnol*. **17**, 768-774.

Kopecky P. and Mudrova B. (1974). [68]Ge-^{68}Ga generator for the production of ^{68}Ga in an ionic form. *Int J appl Radiat Isotopes* **25**, 263-268.

Kuhnast B., Bodenstein C., Haubner R., Wester H. J., Senekowitsch-Schmidtke R., Schwaiger M., Weber W. A. (2004). Targeting of gelatinase activity with a radiolabeled cyclic HWGF peptide. *Nucl Med Biol* **31**, 337-344.

Kurkijärvi R., Yegutkin G. G., Gunson B. K., Jalkanen S., Salmi M., Adams D. H. (2000). Circulating soluble vascular adhesion protein 1 accounts for the increased serum monoamine oxidase activity in chronic liver disease. *Gastroenterology* **119**, 1096-1103.

Laforest R., Sharp T. L., Engelbach J. A. Fettig N. M., Herrero P., Kim J., Lewis J. S. Rowland D. J., Tai Y. C., Welch M. J. (2005). Measurement of input function in rodents: challenges and solutions. *Nucl Med Biol* **32**, 679-685.

Lankinen P., Mäkinen T. J., Pöyhönen T. A., Virsu P., Salomäki S., Hakanen A. J., Jalkanen S., Aro H. T., Roivainen A. (2008). ^{68}Ga-DOTAVAP-P1 PET imaging capable of demonstrating the phase of inflammation in healing bones and the progress of infection in osteomyelitic bones. *Eur J Nucl Med Mol Imaging* **35**, 352-364.

Laitinen I. E., Luoto P., Någren K., Marjamäki P. M., Silvola J. M., Hellberg S., Laine V. J., Ylä-Herttuala S., Knuuti J., Roivainen A. (2010). Uptake of ^{11}C-choline in mouse atherosclerotic plaques. *J Nucl Med* **51**, 798-802.

Larson S. M., Rasey J. S., Allen D. R., Nelson N. J., Grunbaum Z., Harp G. D., Williams D.L. (1980). Common pathway for tumor cell uptake of gallium-67 and iron-59 via a transferrin receptor. *J Natl Cancer Inst* **64**, 41-53.

Lavender J. P., Love J. Barker J. R., Burn J. I., Chaundhri M. A. (1971). Gallium 67 citrate scanning in neoplastic and inflammatory lesions. *Br J Radiol* **44**, 361-366.

Lendvai G., Velikyan I., Bergström M., Estrada S., Laryea D., Välilä M., Salomäki S., Långström B., Roivainen A. (2005). Biodistribution of 68Ga-labelled phosphotiester, phosphorothioate, and 2'-O-methyl phosphodiester oligonucleotides in normal rats. *Eur J Pharm Sci* **26**, 26-38.

Li Q. and Xu W. Novel anticancer targets and drug discovery in post genomic age. (2005). *Curr Med Chem* **5**, 53-63.

Lindholm P., Leskinen-Kallio S., Minn H., Bergman J., Haaparanta M., Lehikoinen P., Någren K., Ruotsalainen U., Teräs M., Joensuu H. (1993). Comparison of fluorine-18-fluorodeoxyglucose and carbon-11-methionine in head and neck cancer. *J Nucl Med* **34**, 1711-1716.

Love C. and Palestro C. J. (2004). Radionuclide Imaging of Infection. *J Nucl Med Technol* **32**, 47-57.

Lundqvist H. and Tolmachev V. (2002). Targeting peptides and positron emission tomography. *Biopolymers (Peptide Science)* **66**, 381-392.

Maina T., Nock B., Mather S. (2006). Targeting prostate cancer with radiolabeled bombesins. *Cancer Imaging* **6**, 153-157.

Mantovani A., Romero P., Palucka A. K., Marincola F. M. (2008). Tumor immunity: effector response to tumour and role of the microenvironment. *Lancet* **371**, 771-783.

Marttila-Ichihara F., Smith D. J., Stolen C., Yegutkin G. G., Elima K., Mercier N., Kiviranta R., Pihlavisto M., Alaranta S., Pentikäinen U., Pentikäinen O., Fülöp F., Jalkanen S., Salmi M. (2006). Vascular amine oxidases are needed for leukocyte extravasation into inflamed joints in vivo. *Arthritis and Rheum* **54**, 2852-2862.

Marx J. Inflammation and cancer: The link grows stronger. (2004). *Science* **306**, 966-968.

Mathias C. J., Lewis M. R., Reichert D. E., Laforest R., Sharp T. L., Lewis J. S., Yang Z. F., Waters D. J., Snyder P. W., Low P. S., Welch M. J., Green M. A. (2003). Preparation of ^{66}Ga- and ^{68}Ga-labeled Ga(III)-deferoxamine-folate as potential folate-receptor-targeted PET radiopharmaceuticals. *Nucl Med Biol* **30**, 725-731.

McQuade P., Miao Y., Yoo J., Quinn T. P., Welch M. J., Lewis J. S. (2005). Imaging of melanoma using 64Cu and 86Y-DOTA-ReCCMSH(Arg11), a cycled peptide analog of α-MSH. *J Med Chem* **48**, 2985-2992.

Medina O. P., Kairemo K., Valtanen H., Kangasniemi A., Kaukinen S., Ahonen I., Permi P., Annila A., Sneck M., Holopainen J. M., Karonen S. L., Kinnunen P. K., Koivunen E. (2005). Radionuclide imaging of tumor xenografts in mice using a gelatinase-targeting peptide. *Anticancer Res*. **25**, 33-42.

Meikle S. R., Eberl S., Iida H. (2001). Instrumentation and methodology for quantitative pre-clinical imaging studies. *Curr Pharm Des* **7**, 1945-1966.

Merinen M., Irjala H., Salmi M., Jaakkola I., Hänninen A., Jalkanen S. (2005). Vascular adhesion protein-1 is involved in both acute and chronic inflammation in the mouse. *Am J Pathol* **166**, 793-800.

Meyer G.-J., Mäcke H, Schuhmacher J., Knapp W. H., Hofmann M. (2004). ^{68}Ga-labelled DOTA-derivatised peptide ligands. *Eur J Nucl Med Mol Imaging* **31**, 1097-1104.

Mintun M. A., Raichle M. E., Kilbourn M. R., Wooton G. F., Welch M. J. (1984). A quantitative model for the in vivo assessment of drug binding sites with positron emission tomography. *Ann Neurol* **15**, 217-27.

Moerlein S. M. and Welch M. J. (1981). The chemistry of gallium and indium as related to radiopharmaceutical production. *Int J Nucl Med Biol* **8**, 277-287.

Mohr P., Eggermont A. M. M., Hauschild A., Buzaid A. (2009). Staging of cutaneous melanoma. *Annals of Oncology* **20**, Suppl 6, vi14–vi21.

Mäcke H. R. and André J. P. (2007). ^{68}Ga-PET radiopharmacy: A generator-based alternative to ^{18}F-Radiopharmacy. In: Schubiger P. A., Lehmann M., Friebe M. (eds). *PET Chemistry, The driving force in molecular imaging,* Springer, New York, pp 215-241.

Mäkinen T. J., Lankinen P., Pöyhönen T., Jalava J., Aro H. T., Roivainen A. (2005). Comparison of (^{18})F-FDG and (^{68})Ga PET imaging in the assessment of experimental osteomyelitis due to Staphylococcus aureus. *Eur J Nucl Med Mol Imaging* **32**, 1259-1268.

Nakao A., Fujii T., Sugimoto H., Kanazumi N., Nomoto S., Kodera Y., Inoue S., Takeda S. (2006). Oncological problems in pancreatic cancer surgery. *World J Gastroenterol* **28**, 4466-4472.

Narayanan T. K., Said S., Mukherjee J., Christian B., Satter M., Dunigan K., Shi B., Jacobs M., Bernstein T., Padma M., Mantil J. (2002). A Comparative study on the uptake and incorporation of radiolabeled methionine, choline and fluorodeoxyglucose in human astrocytoma. *Mol Imaging Biol* **4**, 147-156.

Nanni C., Marangoni A., Quarta C., Di Pierro D., Rizzello A., Trespidi S., D'Ambrosio D., Ambrosini V., Donati M., Aldini R., Zanotti-Fregonara P., Grassetto G., Rubello D., Fanti S., Cevenini R. (2009). Small animal PET for the evaluation of an animal model of genital infection. *Clin Physiol Funct Imaging* **29**, 187-192.

Nicholl C. G., Polak J. M., Bloom S. R. (1985). The hormonal regulation of food intake, digestion, and absorption. *Ann Rev Nutr* **5**, 213-239.

Nikkola J., Vihinen P., Vuoristo M. S., Kellokumpu-Lehtinen P., Kähäri V. M., Pyrhönen, S. (2005). High serum levels of matrix metalloproteinase-9 and matrix metalloproteinase-1 are associated with rapid progression in patients with metastatic melanoma. *Clin Cancer Res* **11**, 5158-5166.

Nunn A. D. (2007). Translating promising experimental approaches to clinical trials, Imaging agents. In: Modo M. M. J. and J. W. M. Bulte (eds). *Molecular and cellular MR imaging*, CRC Press, FL, pp 397-398.

Mun-Bryce S., Lukes A., Wallace J., Lukes-Marx M., Rosenberg G. A. (2002). Stromelysin-1 and gelatinase A are upregulated before TNF-alpha in LPS-stimulated neuroinflammation. *Brain Res* **933**, 42-49.

Nikkola J., Vihinen P., Vuoristo M. S., Kellokumpu-Lehtinen P., Kähäri V. M., Pyrhönen S. (2005). High serum levels of MMP-9 and MMP-1 are associated with rapid progression in patients with metastatic melanoma. *Clin Cancer Res* **11**, 5158-5166.

Okarvi S. M. (2004). Peptide-based radiopharmaceuticals: Future tools for diagnostic imaging of cancers and other diseases. *Med Res Rev* **24**, 357-397.

Oltenfreiter R., Staelens L., Lejeune A., Dumont F., Frankenne F., Foidart J. M., Slegers G. (2004). New radioiodinated carboxylic and hydroxamic matrix metalloproteinase inhibitor tracers as potential tumor imaging agents. *Nucl Med Biol* **31**, 459-468.

O'Reilly T. and Mader J. T. (1999). Rat model of bacterial osteomyelitis of the tibia. In: Zak O., Sande M. A. (eds.) *Handbook of animal models of infection.* Academic Press, Bath, Avon, UK, pp 561-75.

Oude Munnink T. H., Nagengast W. B., Brouwers A. H., Schröder C. P., Hospers G. A., Lub-de Hooge M. N., van der Wall E., van Diest P.J., de Vries E. G. (2009). Molecular imaging of breast cancer. *Breast* **18**, Suppl 3, S66-S73.

Oyama N., Akino H., Kanamaru H., Suzuki Y., Muramoto S., Yonekura Y., Sadato N., Yamamoto K., Okada K. (2002) [^{11}C]acetate-PET imaging of prostate cancer. *J Nucl Med* **43**, 181-186.

Packard A. B., Kronauge J. F., Barbarics E., Kiani S., Treves S. T. (2002). Synthesis and biodistribution of a lipophilic ^{64}Cu-labeled monocationic copper(II) complex. *Nucl Med Biol* **29**, 289-294.

Palestro C. J. (2007). In vivo leucocyte labeling: The quest continues. *J Nucl Med* **48**, 332-334.

Peräkylä H., Huttunen M., Karisalmi E. K., Bergman M., Elo H. (2007). *Peptide conjugates*. U S Pat App Pub US 0231258; O/2007/113386.

Peters A. M. (1998). The use of nuclear medicine in infections. *The British Journal of Radiology* **71**, 252-261.

Phelps M. E. (2002). Molecular imaging with positron emission tomography. *Annu Rev Nucl Part Sci* **52**, 303-38.

Phillips P. G. and Birnby L. M. (2004). Nitric oxide modulates caveolin-1 and matrix metalloproteinase-9 expression and distribution at the endothelial cell/tumour cell surface. *Am J Physiol Lung Mol Physiol* **286**, 1055-1065.

Pool S. E., Krenning E. P., Koning G. A., van Eijck C. H. J., Teunissen J. J. M., Kam B., Valkema R., Kwekkeboom D. J., de Jong M. (2010). Preclinical and clinical studies of peptide receptor radionuclide therapy. *Semin Nucl Med* **40**, 209-218.

Raithatha S. A., Muzik H., Rewcastle N. B., Johnston R. N., Edwards D. R., Forsyth P. A. (2000). Localization of gelatinase-A and gelatinase-B mRNA and protein in human gliomas. *Neuro Oncol* **2**, 145-150.

Reubi J. C. and Mäcke H. R. (2008). Peptide-based probes for cancer imaging. *J Nucl Med* **49**, 1735-1738.

Reubi J. C., Wenger S., Schmuckli-Maurer J., Schaer J.-C., Gugger M. (2002). Bombesin receptor subtypes in human cancers: detection with the universal radioligand ^{125}I-[D-TYR^6], β-ALA^{11}, PHE^{13}, NLE^{14}] Bombesin(6-14). *Clin Cancer Res* **8**, 1139-1146.

Randy L., Scherer J., McIntyre O., Matrisian L. M. (2008). Imaging matrix metalloproteinases in cancer. *Cancer Metastasis Rev* **27**, 679-690.

Rizzello A., Di Pierro D., Lodi F., Trespidi S., Cicoria G., Pancaldi D., Nanni C., Marengo M., Marzola M. C., Al-Nahhas A., Rubello D., Boschi S. (2009). Synthesis and quality control of ^{68}Ga citrate for routine clinical PET. *Nucl Med Commun* **30**, 542-545.

Robertson L., Grip L., Mattsson Hultén L., Hulthe J., Wiklund O. (2007). Release of protein as well as activity of MMP-9 from unstable atherosclerotic plaques during percutaneous coronary intervention. *J Intern Med* **262**, 659-667.

Roivainen A., Forsback S., Grönroos T., Lehikoinen P., Kähkönen M., Sutinen E., Minn H. (2000). Blood metabolizm of [*methyl*-^{11}C]choline; implications for in vivo imaging with positron emission tomography *Eur J Nucl Med Mol Imaging* **27**, 25-32.

Roivainen A., Parkkola R., Yli-Kerttula T., Lehikoinen P., Viljanen T., Möttönen T., Nuutila P., Minn H. (2003). Use of positron emission tomography with methyl-^{11}C-choline and 2-^{18}F-fluoro-2-deoxy-D-glucose in comparison with magnetic resonance imaging for the assessment of inflammatory proliferation of synovium. *Arthritis Rheum* **48**, 3077-3084.

Roivainen A., Tolvanen T., Salomäki S., Lendvai G., Velikyan I., Numminen P., Välilä M., Sipilä H., Bergström M., Härkönen P., Lönnberg H., Långström B. (2004). ^{68}Ga-labeled oligonucleotides for in vivo imaging with PET. *J Nucl Med* **45**, 347-355.

Roivainen A. and Yli-Kerttula T. Whole-body distribution of (11)C-choline and uptake in knee synovitis. (2006). *Eur J Nucl Med Mol Imaging* **33**, 1372-1373.

Ryschich E., Huszty H. P., Knaebel H. P., Hartel M., Büchler M. W., Schmidt J. (2004). Transferrin receptor is a marker of malignant phenotype in human pancreatic cancer and in neuroendocrine carcinoma of the pancreas. *Eur J Cancer* **40**, 1418-1422.

Saha G. B. (2004a). Appendix B, Terms used in the text. In: Saha G. B. (eds). *Funfamentals of nuclear pharmacy*, Springer, New York, pp 357-362.

Saha G. B. (2004b). Radiopharmaceuticals and methods of radiolabeling, In: Saha G. B. (eds). *Funfamentals of nuclear pharmacy*, Springer, New York, pp 79-110.

Saif M. W., Cornfeld D., Modarresifar H., Ojha B. (2008). FDG positron emission tomography CT (FDG-PET-CT) in the management of pancreatic cancer: initial experience in 12 patients. *J Gastrointestin Liver Dis* **17**, 173-178.

Sakata K., Satoh M., Someya M., Asanuma H., Nagakura H,. Oouchi A., Nakata K., Kogawa K., Koito K., Hareyama M., Himi, T. (2004). Expression of matrix metalloproteinase 9 is a prognostic factor in patients with non-hodgkin lymphoma. *Cancer* **100**, 356-365.

Salmi M. and Jalkanen S. (1992). A 90-kilodalton endothelial cell molecule mediating lymphocyte binding in humans. *Science* **257**,1407-1409.

Salmi M. and Jalkanen S. (2001) VAP-1: an adhesin and an enzyme. *Trends Immunol* **22**, 211-216.

Salmi M. and Jalkanen S. (2005). Cell-surface enzymes in control of leukocyte trafficking. *Nature Rev Immunol* **5**, 760-771.

Salmi M., Kalimo K., Jalkanen S. (1993). Induction and function of vascular adhesion protein-1 at sites of inflammation. *J Exp Med* **178**, 2255-2260.

Salmi M., Tohka S., Berg E. L., Butcher E. C., Jalkanen S. (1997). Vascular adhesion protein 1 (VAP-1) mediates lymphocyte subtype-specific, selectin-independent recognition of vascular endothelium in human lymph nodes. *J Exp Med* **186**, 589-600.

Salmi M., Yegutkin G. G., Lehvonen R., Koskinen K., Salminen T., Jalkanen S. (2001). A cell surface amine oxidase directly controls lymphocyte migration. *Immunity* **14**, 265-276.

Sanchez-Crespo A., Andreo P., Larsson S. A. (2004). Positron flight in human tissues and its influence on PET image spatial resolution. *Eur J Nucl Med Mol Imaging* **31**, 44-51.

Sato H., Takino T., Okada Y., Cao J., Shinagawa A., Yamamoto E., Seiki M. (1994). A matrix metalloproteinase expressed on the surface of invasive tumour cells. *Nature* **370**, 61-65.

Schnaeker E. M., Ossig R., Ludwig T., Dreier R., Oberleithner H., Wilhelmi M., Schneider S. W. (2004). Microtubule-dependent matrix metalloproteinase-2/matrix metalloproteinase-9 exocytosis: prerequisite in human melanoma cell invasion. *Cancer Res* **64**, 8924-8931.

Schuhmacher J., Zhang H., Doll J., Mäcke H. R., Matys R., Hauser H., Henze M., Haberkorn U., Eisenhut M. (2005). GRP receptor-targeted PET of a rat pancreas carcinoma xenograft in nude mice with a ^{68}Ga-labeled bombesin(6-14) analog. *J Nucl Med* **46**, 691-699.

Shah S. and Mortele K. J. (2007). Uncommon solid pancreatic neoplasms: Ultrasound, computed tomography, and magnetic resonance imaging features. *Semin Ultrasound CT MRI* **28**, 357-370.

Sharma V., Luker G. D., Piwnica-Worms D. (2002). Molecular imaging of gene expression and protein function in vivo with PET and SPECT. *J Magn Reson Imaging* **16**, 336-351.

Shealy C. N., Aronow S., Brownell G. L. (1964). Gallium-68 as a scanning agent for intracranial lesions. *J Nucl Med* **21**, 161-167.

Scherer R. L., McIntyre J. O., Matrisian L. M. Imaging matrix metalloproteinases in cancer. (2008). *Cancer Metastasis Rev* **27**, 679-690.

Shields A. F., Grierson J. R., Dohmen B. M., Machulla H. J., Stayanoff J. C., Lawhorn-Crews J. M., Obradovich J. E., Muzik O., Mangner T. J. (1998). Imaging proliferation *in vivo* with [^{18}F]FLT and positron emission tomography. *Nat Med* **4**, 1334-1336.

Shuhmacher J., Zhang H., Doll J., Mäcke H. R., Matys R., Hauser H., Henze M., Haberkorn U., Eisenhut M. (2005). GRP receptor-targeted PET of a rat pancreas carcinoma xenograft in nude mice with a ^{68}Ga-labeled bombesin(6-14) analog. *J Nucl Med* **46**, 691-699.

Sipos B., Möser S., Kalthoff H., Török V., Löhr M., Klöppel G. (2003). A comprehensive characterization of oancreatic ductal carcinoma cell lines: toward the establishment of an in vitro research platform. *Virchows Arch* **442**, 444-452.

Smith D. J., Salmi M., Bono P., Hellman J., Leu T., Jalkanen S. (1998). Cloning of vascular adhesion protein 1 reveals a novel multifunctional adhesion molecule. *J Exp Med* **188**, 17-27.

Smith G. (1985). Filamentous fusion phage: Novel expression vectors that display cloned antigens on the virion surface. *Science* **228**, 1315-1317.

Song W. S., Nielson B. R., Banks K. B., Bradley Y. C. (2009). Normal organ standard uptake values in carbon-11 acetate PET imaging. *Nuclear Medicine Communications* **30**, 432-465.

Spraque J. E., Li W. P., Liang K., Achilefu S., Anderson C. J. (2006). In vitro and in vivo investigation of matrix metalloproteinase expression in metastatic tumor models. *Nucl Med Biol* **33**, 227-237.

Stephenson T. J. (2004). Inflammation. In a book: *General and systematic pathology*, edited by Underwood J. C. E. Elsevier, London pp 202-220.

Sternlicht M. D. and Werb Z. (2001). How matrix metalloproteinases regulate cell behaviour. *Annu Rev Cell Dev Biol* **17**, 463-516.

Ståhle-Bäckdahl M. and Parks W. C. (1993). 92kD gelatinase is actively expressed by eosinophils and stored by neutrophils in squamous cell carcinoma. *Am J Pathol* **42**, 995-1000.

Sutinen E., Jyrkkiö S., Alanen K., Någren K., Minn H. (2003). Uptake of [N-methyl-11C]alpha-methylaminoisobutyric acid in untreated head and neck cancer studied by PET. *Eur J Nucl Med Mol Imaging* **30**, 72-77.

Swartzendruber D. C., Nelson B., Hayes R. L. (1971). Gallium-67 localization in lysosomal-like granules of leukemic and nonleukemic murine tissues. *J Natl Cancer Inst* **46**, 941-952.

Tan M. H., Nowak N. J., Loor R., Ochi H., Sandberg A. A., Lopez C., Pickren J. W., Berjian R., Douglass H. O., Chu T. M. (1986). Characterization of a new primary human pancreatic tumor line. *Cancer Invest* **4**, 15-23.

Tsan M.-F. and Scheffel U. (1986). Mechanism of Gallium-67 accumulation in tumors. *J Nucl Med* **27**, 1215-1219.

Underwood J. C. E. (2004a). Carcinogenesis. In: *General and systematic pathology*, edited by Underwood J. C. E. Elsevier, London, pp 223-262.

Underwood J. C. E. (2004b). Exocrine pancreas. In: *General and systematic pathology*, edited by Underwood J. C. E. Elsevier, London, pp 428-432.

Vallabhajosula S. (2007). Radionuclides for PET. In: Biersack H.-J., Freeman L. M. *Clinical nuclear medicine*, Springer-Verlag, Berlin, Heidelberg, pp 51-52.

Vallabhajosula S. R., Harwig J. F., Siemsen J. K., Walter W. (1980). Radiogallium localization in tumors: Blood binding and transport and the role of transferrin. *J Nucl Med* **21**, 650-656.

Vallabhajosula S. R., Harwig J. F., Wolf W. (1981). The mechanism of tumor localization of Gallium-67 citrate: Role of transferrin binding and effect of tumor pH. *Int J Nucl Med Biol* **8,** 363-370.

Van de Wiele C. and Oltenfreiter R. (2006). Imaging probes targeting matrix metalloproteinases. *Cancer Biother Radiopharm* **21**, 409-416.

van Eerd J. E., Oyen W. J., Harris T. D., Rennen H. J., Edwards D. S., Corstens F. H., Boerman O. C. (2005).

Scintigraphic imaging of infectious foci with an 111In-LTB4 antagonist is based on in vivo labeling of granulocytes. *J Nucl Med* **46**, 786-793.

van Waarde A., Been L. B., Ishiwata K., Dierckx R. A., Elsinga P. H. (2006). Early response of sigma-receptor ligands and metabolic PET tracers to 3 forms of chemotherapy: an *in vitro* study in glioma cells. *J Nucl Med* **47**, 1538-1545.

van Waarde A., Cobben D. C. P., Suurmeijer A. J. H., Maas B., Vaalburg W., de Vries E. F. J., Jager P. L., Hoekstra H. J., Elsinga P. H. (2004). Selectivity of ^{18}F-FLT and ^{18}F-FDG for differentiating tumor from inflammation in a rodent model. *J Nucl Med* **45**, 695-700.

van Waarde A. and Elsinga P. H. (2008). Proliferation markers for the differential diagnosis of tumor and inflammation. *Curr Pharm Des* **14**, 3326-3339.

Vartak D. G. and Gemeinhart R. A. (2007). Matrix metalloproteinases: Underutilized targets for drug delivery. *J Drug Target* **15**, 1-20.

Velikyan I. (2005). *Synthesis, characterisation and application of ^{68}Ga-labelled macromolecules*. Acta Universitatis Upsaliensis, Uppsala. (http://uu.diva-portal.org/smash/record.jsf?pid=diva2:166697)

Velikyan I., Lendvai G., Välilä M., Roivainen A., Yngve U., Bergström M., Långström B. (2004). Microwave accelerated ^{68}Ga-labelling of oligonucleotides. *J Label Compd Radiopharm* **47**, 79-89.

Vihinen P., Ala-aho R., Kähäri V. M. (2005). Matrix metalloproteinases as therapeutic targets in cancer. *Current Cancer Drug Targets* **5**, 203-220.

von Forstner C., Egberts J. H., Ammerpohl O., Niedzielska D., Buchert R., Mikecz P., Schumacher U., Peldschus K., Adam G., Pilarsky C., Grutzmann R., Kalthoff H., Henze E., Brenner W. (2008). Gene expression patterns and tumor uptake of ^{18}F-FDG, ^{18}F-FLT, and ^{18}F-FEC in PET/MRI of an orthotopic mouse xenotransplantation model of pancreatic cancer. *J Nucl Med* **49**, 1362-1370.

Wack S., Hajri A., Heisel F., Sowinska M., Berger C., Whelan M, Marescaux J., Aprahamian M. (2003). Feasibility, sensitivity, and reliability of laser-induced fluorescence imaging of green fluorescent protein-expressing tumors in vivo. *Mol Ther* **7**, 765-773.

Wagner S., Breyholz H. J., Höltke C., Faust A., Schober O., Schäfers M., Kopka, K. (2009). A new ^{18}F-labelled derivative of the MMP inhibitor CGS 27023A for PET: radiosynthesis and initial small-animal PET studies. *Appl Radiat Isot* **67**, 606–610.

Wei L., Miao Y., Gallazzi F., Quinn T. P., Welch M. J., Vavere A. L., Lewis J. S. (2007). Gallium-68-labeled DOTA-rhenium-cyclized α-melanocyte-stimulating hormone analog for imaging of malignant melanoma. *Nucl Med Biol* **34**, 945-953.

Weiner R. E. (1996). The mechanism of ^{67}Ga localization in malignant disease. *Nucl Med Biol* **23**, 745-751.

Weiner R., Hoffer P. B., Thakur M. L. (1981). Lactoferrin: Its role as a Ga-67-binding protein in polymorphonuclear leukocytes. *J Nucl Med* **22**, 32-37.

Welch D. R., Bisi J. E., Miller B. E., Conaway, D., Seftor E. A., Yohem, K. H., Gilmore, L. B., Seftor, R. E., Nakajima, M., and Hendrix, M. J. (1991). Characterization of highly invasive and spontaneously metastatic human malignant melanoma cell line. *Int J Cancer* **47,** 227-237.

Wikström S. A., Keski-Oja J., Alitalo K. (2003). Matrix reloaded to circulation hits the tumor target. *Cancer Cell 3,* 513-514.

Wienhard K., Schmand M., Casey M. E., Baker K., Bao J., Eriksson L., Jones W. F., Knoess C., Lenox M., Lercher M., Luk P., Michel C., Reed J. H., Richerzhagen N., Treffert J., Vollmar S., Young J. W., Heiss W. D., Nutt R. (2002). The ECAT HRRT: performance and first clinical application of the new high resolution research tomograph. *IEEE Trans Nucl Sci* **49**, 104-110.

Yang Y., Hong H., Zhang Y., Cai W. (2009). Molecular imaging of proteases in cancer. *Cancer Growth Metastasis* **17**, 13-27.

Yegutkin G. G., Salminen T., Koskinen K., Jalkanen S., Salmi M. (2004). A peptide inhibitor of vascular adhesion protein-1 (VAP-1) blocks leukocyte-endothelium interactions under shear stress. *Eur J Immunol* **34**, 2276-2285.

Younes M., Brown R. W., Stephenson M., Gondo M., Cagle P. T. (1997). Overexpression of Glut1 and Glut3 in stage I non-small cell lung carcinoma is associated with poor survival. *Cancer* **80**, 1046-1051.

Young A. B., Frey K. A., Agranoff B. A. (1986). Receptor Assays: In Vitro and In Vivo. In: *Positron Emission Tomography and Autoradiography: Principles and Applications for the Brain and Heart*, edited by Phelps M., Mazziota J., and Schelbert H. Raven Press, New York, pp 73-107.

Zheng Q. H., Fei X., Liu X., Wang, J. Q., Bin Sun H., Mock, B.H., Lee Stone, K., Martinez, T. D., Miller, K. D., Sledge, G. W., Hutchins, G. D. (2002). Synthesis and preliminary biological evaluation of MMP inhibitor radiotracers [^{11}C]methyl-halo-CGS 27023A analogs, new potential PET breast cancer imaging agents. *Nucl Med Biol* **29**, 761-770.

Zheng Q. H., Fei X., Liu X., Wang J. Q., Stone K. L., Martinez T. D., Gay D. J., Baity W. L., Miller K. D., Sledge G. W., Hutchins G. D. (2004). Comparative studies of potential cancer biomarkers carbon-11 labeled MMP inhibitors (S)-2-(4'-[11C]methoxybiphenyl-4-sulfonylamino)-3-methylbutyric acid and N-hydroxy-(R)-2-[[(4'-[11C]methoxyphenyl) sulfonyl]benzylamino]-3-methylbutanamide. *Nucl Med Biol* **31,** 77-85.

Zorzano A., Abella A., Marti L., Carpene C., Palacin M., Testar X. (2003). Semicarbazide-sensitive amine oxidase activity exerts insulin-like effects on glucose metabolism and insulin-signaling pathways in adipose cells. *Biochim Biophys Acta* **1647**, 3-9.